

Chernihiv Polytechnic National University¹ (Ukraine)
Ministry of Education and Science of Ukraine
University of Extremadura² (Spain)
Department of Electric, Electronic and Automation Engineering
Chernihiv Polytechnic National University¹ (Ukraine)
Ministry of Education and Science of Ukraine

Qualifying scientific work
on the rights of manuscript

AZIZI MOHAMMADREZA

UDC [621.314.5:621.318.43:621.3.051](043.5)

DISSERTATION

ENERGY ROUTER FOR HYBRID MICROGRIDS FOR EFFICIENT AND ROBUST ENERGY AND POWER MANAGEMENT

¹141 – Electrical Power Engineering, Electrical Engineering and Electromechanics

²R024 – Doctorate in Industrial Engineering (R024)

¹14 – Electrical Engineering

Applying for a double degree of Doctor of Philosophy

Based on an agreement between both Universities

The dissertation contains the results of my own research. The use of ideas, results and texts of other authors requires a reference to the appropriate source.

_____ M. Azizi

Scientific supervisor:

¹Oleksandr Velihorskyi, Dr., docent, Professor of Department of Electronics Automation, Robotics and Mechatronics of Chernihiv Polytechnic National University.

²Carlos Roncero-Clemente, Dr., Associate Professor of Department of Electric, Electronic and Automation Engineering of University of Extremadura.

Chernihiv – 2025

ANNOTATION

Azizi M. Energy Router for Hybrid Microgrids for Efficient and Robust Energy and Power Management – Qualifying scientific work on the rights of the manuscript.

Dissertation for a double degree of Doctor of Philosophy in specialty 141 - "Electric Power Engineering, Electrotechnics and Electromechanics." Department of Electrical Engineering and Information Measuring Technologies, Chernihiv Polytechnic National University, Ministry of Education and Science of Ukraine; and R024 - Doctorate in Industrial Engineering, University of Extremadura, Department of Electric, Electronic and Automation Engineering, Badajoz, Spain.

Electric energy consumption is increasing much faster than the predicted growth in energy generation. Although the installed capacity of renewable energy sources is also expanding, grid congestion remains unavoidable without adopting smart energy management systems and flexible power electronics structures. Therefore, the rise of electric energy consumption and electric energy congestion is leading to the necessity of autonomous residential buildings. With the increase of domestic generation resources (mainly photovoltaic), and the use of storage systems in many buildings, moving towards zero-emission buildings (ZEBs) and the utilization of the dc system along with ac system is being developed. For this purpose, a new technology, called an energy router (ER) with ac and dc ports, was proposed in recent years. Researchers have already proposed various topologies and control strategies for ER; however, there are still research gaps and challenges that should be addressed. Safety and protection issues and the control response in dynamic conditions are among these challenges.

Chapter one provides a general review of power electronics solutions for ZEBs. By exploring the promising future of the low-voltage dc industry in ZEBs, the study presents and compares different configurations for ER and grid-connected scenarios, evaluating their overall efficiencies across hybrid, dc, and ac technologies.

Chapter two comprehensively deals with the integration of dc systems and related challenges. Dc microgrids, along with existing ac grids, are a future trend in energy distribution systems. However, there are not yet sufficient standards to integrate dc systems into the ac grid, and safety considerations remain a problem. At the same time,

many related issues are still undefined and unsolved. In particular, uncertainty prevails in isolation requirements between ac grids and novel microgrids, as well as in the grounding approaches. This chapter first deals with different integration solutions and then investigates leakage currents and different grounding types and configurations, both on ac and dc sides. It provides an overview of possible grounding approaches at the connection points and the feasibility of avoiding isolation between ac grid and dc systems. Furthermore, it proposes solutions for challenges related to protection, grounding, and leakage currents. Finally, considering the importance of grounding and protecting personnel and equipment on both ac and dc sides, the use of common-ground structures is introduced as an effective method.

Regarding the integration challenges and scenarios, chapter three introduces the proposed structure of a single-cell three-phase ER based on the common-ground inverter. In this topology, dc link can access all three phases and balance them without the complexities and costs associated with conventional three-phase systems. Common-ground structure creates the same ground on both ac and dc sides that not only provides safety and protection on both sides, but also decreases the cost and weight since it eliminates isolation. Inverter operating mode and modulation, component design of different parts, and then protection and dc circuit breaker are also described in detail.

Chapter four focuses on control strategy and describes different control levels in an ER. The ER system integrates multiple power sources and sinks, and any sudden change in a subsystem can introduce dynamic conditions across the entire system. To enhance the dynamic performance of a multiport ER, flatness-based control (FBC) theory is applied to the low-level control (inner loops) of the ER, ensuring a fast and robust control response in dynamic conditions. The presented method guarantees a robust dc-link in any dynamic conditions. In this method, with the algebraic and analytical relationships, the system can be controlled effectively. Therefore, the amount of system calculations is reduced, and it does not require solving the optimization problem at each time step. While FBC can be used for both dc-link and the grid current control, the proportional resonance (PR) controller is also described in this chapter as a reliable alternative for grid current, which can effectively eliminate different harmonics. At the

end, this chapter examines the high-level energy management system solutions from a simple local-based to a high-tech solution, emphasizing the shift to full digitalization through a combination of cloud-based and edge-computing platforms.

Finally, chapter five presents simulation and experimental results. Simulation results are provided to validate the proposed control solution and compare the control response and quality with conventional control solutions. In the experimental part, the general operating modes are analyzed, and the controller response in dynamic conditions is also investigated. At the end, general conclusions are discussed and highlighted.

Keywords: Zero-emission buildings, energy router, dc microgrid, low-voltage dc, leakage current, grounding, single-cell three-phase, common-ground inverter, dc circuit breaker, flatness-based control theory, dynamic conditions.

АНОТАЦІЯ

Azizi M. Енергетичний маршрутизатор для гібридних мікромереж для ефективного та надійного керування енергією та потужністю – кваліфікаційна наукова робота на правах рукопису.

Дисертація на здобуття подвійного ступеня доктора філософії за спеціальністю 141 – «Електроенергетика, електротехніка та електромеханіка», кафедра електротехніки та інформаційно-вимірювальних технологій, Чернігівський політехнічний національний університет, Міністерство освіти і науки України; та за напрямом R024 – докторантура з промислової інженерії, Університет Естремадури, кафедра електричної, електронної та автоматизаційної інженерії, Бадахос, Іспанія.

Споживання електричної енергії зростає значно швидше, ніж прогнозоване зростання її генерації. Хоча встановлена потужність відновлюваних джерел енергії також зростає, перевантаження електромереж залишається неминучим без впровадження інтелектуальних систем керування енергією та гнучких структур силової електроніки. Тому зростання споживання електроенергії та перевантаження мережі призводить до необхідності автономних житлових будівель. Зі збільшенням кількості локальних джерел генерації (переважно фотоелектричних) та використанням систем зберігання енергії у багатьох будівлях розвивається напрям до будівель з нульовими викидами (ZEB) та використання постійного струму (DC) поряд із системами змінного струму (AC). З цією метою в останні роки запропоновано нову технологію – енергетичний маршрутизатор (ER) із портами змінного та постійного струму. Дослідники вже запропонували різні топології та стратегії керування ER, однак залишаються дослідницькі прогалини та виклики, які потребують вирішення. Питання безпеки, захисту та реакції системи керування в динамічних умовах є серед основних проблем.

У першому розділі представлено загальний огляд силових електронних рішень для ZEB. Досліджується перспективне майбутнє індустрії низьковольтних систем постійного струму в ZEB, порівнюються різні конфігурації ER та сценарії

підключення до мережі, оцінюється їх загальна ефективність у гібридних, DC та AC технологіях.

Другий розділ присвячений інтеграції систем постійного струму та пов'язаним із цим викликам. DC-мікромережі разом із наявними AC-мережами є майбутнім трендом систем розподілу енергії. Проте наразі бракує стандартів для інтеграції DC-систем в AC-мережу, а питання безпеки залишаються актуальними. Багато пов'язаних питань досі не визначено, зокрема вимоги до ізоляції між AC-мережами та новими мікромережами, а також підходи до заземлення. У цьому розділі розглядаються різні рішення інтеграції, досліджуються струми витоку та типи і конфігурації заземлення на сторонах AC та DC. Також наведено огляд можливих підходів до заземлення у точках з'єднання та розглянуто доцільність уникнення ізоляції між AC-мережею та DC-системами. Далі пропонуються рішення для проблем, пов'язаних із захистом, заземленням і струмами витоку. Нарешті, враховуючи важливість захисту персоналу та обладнання на обох сторонах, запропоновано використання структур із загальним заземленням як ефективний метод.

У третьому розділі, з огляду на виклики інтеграції, представлено запропоновану структуру трифазного ER з однією коміркою на основі інвертора із загальним заземленням. У цій топології ланка постійного струму має доступ до всіх трьох фаз і може балансувати їх без складностей і витрат, характерних для традиційних трифазних систем. Структура із загальним заземленням забезпечує однаковий потенціал землі на сторонах AC і DC, що підвищує безпеку, спрощує захист, а також зменшує вартість і вагу системи за рахунок відсутності потреби в ізоляції. Детально описано режими роботи інвертора, модуляцію, проєктування компонентів, а також захист і вимикач постійного струму.

Четвертий розділ зосереджується на стратегії керування та описує різні рівні управління в ER. Оскільки система ER інтегрує кілька джерел та споживачів енергії, будь-яка раптова зміна в підсистемі може створити динамічні умови в усьому комплексі. Для підвищення динамічних характеристик багатопортового ER застосовано теорію керування на основі пласкості (FBC) на нижньому рівні

керування (внутрішніх контурах), що забезпечує швидку та надійну реакцію системи в динамічних умовах. Запропонований метод гарантує стабільну роботу DC-ланки за будь-яких умов. Завдяки аналітичним співвідношенням система керується ефективно, що зменшує обчислювальні витрати та усуває необхідність розв’язування задач оптимізації на кожному кроці. Хоча FBC можна застосовувати як для керування DC-ланкою, так і струмом мережі, у цьому розділі також описано пропорційно-резонансний (PR) контролер як надійну альтернативу для керування струмом мережі, здатну ефективно усувати гармоніки. Наприкінці розділу розглянуто рішення для систем управління енергією верхнього рівня — від простих локальних до високотехнологічних рішень, з акцентом на перехід до повної цифровізації через поєднання хмарних і edge-платформ.

П’ятий розділ містить результати моделювання та експериментів. Результати моделювання підтверджують ефективність запропонованого контролера та порівнюють його характеристики з традиційними методами керування. В експериментальній частині проаналізовано основні режими роботи системи та поведінку контролера в динамічних умовах. Наприкінці наведено загальні висновки та узагальнення.

Ключові слова: будівлі з нульовими викидами, енергетичний маршрутизатор, мікромережа постійного струму, низьковольтна DC-система, струм витоку, заземлення, трифазна структура з однією коміркою, інвертор із загальним заземленням, вимикач постійного струму, теорія керування на основі плоскості, динамічні умови.

List of publications

1. M. Azizi, O. Husev, C. Roncero-Clemente, O. Veligorskyi and R. Strzelecki, "Fast and Robust Energy Router Control in Dynamic Conditions Using Flatness-Based Control Theory," 2025 IEEE 19th International Conference on Compatibility, Power Electronics and Power Engineering (CPE-POWERENG), Antalya, Turkey, 2025, pp. 1-6, doi: <https://doi.org/10.1109/CPE-POWERENG63314.2025.11027260>. Flatness-based control theory is developed to enhance the dynamic performance of a multiport energy router. The presented method controls the grid-side current and regulates the dc-link voltage. The simulation results confirm the proper performance of this method, and the comparisons made validate the high speed and accuracy of the system responses compared to conventional solutions. Keywords: Flatness-based control theory, multiport energy router, dynamic conditions, hybrid nanogrid. Conference Paper, indexed in Scopus.
2. M. Azizi, O. Husev, R. Mbayed, E. Monmasson, J. Martins and O. Veligorskyi, "Energy Router: A Sustainable Solution for Future Residential Buildings," in IEEE Power Electronics Magazine, vol. 12, no. 1, pp. 75-86, March 2025, doi: <https://doi.org/10.1109/MPEL.2024.3525349>. This article provides a detailed review of power electronics solutions for ZEBs and offers strategies to address related challenges. By exploring the promising future of the low-voltage dc (LVdc) industry in ZEBs, it presents and compares grid connection scenarios and evaluates their overall efficiencies across hybrid, dc, and ac technologies. Furthermore, it addresses the integration of dc and ac systems in energy resources (ER), proposing solutions for challenges related to protection, grounding, and leakage currents. Finally, it examines the latest EMS solutions, emphasizing the shift to full digitalization through a combination of cloud-based and edge-computing platforms. Keywords: Photovoltaic systems, Renewable energy sources, Energy consumption, Low voltage, Reviews, Buildings, Standardization, Microgrids, Power electronics, Protection. Paper, indexed in Scopus Q2 Journal.

3. M. Azizi, O. Husev, O. Veligorskyi, M. Turzvínski and R. Strzelecki, "Dc Leakage Current in Isolated Grid-Connected dc Nanogrid - Origins and Elimination Methods," 2024 IEEE 18th International Conference on Compatibility, Power Electronics and Power Engineering (CPE-POWERENG), Gdynia, Poland, 2024, pp. 1-6, doi: <https://doi.org/10.1109/CPE-POWERENG60842.2024.10604426>. This study deals with the leakage current in the galvanically isolated dc nanogrid. Then, it examines the dc leakage current and its relationship with the dc nanogrid grounding and finally provides solutions to remove the dc components in the leakage current. Keywords: Grid-connected dc nanogrid, Isolation, grounding type, dc leakage current, capacitive grounding. Conference Paper, indexed in Scopus.
4. Azizi, M., Husev, O., Veligorskyi, O., Rahimpour, S., and Roncero-Clemente, C. (2023). Grounding and Isolation Requirements in DC Microgrids: Overview and Critical Analysis. *Energies*, 16(23), 7747. <https://doi.org/10.3390/en16237747>. Dc microgrids, along with existing ac grids, are a future trend in energy distribution systems. At the same time, many related issues are still undefined and unsolved. In particular, uncertainty prevails in isolation requirements between ac grids and novel microgrids as well as in the grounding approaches. This paper presents a critical technical analysis and an overview of possible grounding approaches in dc systems and the feasibility of avoiding isolation between ac and dc grids. Keywords: dc microgrids, isolation requirements, grounding approach. Journal paper, indexed in Scopus Q2.
5. M. Azizi, S. Rahimpour, O. Husev and O. Veligorskyi, "Back-to-Back Energy Router Based on Common-Ground Inverters," 2023 IEEE 17th International Conference on Compatibility, Power Electronics and Power Engineering (CPE-POWERENG), Tallinn, Estonia, 2023, pp. 1-6, <https://doi.org/10.1109/CPE-POWERENG58103.2023.10227480>. This paper proposes an energy router based on a back-to-back structure with common-ground inverters. Connecting the neutral wire of the ac system to the negative port of the dc link eliminates leakage currents and ensures safety. The operation mode of the common-ground inverter has been investigated, and the simulation results confirm the accuracy of the overall

structure and benefits compared to the classical H-bridge inverter. Keywords: Energy router, non-isolated, common-ground inverters, back-to-back structure. Keywords: Energy router, non-isolated, common-ground inverters, back-to-back structure. Conference paper, indexed in Scopus.

6. M. Azizi, O. Husev, D. Vinnikov and O. Veligorskyi, "Comparative Evaluation of Isolated dc-dc Converters for Low Power Applications," 2022 IEEE 20th International Power Electronics and Motion Control Conference (PEMC), Brasov, Romania, 2022, pp. 7-12, doi: <https://doi.org/10.1109/PEMC51159.2022.9962944>. This article examines and evaluates five popular types of isolated dc-dc converters for low-power applications. Using simulations, converters have been evaluated and compared from different perspectives. Keywords: Isolated dc-dc converters, Component design, Flyback, Forward, Push-pull, Full-bridge. Conference paper, indexed in Scopus.
7. M. Azizi, O. Husev, and D. Vinnikov, "Single-stage buck–boost inverters: A state-of-the-art survey," *Energies*, vol. 15, no. 5, p. 1622, Mar. 2022, doi: 10.3390/en15051622. In this paper, the state of the art of single-stage buck–boost inverters is discussed. The advantages and disadvantages of each structure are examined from different perspectives, such as the number of components, losses, and performance. Finally, in a general comparison, the properties of all structures are discussed and summarized in a table. Keywords: single-stage inverter; buck–boost operation; survey, Journal paper, indexed in Scopus Q2.

CONTENT

| | |
|--|----|
| LIST OF CONVENTIONAL ABBREVIATIONS | 14 |
| INTRODUCTION..... | 16 |
| 1 POWER ELECTRONICS SOLUTIONS FOR PV-INTEGRATED RESIDENTIAL BUILDINGS | 25 |
| 1.1 State of the art of power electronics for PV systems | 25 |
| 1.1.1 Protection measures | 28 |
| 1.1.2 Control system of energy router | 29 |
| 1.2 Dc-oriented future distribution network | 34 |
| 1.3 Possible configurations | 39 |
| 1.4 Conclusion..... | 42 |
| 2 DC SYSTEM INTEGRATION AND RELATED CHALLENGES | 44 |
| 2.1 Dc system integration..... | 44 |
| 2.2 Protection and safety in the dc microgrid | 46 |
| 2.3 Leakage current in dc systems | 49 |
| 2.3.1 Ac leakage current | 49 |
| 2.3.2 Dc leakage current | 51 |
| 2.4 Grounding in ac system..... | 53 |
| 2.4.1 Ac grounding type | 53 |
| 2.4.2 Ac grounding configurations | 54 |
| 2.5 Grounding in dc microgrids | 57 |
| 2.5.1 Grounding type | 58 |
| 2.5.2 Grounding configuration in dc microgrids | 60 |
| 2.6 Impact of grounding on the dc leakage current..... | 64 |
| 2.7 Grounding configuration for several decentralized sources | 65 |
| 2.8 Grounding in the connection point of the dc microgrid to the ac grid..... | 67 |
| 2.8.1 Isolated case | 68 |
| 2.8.2 Non-isolated case | 69 |
| 2.9 Conclusion..... | 71 |

| | | |
|-------|---|-----|
| 3 | PROPOSED HYBRID ENERGY ROUTER..... | 73 |
| 3.1 | Proposed structure | 73 |
| 3.2 | Inverter, modulation, and designing the passive element | 75 |
| 3.2.1 | Single-stage common-ground inverter | 75 |
| 3.2.2 | Inverter component design..... | 81 |
| 3.2.3 | dc-dc converters component design..... | 82 |
| 3.3 | Safety and protection..... | 83 |
| 3.4 | Solid-state circuit breaker..... | 84 |
| 3.5 | Conclusion..... | 86 |
| 4 | CONTROL SYSTEM | 87 |
| 4.1 | Proposed solution in low-level control | 87 |
| 4.1.1 | Theoretical foundation of the single-phase rotating dq reference frame transformation..... | 88 |
| 4.1.2 | Flat system | 90 |
| 4.1.3 | Dc-link voltage regulation | 93 |
| 4.1.4 | Inverter current control | 94 |
| 4.1.5 | Design process | 94 |
| 4.1.6 | PR controller as an alternative for the grid current controller | 96 |
| 4.2 | Possible high-level control and EMS | 99 |
| 4.2.1 | Simple local EMS | 99 |
| 4.2.2 | From distributed control to full Digitalization of EMS | 100 |
| 4.3 | Conclusion..... | 103 |
| 5 | SIMULATION AND EXPERIMENTAL VERIFICATION OF PROPOSED ENERGY ROUTER SOLUTION | 105 |
| 5.1 | Simulation results for the FBC solution in dynamic conditions | 106 |
| 5.1.1 | Step change in ac load (grid-forming) | 107 |
| 5.1.2 | Step change in dc load (grid-following) | 107 |
| 5.1.3 | Step changes in PV (grid-following) | 108 |
| 5.1.4 | Step change in the BSS reference current (grid-following) | 109 |
| 5.1.5 | Grid-side evaluation with FBC | 109 |

| | | |
|-------|--|-----|
| 5.1.6 | Grid-side evaluation with PR controller | 110 |
| 5.2 | Experimental verification | 111 |
| 5.2.1 | Dc-mode | 114 |
| 5.2.2 | Grid-forming mode | 115 |
| 5.2.3 | Grid-following mode | 116 |
| 5.2.4 | Dynamic conditions | 117 |
| 5.3 | Conclusion | 119 |
| 6 | CONCLUSION | 121 |
| 7 | REFERENCES | 124 |
| | APPENDIX A List of publications of the applicant | 146 |
| | APPENDIX B | 150 |

LIST OF CONVENTIONAL ABBREVIATIONS

| | | |
|-------|---|----------------------------------|
| RES | – | Renewable energy source |
| PV | – | Photovoltaic |
| NZEB | – | Nearly-zero energy building |
| ZEB | – | Zero emission building |
| LVdc | – | Low-voltage direct current |
| MPPT | – | Maximum power point tracking |
| ER | – | Energy router |
| API | – | Adaptive proportional integrator |
| FLC | – | Fuzzy logic control |
| MPC | – | Model predictive control |
| SMC | – | Sliding mode control |
| FBC | – | Flatness-based control |
| SoC | – | State of charge |
| PR | – | Proportional resonant |
| PLL | – | Phase-lock-loop |
| ANN | – | Artificial neural network |
| MPPT | – | Maximum power point tracking |
| B2B | – | Back-to-back |
| EMS | – | Energy management system |
| RCD | – | Residual current device |
| ELV | – | Extra low voltage |
| CMV | – | Common-mode voltage |
| PE | – | Protective earth |
| HRG | – | High-resistance ground |
| BSS | – | Battery storage system |
| SC-TP | – | Single-cell three-phase |
| SC | – | Single cell |
| SSCB | – | Solid-state circuit breaker |
| DCCB | – | Direct current circuit breaker |

| | | |
|--------|---|---|
| SCR | – | Silicon controlled rectifiers |
| MOV | – | Metal oxide varistor |
| MOSFET | – | Metal-oxide-semiconductor field-effect transistor |
| IoT | – | Internet of Things |
| CCP | – | Cloud computing platform |
| ECP | – | Edge computing platform |
| THD | – | Total harmonic distortion |

INTRODUCTION

Justification of the choice of research topic. With the increasing utilization of renewable energy and the development of zero-emission building (ZEB) concepts and the move towards dc or hybrid systems, the development of interface converters between dc buildings and ac grids is crucial. While the way to decrease cost, weight, and volume is always open, existing structures face challenges in terms of supplying dc loads and ensuring the safety of personnel and equipment at the connection point of the dc system to the ac grid. On the other hand, considering the connection of different sources and loads in this interface converter, improving the control system to manage loads and dynamic conditions is another important aspect of this study.

Energy supply has always been a critical issue of concern for governments. In the last few years, the combined challenges of the supply gas crisis to power plants and the increase in electricity demand, following the removal of the restrictions of Covid-19, have caused a significant increase in the price of electricity. On the other hand, energy production from clean and renewable energy sources (RES) has become crucial due to environmental reasons and the need to reduce greenhouse gases. While many countries incorporated the production of electricity from RES into their general policies and numerous renewable power plants have been built, a significant part of the electricity generated is still produced by combustion power plants. According to recent statistics, for the contribution of different sources of electricity generation in the EU, nearly 40% of the produced electricity comes from combustion plants, while wind plants provide nearly 16% and solar plants only account for 7% [1]. Fig. 1 illustrates the electricity production share from various sources and the solar energy share in the utility-scale and rooftop sectors for EU countries [1]. In 2023, the share of solar power was close to 263 GW, 66% of which was produced in the rooftop sector [2].

Along with the increase in photovoltaic (PV) installed in the distribution network, battery storage systems (BSS) have also faced significant growth for grid-independent operations. According to Solar Power Europe statistics, the annual capacity growth of BSSs in 2023 has reached 17.2GWh, with a 94% growth compared to 2022 [3].

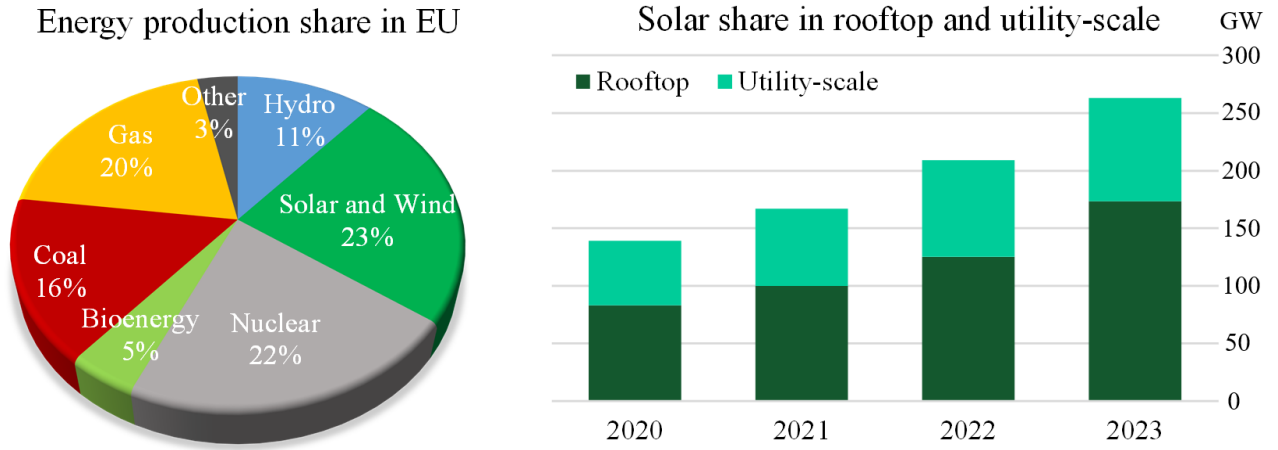


Fig. 1 Energy production and solar shares at utility-scale and rooftop parts from 2020 to 2023 in the EU.

In 2022, the European Union adopted a roadmap to accelerate solar energy strategies [4], specifically aiming to require rooftop solar on all new buildings. Therefore, dealing with small-scale solar power plants and providing solutions to improve efficiency and performance becomes particularly crucial.

Residential or industrial units equipped with PV and storage systems in the distribution sector not only contribute effectively to electricity production but also offer uninterrupted power supply capabilities, along with bringing economic benefits to the owners of these small-scale power plants. Therefore, such solutions fully accomplish the Nearly-Zero Energy Buildings (NZEBs) [5] and ZEB concepts [6].

At the same time, electric energy consumption is rising much faster than predicted energy generation. The electrification of public and private transportation exacerbates the problem. Considering the unpredictable nature of RESs, grid congestion is unavoidable in most developed countries without increasing grid capacity and the adoption of smart energy management systems (EMS). In this context, with the development of control methods and the application of management strategies, the new intelligent and integrated power electronics interface, often called the energy router (ER), is needed.

This thesis first reviews the current power electronics solutions for ZEBs and analyzes different scenarios of dc system integration. Given the importance of protection and safety, it comprehensively examines the dc system, grounding, and leakage currents at the point where the dc system connects to the ac grid. Analyzing different

configurations and connection scenarios and protection levels, this work proposes using an ER structure based on a common-ground inverter. Having the same ground on both dc and ac sides eliminates leakage currents and provides safety criteria in dc nanogrid. The proposed ER is a single-cell three-phase (SC-TP) type, which allows access to all three phases and phase balancing through a smart EMS. The proposed structure not only enhances PV self-consumption and reduces phase unbalance compared to single-phase systems but also offers significant cost advantages relative to the three-cell three-phase architecture. Control strategies at different levels are analyzed, and then an effective solution in low-level control is applied to enhance the dc-link robustness in dynamic conditions. Unlike conventional control methods that may halt system operation for protection during severe dynamic disturbances, the proposed method delivers a precise and fast control response, thereby significantly enhancing system reliability. Finally, the simulation and experimental results validate the operation of this structure and the control solution.

The connection of the work with scientific programs, plans, topics, and grants.

The doctoral research presented in this thesis, which focuses on the design and implementation of a power electronic converter enabling the integration of BSS with PV generation at the residential scale, is closely aligned with the strategic priorities of the European Union in the fields of energy transition, sustainability, and technological innovation.

First, the work directly addresses the objectives of the European Green Deal, particularly the decarbonization of the energy system and the large-scale deployment of renewable energy sources. By enabling the efficient coupling of photovoltaic generation with residential battery storage, the proposed solution contributes to enhancing self-consumption, reducing greenhouse gas emissions, and lowering the dependence on fossil fuels in the domestic sector.

Moreover, the research aligns with the goals of the Horizon Europe framework program, particularly within the thematic clusters related to Climate, Energy, and Mobility. The proposed converter technology supports the integration of distributed renewable generation and storage, contributing to improved system efficiency, enhanced

grid flexibility, and greater resilience, key enablers for the modernization of the European energy infrastructure.

In addition, the thesis aligns with the EU's strategy on the digitalization of the energy sector, as advanced power electronic interfaces facilitate active demand-side management and dynamic interaction with the grid. Such functionalities create opportunities for the development of local energy communities and foster greater citizen participation in the energy market, both of which are central elements of the Union's vision for a sustainable and decentralized energy system.

Overall, the contributions of this doctoral work resonate with several of the EU's priority thematic areas, including:

- The transition towards a climate-neutral energy system.
- The promotion of distributed renewable generation and energy storage solutions.
- The improvement of energy efficiency and sustainability in the residential sector.
- The advancement of technological innovation in power electronics applied to renewable integration.

In this context, the outcomes of the research represent not only a scientific and technological contribution but also a tangible step in support of the European Union's overarching strategies for a cleaner, more decentralized, and resilient energy future.

This project has received funding from the European Union's Framework Program for Research and Innovation Horizon 2020 (2014–2020) under the Marie Skłodowska-Curie Grant Agreement No. 955614.

Additional support for this PhD was provided by the Grant PID2022-137345OA-I00, funded by MCIN/AEI/10.13039/501100011033 and co-financed by the European Regional Development Fund (ERDF) under the slogan 'A way of making Europe'.

The purpose and objectives of the study.

The objective of the study is to develop an ER for a hybrid nanogrid or building that not only solves challenges of the previous ER in literature, but also improves and proposes new features that ultimately lead to higher reliability, efficiency, and protection. This goal was implemented by reviewing, analyzing, comparing, calculating,

substantiating, modeling, and implementing a set of scientific and practical technical and software methods and tools.

Solving the scientific problem set in the dissertation includes solving the following set of problems:

1. While ensuring the required safety and protection, a non-isolated structure is proposed, which offers reduced volume, weight, and cost by eliminating the isolation transformer.
2. Although using isolation between the ac grid and the dc nanogrid does not completely suppress leakage currents, the proposed structure effectively eliminates them by establishing a common ground for both ac and dc sides.
3. Considering the growing expansion of dc nano/microgrids, the implementation of appropriate grounding systems is essential to ensure the protection of both personnel and equipment. Unlike previous studies and conventional structures, which often overlook comprehensive protection strategies in the dc link, this study investigates and applies effective grounding techniques. Various connection scenarios and tailored grounding methods are analyzed to provide reliable protection on both the ac and dc sides.
4. Unlike conventional architectures that employ a single-cell configuration for single-phase systems and a three-cell design for three-phase systems, the proposed structure adopts a single-cell approach for three-phase operation. This configuration enables dynamic phase selection, contributing to grid balancing and offering considerable economic advantages by reducing hardware complexity and cost.
5. Conventional structures typically rely on classical control methods at the low-level control stage, which often exhibit sluggish performance under dynamic conditions. The limited responsiveness of these controllers during significant transients may trigger protective shutdowns. In this thesis, the flatness-based control (FBC) method is selected to enhance dynamic performance. Despite requiring relatively low computational effort, the proposed approach

demonstrates notable improvements in dynamic response and significantly enhances the overall reliability of the system.

The objective of the study is to realize an ER for hybrid nanogrids or ZEBs that not only solves challenges of the previous prototype but also improves and proposes new features that ultimately lead to higher reliability, efficiency, and protection.

The subject of research is an energy router for hybrid microgrids for efficient and robust energy and power management.

Research methods. When solving the problems set in the dissertation, the study and discussion of research literature, the theory of electrical and electronic circuits, average modeling, control system design and tuning, simulation tools, and physical experiments were used.

Mathematical modeling and calculations of processes in the hybrid ER were performed using MATLAB, PSIM and PLECS software packages; design of the printed circuit board was carried out by Altium Designer, and software development was performed in Code Composer Studio.

Mathematical and computer modeling were used to verify the proposed structure and control solutions. Computer modeling was generally performed in the PLECS and MATLAB software packages, which are available in the project implementing organization in the form of licensed or limited versions. The proposed control method was compared with conventional solutions using simulation in PLECS. Final proof of the effectiveness of the proposed solutions was determined based on experimental studies. The proposed structure was designed, assembled, and then experimental tests were performed in the laboratory to validate the control method under general and dynamic conditions.

Scientific novelty of the obtained results:

1. Different types of ER topologies as interlink solutions between dc systems and ac grid were investigated, and an ER topology based on the SC-TP concept is developed. The proposed approach helps mitigate phase imbalance, offering economic advantages by eliminating the need for two additional conversion cells.

2. A comprehensive study analyzing grounding and leakage currents at the connection point of an isolated dc system to ac grid was performed. It was first time demonstrated, that in some specific cases, the isolation itself is not enough for dc leakage current elimination. It is recommended to equalize the potential between dc middle point and ac neutral point.

3. For the first time, it is demonstrated that a non-isolated ER based on a common-ground inverter can act as an interlink solution between residential dc and ac grids and can be connected to the residential ac system using special grounding and classical protection scheme.

4. FBC theory was for the first time applied to the ER to improve control response in dynamic conditions and enhance the reliability level of the multiport ER. While conventional methods have a relatively slow response in dynamic conditions, which may trip the protection system, FBC provides a very fast and robust response in these conditions.

Practical significance of the results obtained:

1. Different tests, including dc-mode, grid-forming and grid-following approaches, were conducted. In the case of the connection of PV and battery, energy flow was checked based on the proposed EMS. These tests were done at different power levels and different dc and ac load conditions to check the reliability of the system. Oscillogram results were captured to be used in the thesis and related publications.

2. FBC theory was applied to enhance control response in dynamic conditions. An attempt was made to reach the best coefficients for the best responses in dynamic conditions, such as a huge step change in loads. Oscillogram results obtained for these cases prove the significant contribution of this work.

3. The results of the research obtained during the project can be used in the educational process to improve lecture courses and update laboratory work cycles in the disciplines "Foreign language for professional purposes" (specialty 141 Electrical power engineering, electrical engineering and electromechanics", educational and qualification level "Master") and "Modern electricity generation and distribution systems", "Electrical energy converters for renewable energy systems" (specialty 141 "Electrical power

engineering, electrical engineering and electromechanics"), educational and scientific level "Doctor of Philosophy".

Personal contribution of the applicant. The author directly carried out:

- Reviewing the existing structure of ERs and analyzing their performance in different modes and safety conditions.
 - Comparative analysis of different isolated dc-dc converters for low-power applications to be used in the overall ER structure.
 - Comparative analysis for different scenarios of NZEB connection to the ac grid.
 - Development of the simulation model in PLECS software to analyze the open-loop and closed-loop operation, as well as the control system at different levels.
 - Studying, modeling and simulating common-ground structures to be used in the general structure of the ER to enhance safety.
 - Analyzing and applying modulation techniques for the common-grounded inverter in ERER for an accurate operation in boost, buck and buck-boost modes.
 - Reviewing and analyzing dc and ac leakage current and grounding type and configurations in dc and ac systems.
 - Analyzing and modeling different scenarios for connecting dc and hybrid NZEB to the ac grid, regarding safety issues in both dc and ac sides.
 - Analyzing and simulating dc leakage current in the isolated connection of the ER to ac grid.
 - Proposing and tuning of the control system based on FBC theory in ER simulation to enhance control response in dynamic conditions.
 - Assembling the experimental setup to analyze the general open-loop operation of different parts and converters in the ER system.
 - Running experimental tests for different operation modes, including dc-mode, grid-forming, and grid following, as well as dynamic conditions of step changes in loads.
- Scientific works published in co-authorship with O. Husev, O. Veligorsky, C.R. Clemente, S. Rahimpour, as well as with Professors R. Strzelecki, D. Vinnikov, J. Martins, and E. Monmasson.

Co-authors of scientific works are the scientific supervisor, O. Husev, and the scientists with whom the research was conducted. In scientific works published in co-authorship, the doctoral candidate owns the factual material and the main creative work.

Setting the goal and objectives, and discussing the results, were carried out together with the scientific supervisor.

Approval of the results of the dissertation. The main provisions of the dissertation were reported and discussed at four international scientific and technical conferences, namely:

- 20th International Power Electronics and Motion Control Conference (PEMC) IEEE 2022 (Brasov, Romania) 25-28 September 2022.
- 17th International Conference on Compatibility, Power Electronics and Power Engineering (CPE-PowerENG) 2023 (Tallinn, Estonia), 14-16 June 2023.
- 18th International Conference on Compatibility, Power Electronics and Power Engineering (CPE-PowerENG) 2024 (Gdynia, Poland), 24-26 June 2024.
- 19th International Conference on Compatibility, Power Electronics and Power Engineering (CPE-PowerENG) 2024 (Antalya, Turkey), 20-22 May 2025.

Thesis scope and structure. The dissertation is presented on 150 pages of typewritten text, consists of an introduction, five chapters, general conclusions, a list of sources used, and 1 appendix. The main text of the dissertation is 128 pages of printed text. The work is illustrated with 13 tables and 57 figures. The list of sources used contains 169 references.

1 POWER ELECTRONICS SOLUTIONS FOR PV-INTEGRATED RESIDENTIAL BUILDINGS

1.1 State of the art of power electronics for PV systems

The increasing integration of PV systems and energy storage solutions in residential buildings, coupled with the new trends in PV-integrated energy communities, has led to the development of various power electronics devices and energy management systems (EMSs). During the last few decades, solar inverters have been used to supply buildings and inject solar power into the grid [7]. Within the past few decades, companies like SMA, Fronius, Growatt, etc. have produced solar inverters in different power ranges for single-phase and three-phase grid connections. In these inverters, the focus has been more on the number of maximum power point trackings (MPPTs) and the overall efficiency.

Considering the importance of reliability and a constant supply of electricity, hybrid inverters were introduced, offering the option of integrating a storage system through their dc-link. In primary models of hybrid inverters and certain current products (Voltronic Axpert VP 3000 24V), the storage system lacks intelligent functionality and operates independently. In contrast, the latest generation of hybrid inverters from companies such as SMA (Sunny Boy) and Growatt integrate seamlessly with EMSs. These advanced inverters not only optimize energy usage but also provide intelligent management of loads and storage systems through dedicated applications, which ultimately leads to increased economic efficiency [8].

In recent years, focusing on storage and backup during power grid blackouts, Powerwall systems have entered the market. In its newest version, it is also equipped with a solar inverter and has the concept of all-in-one. This smart structure also has the ability to control and monitor the stored energy, load consumption, and PV system production via the developed application. Fig. 1.1 shows these technologies for ZEBs.

At the same time, all devices available on the market do not provide smart functionality, and smart meters are required for energy-flow monitoring [9]. With the advancement of power electronic converters and intelligent control methods, including

optimization capabilities, the Energy Router (ER) title was given to the future smart structures. An ER is an advanced power electronic interface designed not only to convert power between ac and dc, but also to manage and route energy flows among multiple sources, storage units, and loads. Unlike conventional PV inverters, which only convert solar dc to grid-synchronized ac, and hybrid inverters, which combine solar and battery management, the ER acts as a central hub enabling coordinated control, optimal utilization, and intelligent energy distribution in modern power systems. Fig. 1.2 illustrates an ER system and its wireless communication. As can be seen, different parts send data to the ER and based on the EMS, energy routing will be done between different parts.

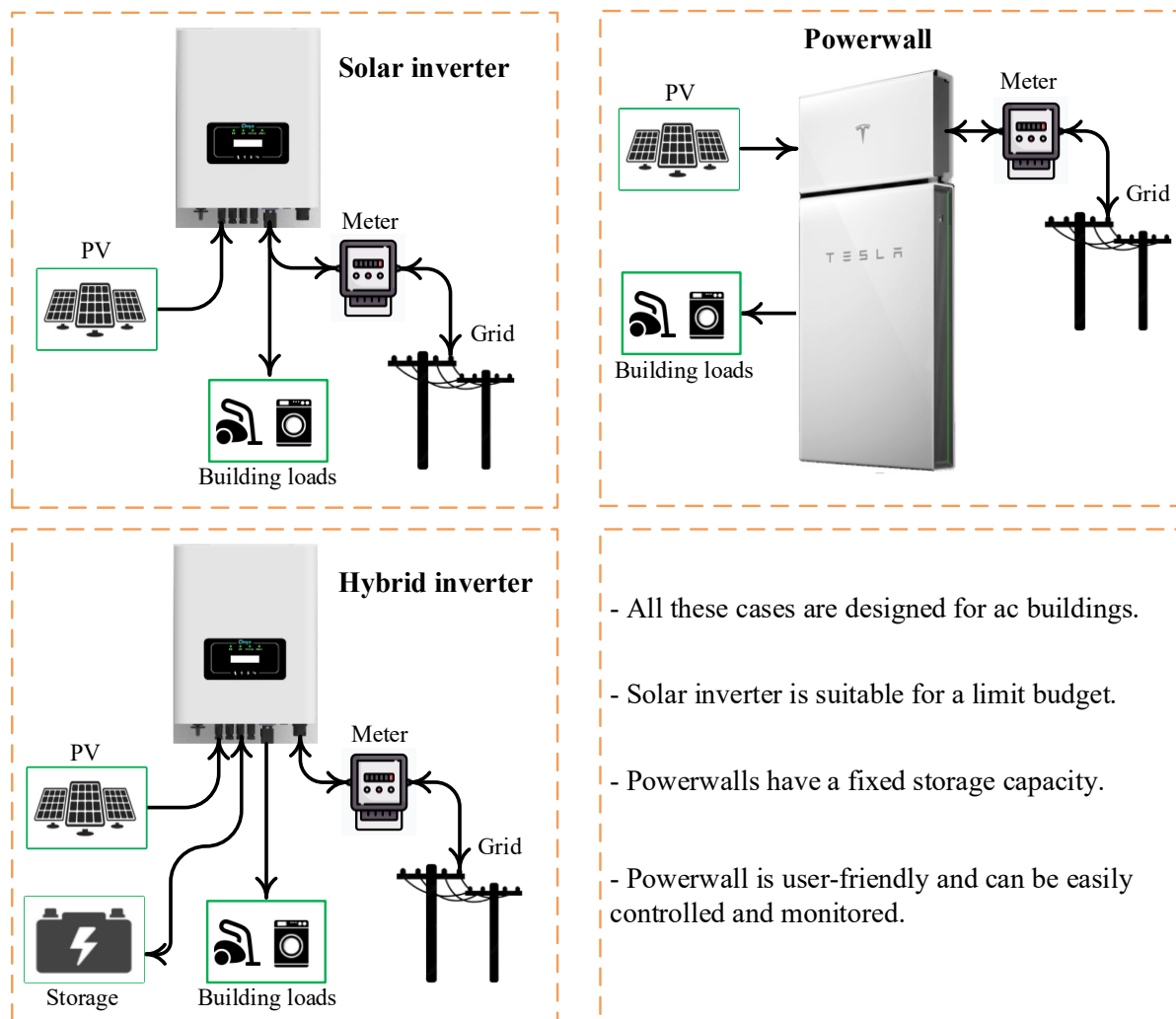


Fig. 1.1 Latest technologies for residential buildings equipped with PV and storage systems.

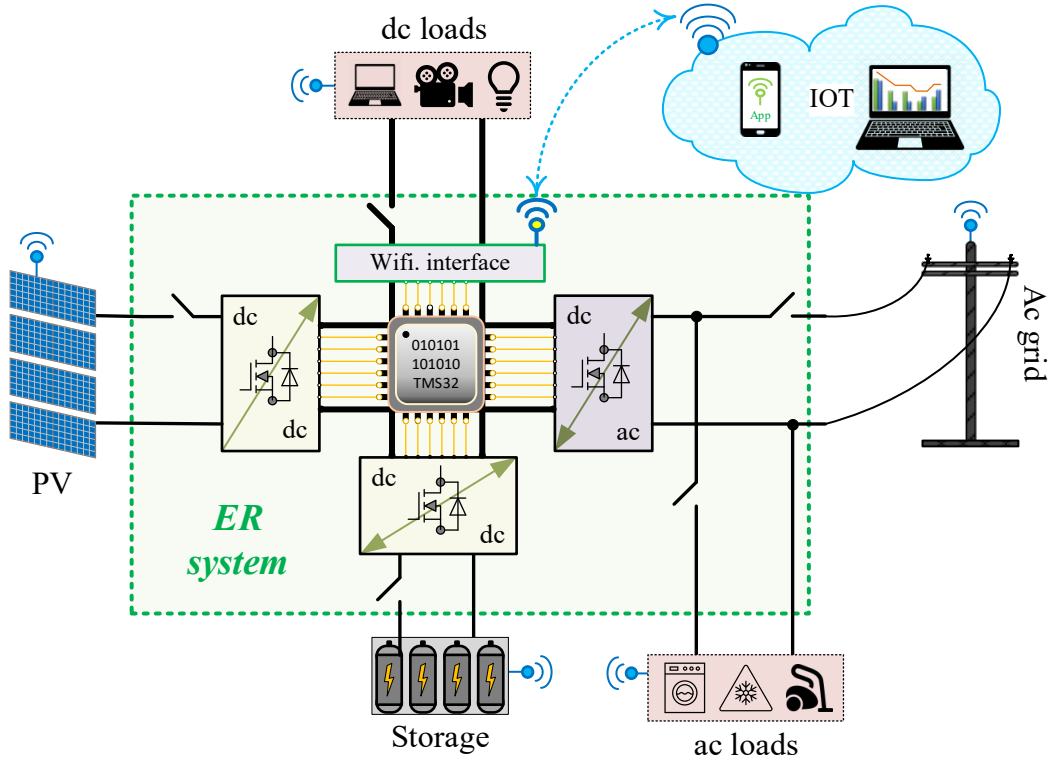


Fig. 1.2 General structure of an ER system and its wireless communication.

Over the past decade, the ER concept has evolved through various perspectives. While numerous studies have emphasized high-level control approaches and the development of efficient EMS tailored for conventional ER configurations [10]-[16], other research efforts have focused on proposing alternative ER architectures. These architectures differ primarily in terms of galvanic isolation, single-phase versus three-phase design, circuit topology, and their ability to supply dc loads. For instance, in [17], a back-to-back (B2B) structure is suggested, which utilizes two inverters: one for supplying ac loads and one to interact with the grid. These recent studies primarily address the issue of energy optimization and management, and occasionally introduce new structures. However, an ER comes with issues related to protection, safety, and energy management. Galvanic isolation or special topology should be used to eliminate leakage current. Grounding and other protections should also be implemented on both the dc and ac sides to prevent electric shock and damage to equipment. A non-isolated three-phase multiport ER with dc load supply capability is presented in [18], where a comprehensive multi-level control strategy is proposed with an emphasis on battery management.

However, critical aspects such as safety and grounding are not discussed. In contrast, [19] introduces an isolated three-phase ER for high power applications, employing a cascaded configuration, where power balance across different subsystems is analyzed. Nonetheless, this study lacks the ability to supply dc loads or establish connections with other dc nanogrids.

The transition toward dc or hybrid architectures has received increasing attention in recent years. This growing interest is largely attributed to the intrinsic advantages of dc systems, including the elimination of synchronization and the absence of reactive power issues. As a result, dc-adaptive topologies have emerged as promising solutions, particularly due to their high compatibility with PV and BSS, thereby enabling improved overall efficiency. A substantial body of research has been dedicated to evaluating efficiency improvements and addressing the technical challenges associated with dc systems [20],[21]. One major research focus involves the design and implementation of Direct current circuit breakers (DCCBs) with various topological configurations, driven by the lack of a natural current zero-crossing, which complicates interruption mechanisms [22].

1.1.1 Protection measures

Since an ER has a dc link to supply dc loads or connect to other dc nanogrids, it is essential to protect the dc link from short-circuits and provide an effective solution for the timely interruption of the fault current. Considering the absence of a zero-crossing point in the dc system and the high current increase ratio in the event of a fault, it is essential to use an efficient and highly reliable structure. In recent years, dc microgrids have received attention and various structures have been proposed for DCCBs [23],[24]. DCCBs are generally divided into three categories: Electromechanical, Solid-state, and Hybrid. The operation of the electromechanical structure is associated with the creation of an arc and a relatively low interruption speed. The low speed of operation in this structure causes the loss of circuit components (switches, etc.), and the arc created also causes corrosion of the conductors [25].

To increase the speed of operation in recent years, solid-state DCCBs have been proposed. This type of circuit breaker is itself divided into two types: semi-controlled devices, such as silicon controlled rectifiers (SCRs) [26],[27] and fully controlled switching devices such as IGBTs and MOSFETs [28]. The characteristics of each of these structures are found in detail in [22]. The hybrid structure is also the result of combining the electromechanical structure with the solid-state. The hybrid structure has lower losses than the electromechanical structures, but still has disadvantages such as low operating speed and high cost. A review and comparison of different technologies can be found in [29]. The DCCB used in the ER of this work is of the solid-state type, introduced in [22], which is accompanied by a higher reliability and safety level.

Additionally, in efforts to improve safety and grounding performance, the use of common-ground inverters has gained significant traction as an effective approach to mitigate leakage current issues, especially in PV-based applications [20]-[30]. Common-ground inverters provide a common ground for both the dc source and ac output to eliminate the leakage current induced by the parasitic capacitance. Among the different studies, it was found that the topology introduced in [31] has a higher reliability and lower voltage stress on semiconductor devices, and it was used for the proposed ER structure in this work.

1.1.2 Control system of energy router

Along with the structural layout, the control system of ER at different levels is also a topic of much research. Fig. 1.3 shows the simplified sketch of the classical control system of the ER. The ER's control system includes different levels. As can be seen, high-level control is responsible for EMS, determining reference values based on provided information on consumption levels and the state of charge (SoC) of BSS. EMS can be local (simple rule-based) or cloud-based, incorporating advanced communication and optimization algorithms. The control of dc-dc converters for the PV and BSS is at mid-levels and uses PI controllers and reference values to regulate the power flow of PV and BSS. In mid-level, the PV and BSS reference currents are set based on the grid connection state, through the dc-link voltage error and an outer PI controller, or by EMS at a higher

level. Once the reference values (I_{PV}^* and I_{BSS}^*) are obtained, they will be compared to the corresponding reference currents, and then the error will be sent to the inner PI controllers to produce modulation signals. Low-level control handles the grid current, regulates dc link voltage and grid synchronization. In low-level control, a PI outer control loop along with a Phase Lock Loop (PLL) sets the grid reference current (i_g^*) to regulate dc link voltage, and the i_g^* is compared to i_g in an inner loop, and the error is sent to another PI or a proportional resonance (PR) controller in dq frame to produce a modulation reference voltage and control the grid current.

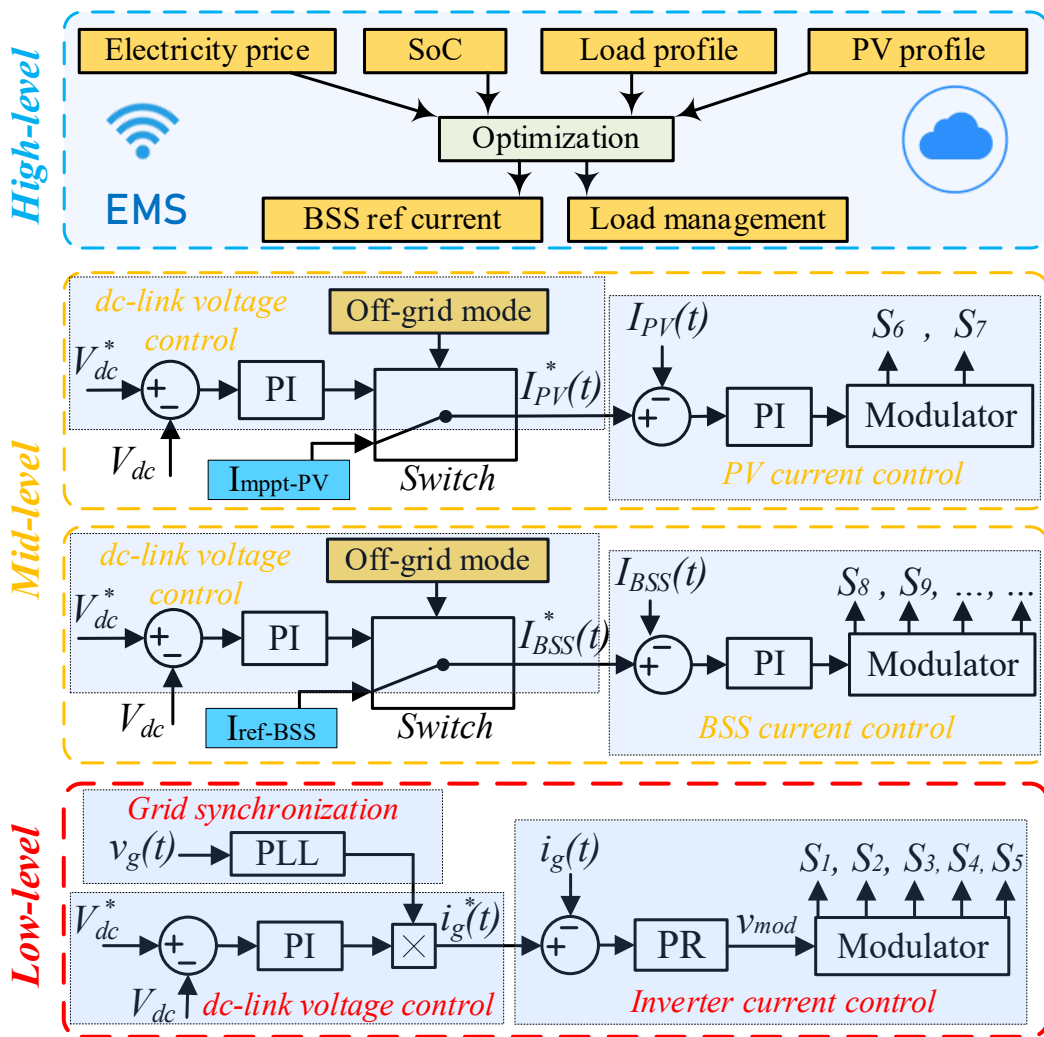


Fig. 1.3. The simplified block diagram of the classical control strategy of ER for different control levels.

In low and mid-level control, classical control strategies are primarily used and designed to regulate the dc-link and manage power exchange with the grid. While these

methods demonstrate acceptable performance, they often exhibit relatively slow dynamic responses [323232]. An ER integrates multiple sources and loads through a common dc link, where any dynamic disturbance in one component can affect the entire system or even trigger protection mechanisms and interrupt operation. Therefore, a robust control strategy with fast dynamic response is essential to ensure stable operation and enhance system reliability.

To enhance system response in dynamic conditions, various solutions have been proposed in studies. For instance, adaptive PI controllers (APIs) dynamically adjust parameters based on operating conditions, improving system performance under uncertainties [33]. However, they introduce higher design complexity and difficulties in defining adaptive tuning rules. Another approach to improve dynamic response is fuzzy logic control (FLC). This method particularly benefits nonlinear systems, offering high flexibility and independence from an accurate system model [34]. Nevertheless, its effectiveness is highly dependent on the design of rule sets, and its optimality cannot always be guaranteed, leading to performance uncertainties. Model predictive control (MPC) has also been widely investigated [16], [35], [36]. While MPC can handle multi-variable systems and constraints efficiently, it demands high computational power, complex tuning procedures, and an accurate system model to ensure precision and stability. Reference [36] integrates an MPC controller with an artificial neural network (ANN), where the ANN is employed as the internal current controller to alleviate the computational burden of MPC. Fig. 1.4 illustrates the general block diagram of this approach. Although this method reduces the computational demand to some extent, it still results in a relatively complex control structure with significant mathematical computations.

In addition to these methods, sliding mode control (SMC) and other nonlinear control techniques have been explored in various studies [37], [38]. While SMC is robust and has a fast dynamic response, the practical implementation is complex due to high-frequency oscillations near the sliding surface. Therefore, as it is clear, each solution presents unique advantages and drawbacks, requiring a trade-off between performance, complexity, and implementation feasibility, depending on the specific application.

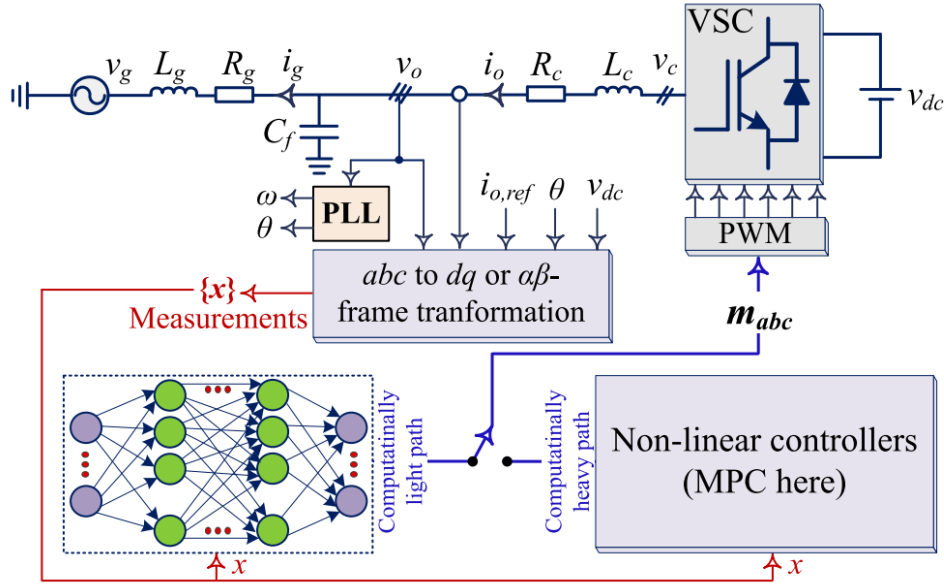


Fig. 1.4. Block diagram of the MPC-based control strategy used in [28].

Among the control methods suitable for dynamic conditions and nonlinear systems, FBC theory has been introduced as a fast and reliable solution in dynamic conditions [39]. This control method, initially introduced by M. Fliess, demonstrates excellent performance in managing nonlinear systems and provides robust capabilities for systems with multiple state variables and inputs. Therefore, it can be a promising control solution for ER where there are multiple power sources and sinks.

On High-level control, when it comes to EMS, different strategies can be adopted [45]. The commonly used method for power sharing in microgrids is droop control. A similar approach can be defined for the ER. Ideally, power can be distributed proportionally according to a specific droop coefficient without using communication. This plug-and-play solution is reliable, low-cost, and easy to expand. It remains the preferred control method for many power electronics researchers [46]. However, droop control involves several issues such as impedance dependency, inaccurate power sharing, and low transient response [47], [48].

Consequently, variants of the conventional droop control have been proposed to address some of these problems: adaptive droop control [49], [50], robust droop control [51], and neural network droop-based control [52]. The latter collects input and output data for training to develop the droop-based controller. In one variant [53], the voltage

droop controller is combined with a secondary communication-based controller in order to improve control performance. The set points for secondary control can be determined based on an optimization scheme.

To achieve multiple control objectives, a distributed hierarchical control paradigm consisting of two or three levels has become a standard solution for dc microgrids [54]. The primary level is a local droop-based controller. For higher-level controllers, low-bandwidth communication links are commonly used for data transmission [55]. The consensus algorithm is often applied since it facilitates the information synthesis and aggregation among a set of distributed agents [56]. Optimization methods can be implemented at the tertiary level to improve the system's efficiency [57].

Yet, distributed control (whether hierarchical or not) cannot guarantee the optimization of the power flow from an economic point of view. An overall optimization requires centralized communication, data acquisition, computation, and management. The first step in full digitalization is monitoring and measuring production, storage, and consumption, and then sending this information to a centralized EMS. Nowadays, with the increase of full digitalization in new buildings and the connection of all parts to a central system, the initial investment to implement a fully centralized control is no longer an issue. In addition, most centralized EMSs are cloud-based. In fact, the use of the cloud plays a significant role by providing a flexible and scalable platform for managing, analyzing, and storing the large amount of information produced by energy sources, storage devices, and loads, in addition to the high computational capacities. Furthermore, the stored data can be used for prediction or to train models based on machine learning. Thus, the cloud-based EMS structure is an accurate, fast, efficient and cost-effective tool for powering smart buildings or microgrids. The proposed EMS for ER in this work introduces a hybrid and reliable solution based on a cloud and edge computing platform to reach a very optimized EMS.

Following the above-reviewed literature, some other studies around ER are listed in Table 1.1. This table summarizes and compares ER features in different aspects, including the structure, isolation and EMS.

Table 1.1

Several studies around ER

| Ref. | Structure | Loading | Power | Energy management system | Safety & Isolation |
|------|---------------------------|-----------------------------|-------|--|--|
| [9] | Hybrid | Ac loads at PCC. | 1 kW | Smart Community EMS which works Based on optimization algorithms considering SoC, weather forecasts, energy prices, load profiles, etc. | Low-frequency isolation. Grounding and safety are not discussed. |
| [10] | Multiport | Ac and dc loads feed by ER. | 6 kW | Hierarchical management control strategy based on decentralized module control and power dispatch control. | Non-isolated. Grounding and safety are not discussed. |
| [11] | Multiport | Ac and dc loads. | 30 kW | Constant current/voltage control or fuzzy control is recruited for the storage system. | High-frequency isolation for dc loads and dc microgrid connection. |
| [12] | 3Ph B2B | Ac and dc loads. | 5 kW | Fuzzy logic is used for battery charging/discharging. | Non-isolated. Grounding and safety are not discussed. |
| [18] | 3Ph B2B | Ac and dc loads feed by ER. | 30 kW | Fuzzy logic is used to control the current of the storage system to ensure reliable operation, economical uses, and increased battery life. | Non-isolated. Grounding and safety are not addressed. |
| [40] | Multiport | Ac and dc loads. | 12 kW | Fuzzy logic-based hierarchical control strategy. | Non-isolated. Grounding and safety are not discussed. |
| [41] | B2B | Ac loads feed by ER. | 3.6kW | EMS is not discussed. Focus is on Model Predictive Control for the load-side inverter. | Non-isolated. Grounding and safety are not discussed. |
| [42] | - | Ac loads. | 8 kW | Fuzzy logic with 3 inputs of electricity price, SoC, and net power, and then by forecasting production and price the optimization problem is solved. | Isolation, grounding, and safety are not discussed. |
| [43] | Multiport | Ac and dc loads feed by ER. | - | Hierarchical management system with a hybrid communication method. | Isolation, grounding, and safety are not discussed. |
| [44] | cascaded H-bridge and DAB | Ac and dc loads. | 5 kW | EMS based on the power imbalance theory. | High-frequency isolation. Grounding and safety are not discussed. |

1.2 Dc-oriented future distribution network

In addition to control systems and EMS, the projected rise in energy demand necessitates the expansion of grid capacity. One prominent research direction in recent

years has been the transition toward low-voltage dc (LVdc) distribution networks, driven by the inherent dc characteristics of PV systems, energy storage solutions, and the increasing prevalence of dc loads [58]. Fig. 1.5 illustrates a conceptual vision of the future grid, where LVdc networks operate in parallel with the existing ac infrastructure. As depicted, the distribution network accommodates conventional ac buildings alongside hybrid and fully dc-enabled buildings. The coexistence of both dc and ac wiring aims to reduce power conversion stages, thereby enhancing overall system efficiency.

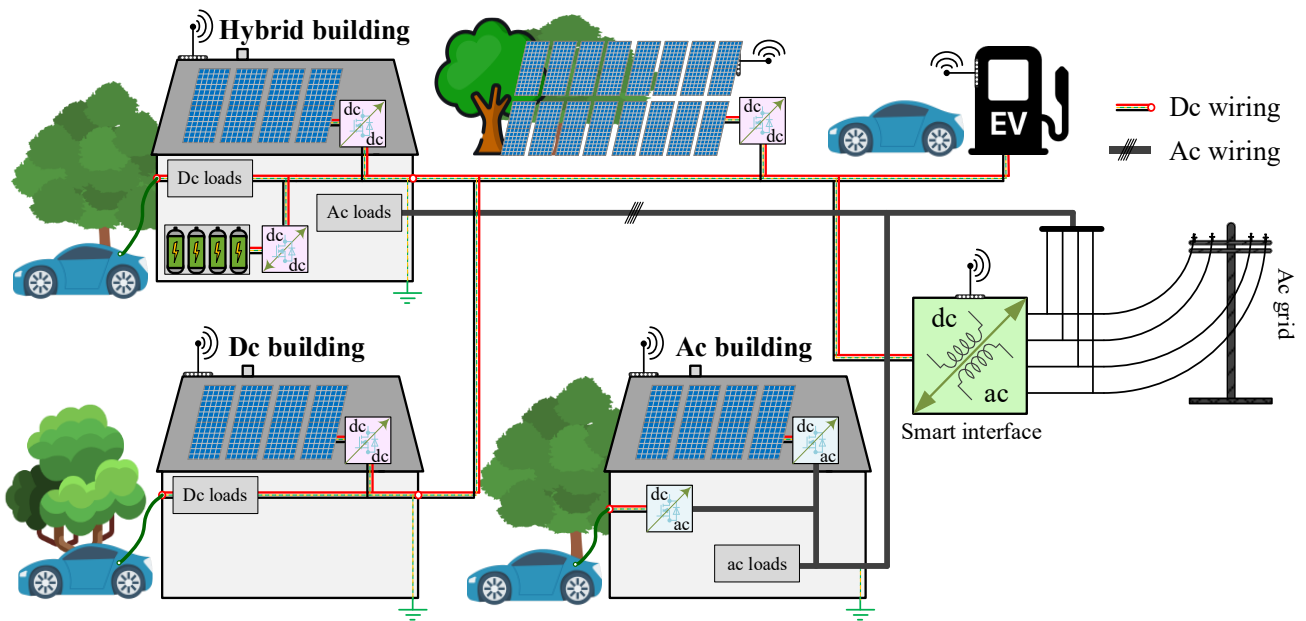


Fig. 1.5 Future energy distribution system with the integration of dc system.

In this context, evaluating the performance of various hybrid ac/dc system configurations is essential. Table 1.2 presents a comparison of the maximum achievable efficiencies of different power converters used in ac and dc distribution networks, as reported in [59]. According to the study, dc-dc employed LVdc systems can achieve efficiencies as high as 99%. In contrast, the maximum efficiency of dc-ac and ac-dc converters typically used in conventional ac grids is generally limited to 97% and 95%, respectively, occasionally reaching up to 98% at the expense of increased cost and complexity. Therefore, moving towards dc system in PV-integrated buildings and using dc-dc converters will lead to higher overall efficiency.

Table 1.2

Maximum achievable efficiency in different converters for LVdc nanogrid

| Type of converter | Techniques | Maximum achievable Efficiency | Power range [kW] | Reference |
|-------------------|------------------------|-------------------------------|------------------|------------|
| dc-dc | Resonance | 98% | 0.1 - 10 | [60], [61] |
| dc-dc | Dual-Phase-Shift | 99% | 0.3 -15 | [62], [63] |
| dc-ac | Resonant | 97% | 0.6 - 6 | [64] |
| ac-dc | Active devices | 98% | 1 - 3 | [65] |
| ac-dc | Passive devices | 95% | 0.1 - 5 | [66] |
| ac-dc | Phase-Shift Modulation | 90% | 0.5 - 5 | [59], [67] |
| ac-ac | Phase-Shift Modulation | 98% | 0.5 - 15 | [68],[69] |

Fig. 1.6 illustrates various potential configurations for integrating future residential buildings into the power system. Case (a) represents the conventional ac system, which underpins the operation of current hybrid inverters. In Case (b), a hybrid ac/dc system is depicted, where ac loads are supplied by the ac grid and dc loads are connected via a 48 V dc interface, corresponding to the ER configuration. Case (c) shows a ZEB with an internal dc infrastructure interfaced to the ac grid through an isolated ac-dc converter. Lastly, Case (d) represents a fully dc-based grid in which PV systems, energy storage, and dc loads are directly connected to a common dc link through dedicated dc-dc converters. Despite their potential advantages, configurations (c) and (d) remain constrained by the limited availability and standardization of dc technologies and loads.

To evaluate the power losses and efficiency of the considered scenarios in Fig. 1.6, the daily electricity consumption data for buildings has been extracted [70]. A building equipped with a 5-kW solar power plant and a storage system capable of supplying up to 5 kWh has been considered. For this study, the building is in the city of Berlin and the comparison is performed for two days: one in June and one in December, which have the longest and shortest radiation time, respectively. The losses in different elements have

been computed, and it is also assumed that the efficiency drop due to load rating is the same and insignificant for all cases. Fig. 1.7 shows the results of these comparisons. As expected, in the pure dc mode (case d), the losses are the lowest for both days in June and December.

However, this result is obvious and cannot be generalized, as the pure ac system is less efficient (case a). The attention is paid in particular to hybrid ac/dc systems (case b). In this context, the location of the building is very important. In a soft climate without a huge difference between summer and winter, very high energy autonomy is expected. It means that even a dc system connected to an ac grid with minimal grid interaction can be efficient, due to the very low interlink converter utilization. The opposite case may lead to an overall efficiency drop due to the lower efficiency of the isolated interface.

In this regard, some other studies [71]-[74] also compare the dc and ac residential nanogrid efficiency in the presence of different PV and storage capacities. In [72] an office building has been considered, and it has been proven that the overall efficiency can be increased by 11 to 17 % if the dc system is used.

It is also worth noting that redesigning existing ac appliances will lead to an additional efficiency boost. For example, in the case of motor-based loads, which are used for cooling, refrigerating, cleaning, etc. it has been stated that by moving towards brushless dc electric motors, 50% of energy saving in the heating sector, 30-50% in the cooling sector, and 5-15% in the cleaning sector can be achieved [74].

Therefore, considering the higher efficiency of the dc system and the time-consuming transition from ac to dc system and loads, the ER solution (case b) seems to be the right solution for the present and future nanogrids.

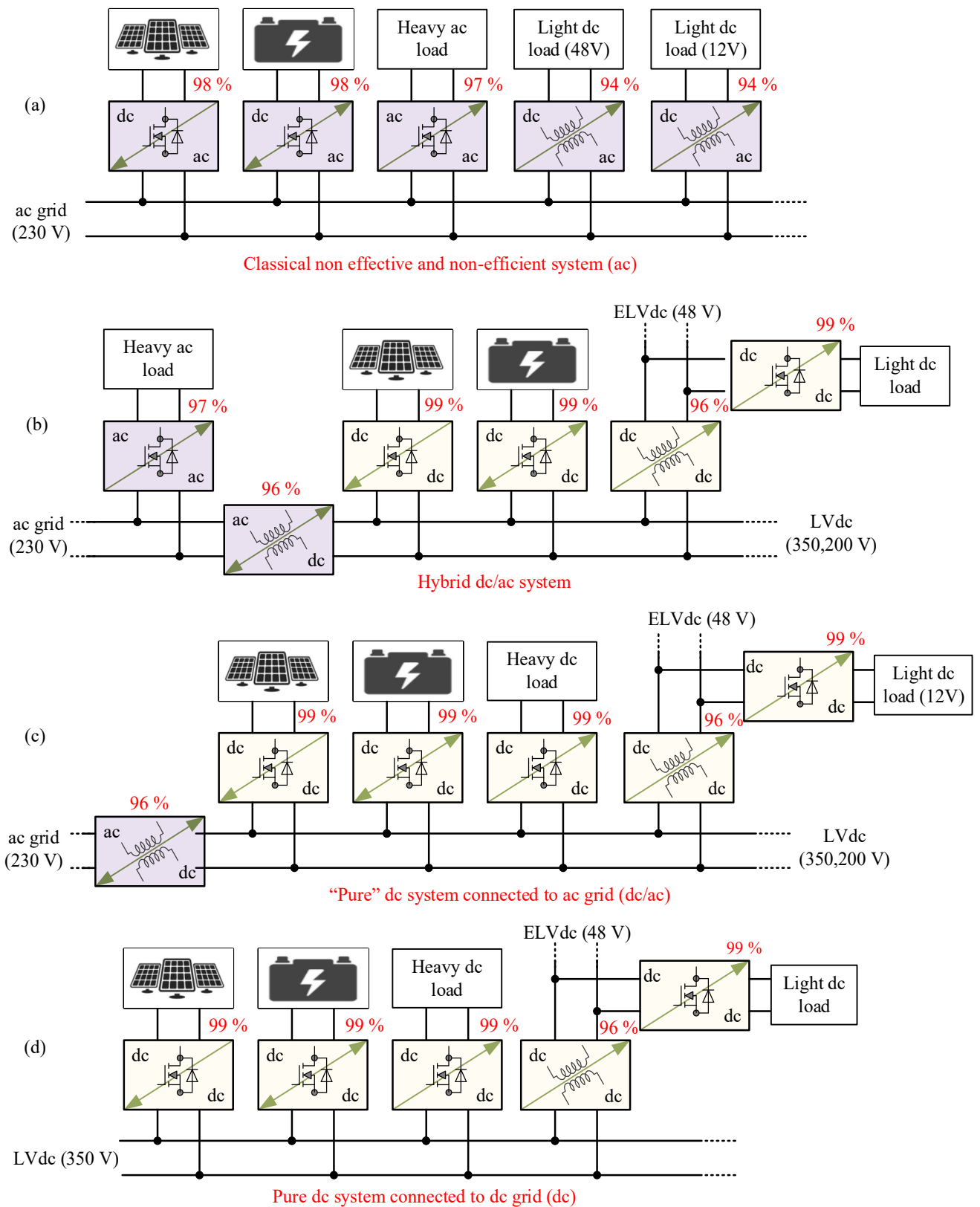


Fig. 1.6 Different scenarios for connecting ZEB to the power grid.

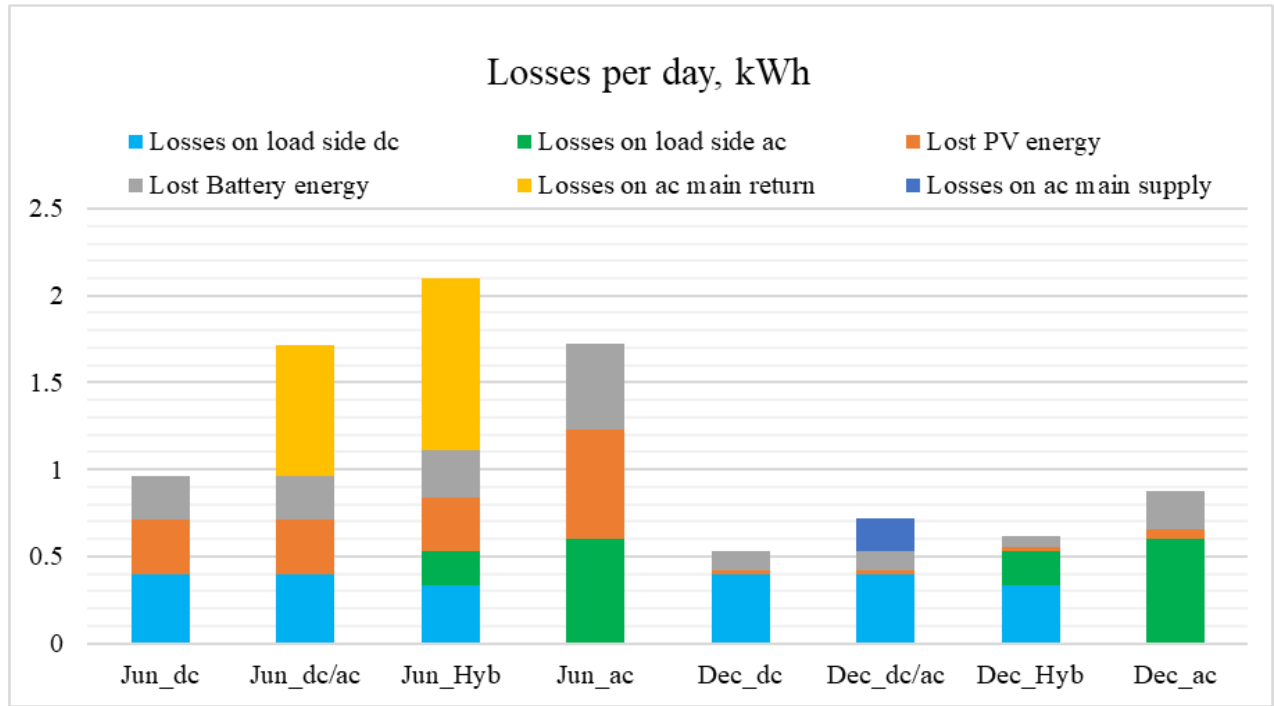


Fig. 1.7 Losses for four scenarios of connecting ZEBs to the grid for a day in June and a day in December based on the electricity consumption profile in [70].

1.3 Possible configurations

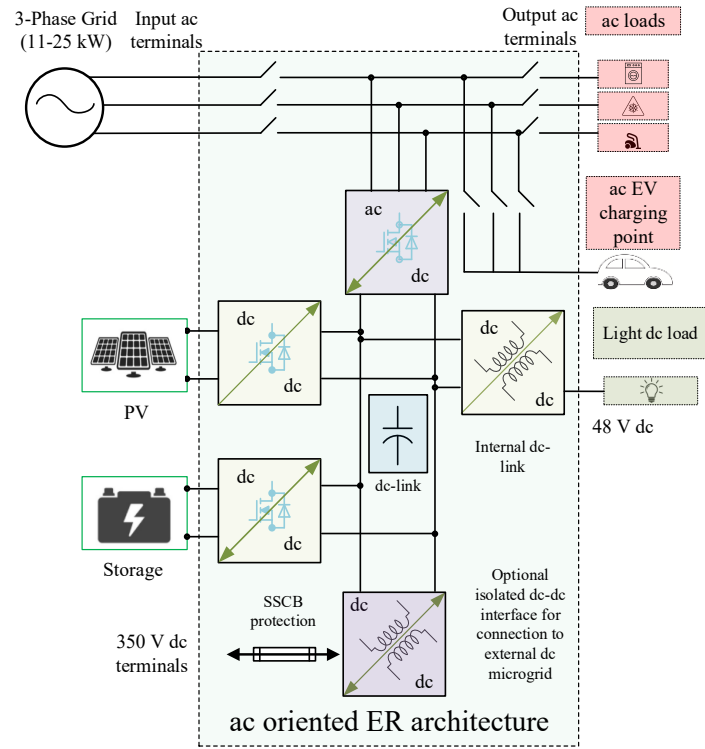
Based on the preceding discussion, a dc structure emerges as a highly suitable option for ZEBs due to its superior flexibility in integrating PV and BSS, alongside potential efficiency gains. However, considering the current grid infrastructure, which is dominated by ac systems, a pure dc connection scenario is currently unlikely to be considered as a valuable option. In this case, the adopted ER structure can be the one depicted in Fig. 1.8(a). It is very similar to hybrid inverter structures but has relays as an optional feature to provide load-shifting demand as well as a dc interface for light dc loads. In advance, an optional isolated dc-dc interface can be connected to an external dc microgrid as an auxiliary supply. Relays as optional features can be removed if we consider loads with IoT communication capabilities, as is the case with new appliances.

As only isolation between future ac and dc grids is accepted in the current discussion, the isolation between hybrid ac/dc and dc microgrids is mandatory. At the same time, considering that energy exchange with dc microgrids is expected in minor cases only, it will not cause significant energy losses.

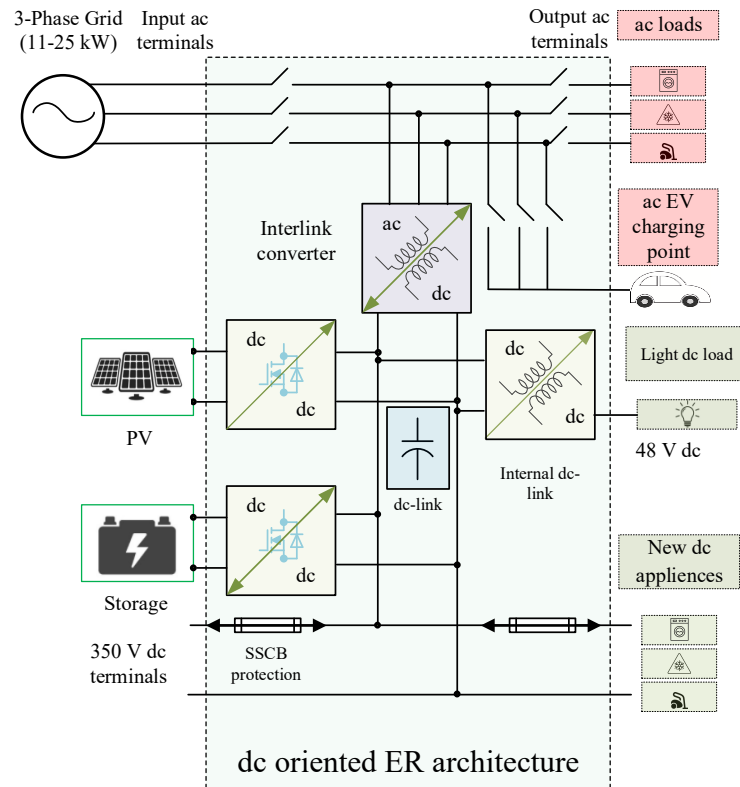
The second case under serious consideration is depicted in Fig. 1.8(b). In this case, the internal dc link should be connected to the dc microgrid as a prior energy source. At the same time, due to the isolation requirements between dc and ac grids, the isolated interlink converter is required. This structure may become feasible when in parallel to conventional ac heavy appliances, heavy dc appliances will be available on the market.

The possible dc loads may require different specific voltage levels. For example, low power loads can be mentioned 5V USB or 12V for security systems or other loads, including lighting or electric chargers. Fig. 1.9 shows the distribution list of dc loads based on voltage level as listed in [75]. Considering that there is only one voltage level in the general structure of ER available for users, the 48V dc interface can be the optimal solution in case of feeding light loads. USB Type-C also supports this voltage level and there are lots of compliant appliances on the market.

These structures can manage energy flow between generation, storage, and consumption, and can be developed as a single power electronics module with all required functionalities, including energy metering and integrated components. EMS will also be done via the same structure through the received information and optimization algorithms.



(a)



(b)

Fig. 1.8 The possible overall structure of ER in case of ac domination (a) and dc domination (b).

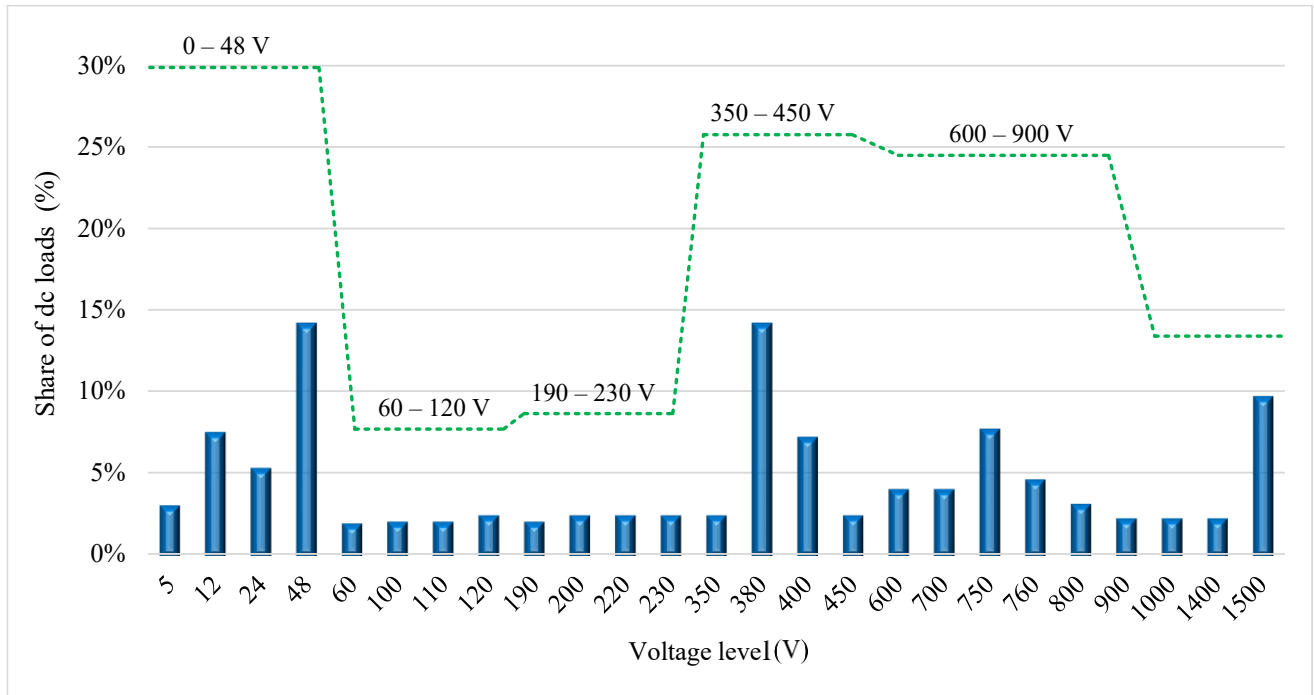


Fig. 1.9. Dc load dispersion at different voltage levels [75].

1.4 Conclusion

This chapter reviewed and further analyzed the literature on the topic of the study, which resulted in the following findings:

1. Based on the literature review of the latest findings in industrial solutions' development for integration of RES to residential buildings, it was shown that the technology of ER can effectively combine RES with energy storage, and this technology is the most promising for further integration of dc components to existing ac electric networks.
2. Based on the evaluation of the efficiency of power converters, various structures of ER were analyzed. It was found that the so-called "hybrid dc/ac system" is the most promising solution for future residential buildings utilizing existing ac grid and incorporating dc sources, loads and energy storage with the highest efficiency. Two possible structures of ER, utilizing "hybrid dc/ac system" approach, were introduced.
3. Literature review shows that low-level control (level of power converters) for ER is mostly based on classical controllers, which demonstrate acceptable performance, but suffer in case of dynamic conditions, which is one of the

challenges, still looking for a solution. More complex algorithms, such as Flatness-based theory, are promising candidates for fast and robust solutions with high static and dynamic performance.

4. On high-level control, EMS was investigated, and it was concluded that cloud-based EMS is an accurate, fast, efficient and cost-effective tool for powering smart buildings or microgrids.
5. Safety issues for power electronic solutions for residential ac systems were already deeply analyzed by researchers, but the grounding and safety measures for hybrid ac and dc systems are still open and should be solved.

These findings emphasize the importance and urgency of the scientific tasks posed in this work and create a basis for finding their solutions.

2 DC SYSTEM INTEGRATION AND RELATED CHALLENGES

Due to environmental problems and global warming, and on the other hand, the need for more energy, the share of renewable resources in the distribution network is increasing [76]. Since RES are intermittent and unpredictable, storage systems are commonly integrated alongside [77]. In such a situation, the distribution network is not only a consumer but also a producer and a consumer, and since there is storage capability, it can operate independently as a microgrid [78],[79]. Considering the nature of most renewables that produce most of dc electricity and on the other hand, the storage systems that are dc, a dc-based system can be a more effective solution to achieve a higher efficiency [80],[81].

Regarding the advantages of using dc microgrids, i.e., high reliability and higher efficiency, dc microgrids in the distribution network are attracting higher attention [82]-[84]. Although some dc nano/microgrids are designed for off-grid operation, in most cases, these microgrids must be connected to the ac grid [85]. Connecting to the main ac grid not only increases the reliability of the electricity supply, but it can also transfer the excess power produced into the grid and bring economic benefits.

2.1 Dc system integration

There are different methods to connect dc microgrids to ac grids. In general, the use of a transformer is suggested to increase reliability and isolate the two sides. In the initial structures, it was suggested to use a low-frequency transformer followed by an ac-dc interface converter [86]. Due to the high volume and weight of the low-frequency transformer, attention was directed to the use of a high-frequency isolation structure. With a high-frequency transformer, an ac-dc interface is used first, and then a high-frequency isolated dc-dc converter structure is applied [87]-[89]. In these cases, galvanic isolation is used to increase reliability and eliminate leakage currents. In isolated cases, the transformer increases the size and cost and reduces the overall efficiency. While many studies have considered it necessary to use isolation for connecting the LVdc microgrid to the ac grid, there is no obligation to use an isolation method, especially if it is defined as a hybrid dc/ac system [90].

Transformerless solutions are possible as well. In the structure without a transformer, only one ac-dc interface converter is used. Fig. 2.1 shows a generalized schematic of this connection. According to the desired features, the interface converter can be full-bridge, NPC, ANPC, T-type, etc. Different isolated and non-isolated structures have been studied in the literature [91], [92]. In transformerless mode, it is especially important to pay attention to protection issues and the elimination of leakage current. Different solutions have been attempted to eliminate or reduce the leakage current by providing novel structures or modified modulation techniques that decouple ac and dc sides [93]-[98].

Recent studies on dc microgrid mostly analyze the types and configuration of grounding and their effect on the types of faults [99]-[101]. Some other studies examine the types of grounding in the dc microgrid for fault detection methods and protective devices [102]. This is while the issue of grounding and its effect on various types of leakage currents has not been comprehensively investigated.

Regarding the lack of sufficient studies and standards for a dc microgrid, the issue of grounding in the dc system and particularly at the connection point of the dc microgrid to the ac grid and its challenges have not been comprehensively examined in a single study. In the current study, the dc microgrid grounding is described in detail and its challenges at the connection point with the ac grid are investigated. The leakage current at the connection point, which is directly related to the type of grounding of both sides, is also examined. More specifically, the issue of the dc leakage current and various grounding methods to eliminate or reduce it in the dc microgrid or at the connection point are all studied to clarify and solve the basic hidden challenges in the dc microgrid as much as possible. Finally, a sustainable solution at the connection point that minimizes the challenges related to grounding and leakage current in the non-isolated mode has been proposed.

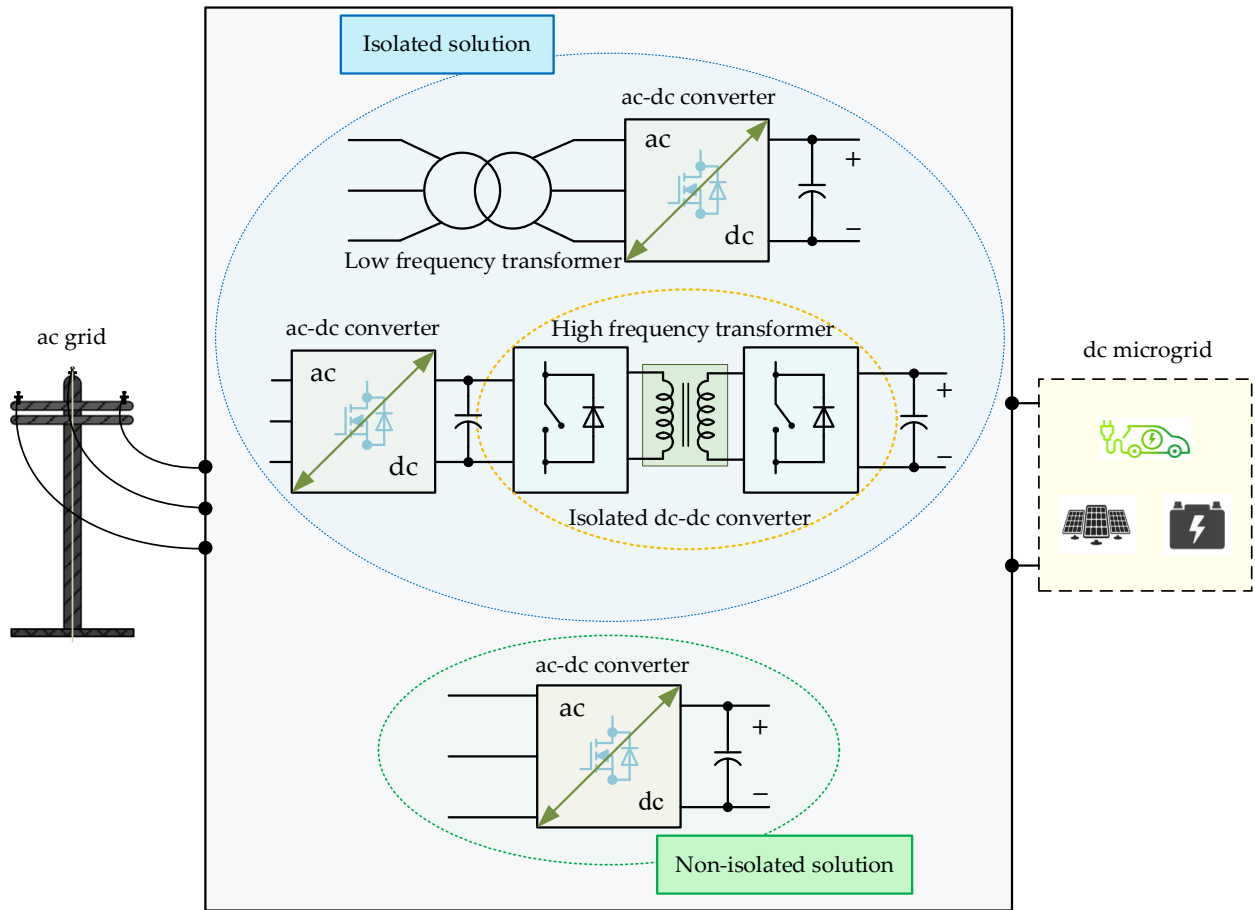


Fig. 2.1 Different solutions for connecting a dc microgrid to an ac grid.

2.2 Protection and safety in the dc microgrid

Although dc microgrids have advantages such as higher efficiency, without a proper protection system, they will face problems and will not be practical. Dc system protection is different from that of an ac system. There are many active sources in the dc system and each of these sources has a different power level that should be considered in the comprehensive protection system. In case of a fault in the dc microgrid, the dc current fault increases suddenly and since it does not have a zero crossing, it is not possible to suppress it easily; it needs extra equipment [103]. Therefore, from the protection point of view, several aspects should be considered. In recent years, only a few studies have focused on the protection of dc systems [104]-[113]. Due to the lack of necessary standards and sufficient experience, the dc system is still developing at a slow pace. As mentioned, the dc microgrid can operate independently or in the grid-connected mode and work bidirectionally. These operation modes also introduce more challenges to the

protection system. The diagnosis of high impedance faults and issues related to grounding and the ground current are other concerns that should be considered [102]. In the dc system, the short-circuit current depends on the source current. Some sources, such as batteries, have a high-rated current and subsequently a high short-circuit current, and others, such as PV have a low short-circuit current. It should also be pointed out that the dc microgrid is decentralized and each production unit operates independently. All of these points make the protection operation more complicated. Therefore, a risk classification according to voltage and current level and protection type is recommended in NPR 9090 [114],[115].

The NPR 9090 standard includes parts that are intended to describe classification, protection, and grounding in low-voltage dc systems. According to the hazardous level, this classification is divided into five classes from zone 0 (high risk) to zone 4 (low risk). Fig. 2.2 shows this classification. According to each zone and the level of voltage and current, different protection and safety requirements are defined.

As can be seen in Fig. 2.2, unprotected resources, including batteries, grids, large solar power plants, synchronous machines, etc., are placed in zone 0. The characteristic of this zone is a relatively high capacity and absence of protection, and a current limiter.

In Zone 1, the sources have short-circuited protection, and several sources could also be the case. The voltage level is less than 1500 V, and extra-low voltage (ELV) can be less than 120 V.

Zone 2 also has short-circuit protection, with the difference that the short-circuit current level is limited (lower). Other characteristics of this zone are: bidirectional operation, a current of less than 50 A for each device, and the use of the residual current device (RCD).

Production and consumption can exist in Zone 3. The voltage level of the line to the ground can be a maximum of 400 V line-to-ground and 800 V line-to-line. The overload current is limited and the maximum current for each device is 50 A.

In Zone 4, only consumers are present, and it is also called a safe zone. The maximum voltage level is the same as in Zone 3, and all types of consumers with a current of less than 50 A are present in the zone only as consumers.

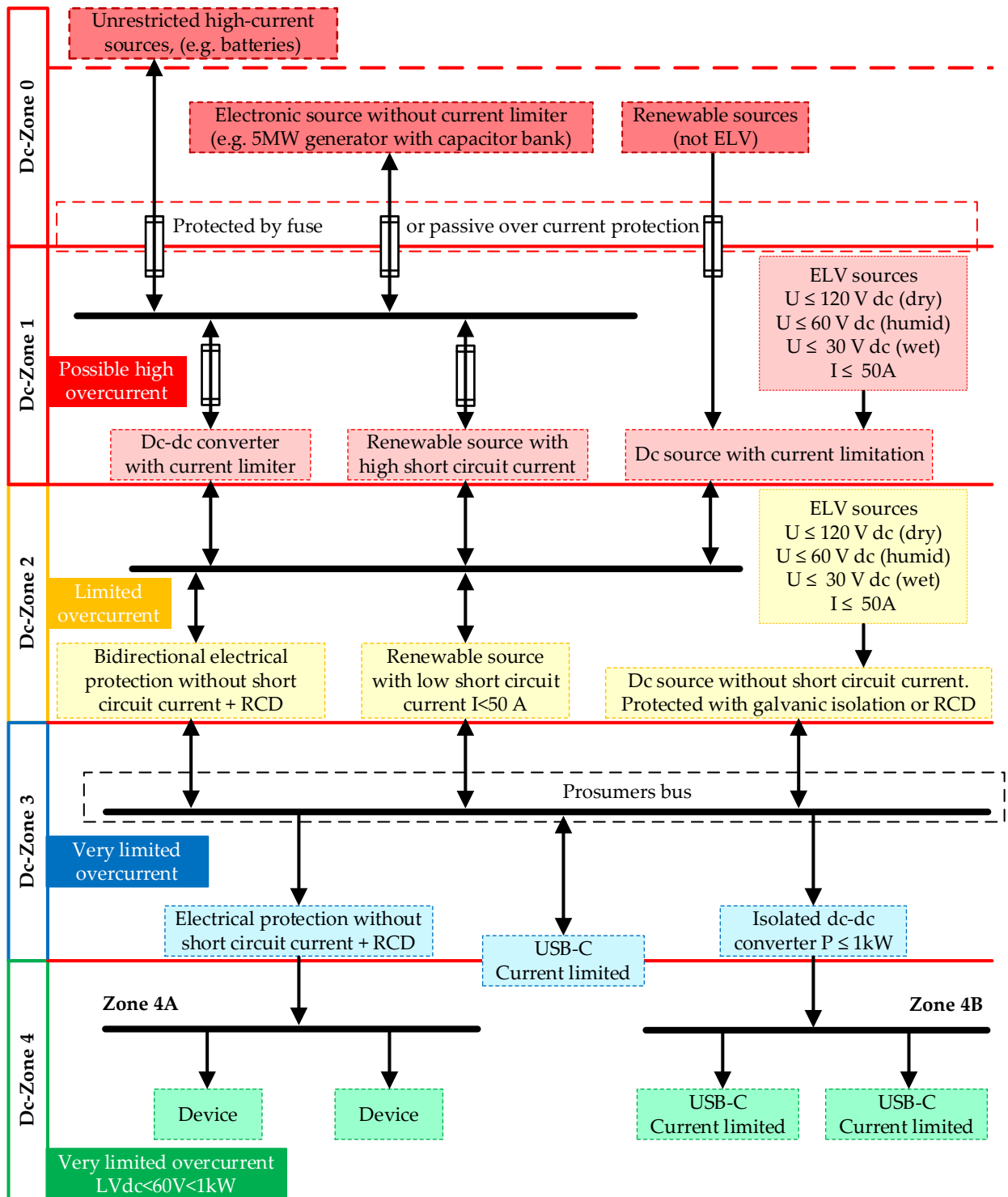


Fig. 2.2 Safety and risk classification in the dc system proposed in NPR 9090 [114],[115].

Based on this classification, the protection method should be chosen according to each zone. As mentioned in this standard, it is possible to ignore zones 2 and 3. However, attention should be paid to the current limits of circuit breakers and fuses and the

minimum short-circuit current of each zone. In NPR 9090, voltage levels of 350 V and ± 350 are suggested. This voltage level is comparable to a single-phase 230 V ac system and in the line-to-line mode, 700 V can be similar to a three-phase 400 V ac, and can also transmit similar power using existing ac cables.

The voltage level in dc microgrids should conform to the power level, length of the cable, and the type of system protection. While in the ac grid, the slight frequency deviation shows the overload or underload, in the dc microgrids, it is the voltage value that determines the underload or overload. Therefore, the voltage level is involved in energy management.

2.3 Leakage current in dc systems

Another important issue in the dc system protection is related to the leakage current. There are two types of leakage current: ac leakage and dc leakage. These leakage currents can cause serious issues or even endanger the safety of personnel. Therefore, it is important to understand how they form and how they can be removed and limited.

2.3.1 Ac leakage current

Ac leakage current is mostly caused by common-mode voltage (CMV). CMV induces a voltage fluctuation with respect to the ground and produces an undesirable leakage current when there is a conduction path. The path of the leakage current is formed through the stray capacitors between the active conductor of equipment (such as PV and batteries, etc.) and their grounded body on the dc side and the filters of the grounded ac grid or stray capacitance of EMI filters [116],[117]. The stray capacitance may be intentional (such as in EMI filter capacitors) or unintentional. Examples are spacings on printed boards, insulations between semiconductors and grounded heatsinks, and the primary-to-secondary capacitance of high-frequency isolating transformers.

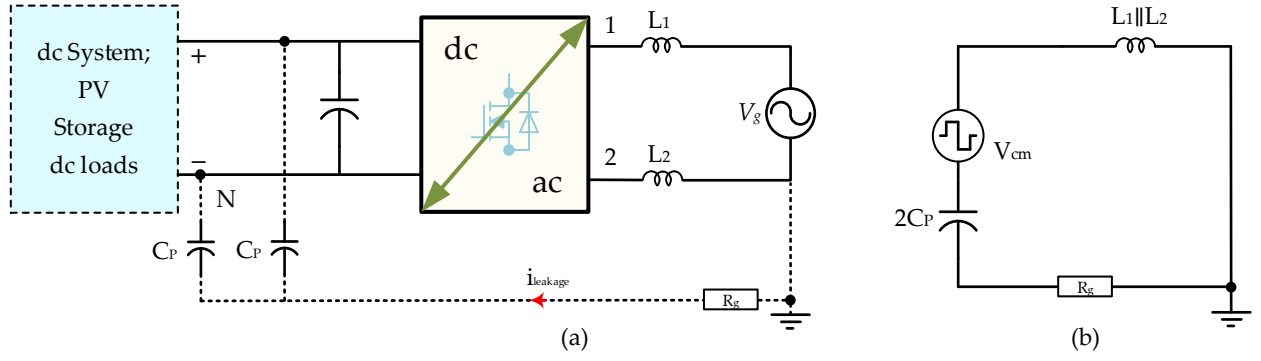


Fig. 2.3. The leakage current path through a parasitic capacitor on the dc side and the grounded ac side. (b) Equivalent circuit of the leakage current.

Fig. 2.3 shows the general condition of creating the leakage current. Due to the presence of stray capacitance (C_P) between the dc system and the grid ground, the high-frequency varying CMV can produce a leakage current through the parasitic capacitors, inverter filters and ground resistance (R_g)[117].

Differential-mode voltage V_{dm} is expressed by:

$$V_{dm} = V_{1N} - V_{2N}, \quad (2.1)$$

where V_{1N} and V_{2N} are the voltages of terminals 1 and 2 to terminal N . This equation defines the useful current injected to the grid. Fig. 2.3(b) illustrates the equivalent circuit of the leakage current, which is defined by the common-mode voltage V_{cm} :

$$V_{cm} = \frac{V_{1N} + V_{2N}}{2}. \quad (2.2)$$

Using equations (2.1) and (2.2), the paths of high-frequency elements can be extracted. It can be inferred that differential voltage can also encompass high-frequency elements, which are effective in generating leakage current. These additional high-frequency elements from V_{dm} can be written as V_{cm-dm} in equation (2.3).

$$V_{cm-dm} = V_{dm} \cdot \frac{L_2 - L_1}{2(L_2 + L_1)}. \quad (2.3)$$

In the asymmetric condition of the output inductances (L_1 not equal to L_2), the differential voltage can also affect the CMV and can lead to extra leakage current. In this case, the total high-frequency CMV can be written as V_{tcm} as (2.4).

$$V_{tcm} = V_{cm} + V_{d-to-c} = \frac{V_{1N} + V_{2N}}{2} + \frac{V_{1N} - V_{2N}}{2} \frac{L_2 - L_1}{(L_2 + L_1)}. \quad (2.4)$$

If $L_1 = 0$ or $L_2 = 0$, V_{tcm} is simplified by:

$$V_{tcm} = V_{cm} + V_{d-to-c} = \frac{V_{1N} + V_{2N}}{2} + \frac{V_{1N} - V_{2N}}{2} = V_{1N}. \quad (2.5)$$

$$V_{tcm} = V_{cm} + V_{d-to-c} = \frac{V_{1N} + V_{2N}}{2} - \frac{V_{1N} - V_{2N}}{2} = V_{2N}. \quad (2.6)$$

When the dc-ac converter has an asymmetrical inductor configuration ($L_1 = 0$ or $L_2 = 0$), the sufficient condition to cancel the leakage current is that the terminal voltage V_{1N} or V_{2N} remains constant. If $L_1 = L_2$, V_{tcm} is simplified by

$$V_{tcm} = \frac{V_{1N} + V_{2N}}{2} = V_{cm} \quad (L_1 = L_2). \quad (2.7)$$

Then, in the symmetrical inductor, the total common-mode voltage will be constant and has no high-frequency variation. This is the condition to cancel the ac leakage current.

2.3.2 Dc leakage current

Besides the ac leakage current, the dc leakage current is the dc current passing through the insulation resistance of the conductor or in situations where there is a potential difference between the grounds of the dc system [118]-[120]. The dc leakage caused by the insulation resistance is usually insignificant compared to the ac leakage. The insulation resistance of the conductor decreases over time or due to humidity and dust, and this can increase the dc leakage current. As mentioned, to eliminate the ac leakage current, CMV should be fixed. In this case, the parasitic capacitor is open-circuited. But still, a constant voltage falls on the insulation resistance, and the dc leakage current passes through the insulation resistance and the grounds of the system. The value of the dc leakage current can easily be calculated by Ohm's law, as in (2.8). But the point is in the estimation method of insulation resistance. Several techniques for testing and estimating insulation resistance have been reviewed in the literature [112], [121].

$$i_{dc} = \frac{V_{conductor-Gnd}}{R_{iso}}, \quad (2.8)$$

where i_{dc} is the dc leakage current, $V_{conductor-Gnd}$ is the voltage on the conductor to the ground point and R_{iso} is the insulation resistance of the conductor. Fig. 2.4 shows a simple representation of two modes of creating dc leakage current in a dc system. In this figure, \underline{G} refers to a dc energy source, and V_d is the voltage drop due to the conducting resistance. In the first case, the leakage current passes through the insulation resistance of the conductor and the ground of the dc system. The path of the leakage current is shown by the dashed line in Fig. 2.4(a). For the second case, as mentioned earlier, the dc system is decentralized and has several energy sources. To have an effective grounding, usually, each source has a separate ground. As shown in Fig. 2.4(b), the dc leakage current in this case is caused by the voltage drop in the current-carrying conductor (due to the resistance of the conductor) and the grounds of the two sources. The path of the leakage current can also be seen in this case.

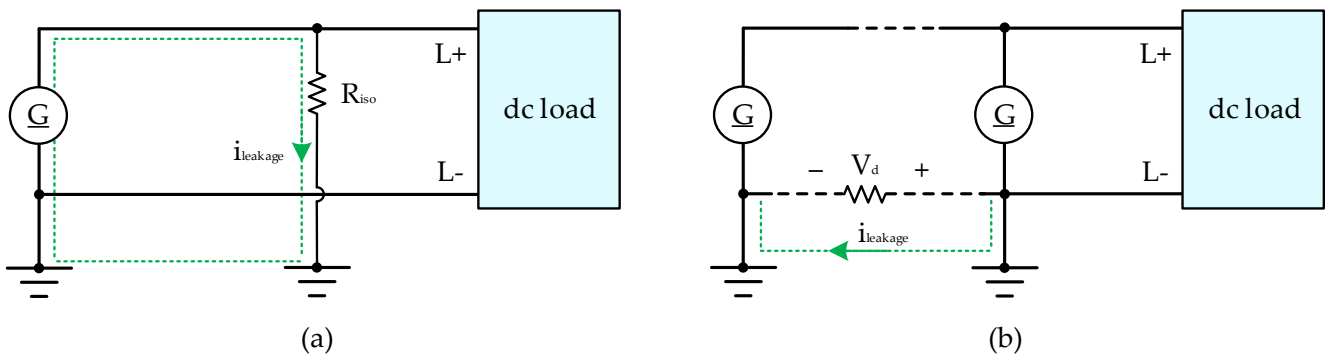


Fig. 2.4. The dc leakage current is created through: (a) the insulation resistance of the conductor and the ground of the system; (b) the potential difference created by the conductor resistance in the live conductor and the grounds of the system.

Based on the standard IEC-60950 for the leakage current, the value of total leakage current should be lower than 3.5 mA for a non-handheld device to ensure that the current is very low and cannot harm the person who touches the case of the device. In the case of a handheld device, this current should be lower than 0.25 mA [122]. Also, the injected dc current into the ac grid should not be greater than 0.5 percent of the nominal current [123].

Until now, many structures and control methods have been provided to eliminate or reduce the leakage current. One of the factors that has a direct effect on the leakage current is the way of grounding at the dc or ac system, and especially at the connection

point of the dc system to the ac grid. In the following, different states of grounding and leakage current will be investigated in different states.

2.4 Grounding in ac system

Though dc grounding has its features and requirements, it is not possible to consider it without consideration of ac grid grounding because of the possible coupling with ac. Therefore, it is helpful to review the different types and configurations of grounding methods in the ac system. In this part, grounding in the ac system is briefly reviewed.

The primary purpose of using earth in ac systems is to protect the personnel and equipment, prevent overvoltage due to any imbalance, etc. In the ac system, the neutral point of the transformer/generator is connected to the earth in different ways, and regarding the way of connection, different configurations can be defined. Each of these methods and configurations has advantages and disadvantages, and the best option should be used according to the conditions (power level and protection system) [124].

2.4.1 Ac grounding type

As mentioned, the earthing of ac systems is usually done through the neutral point in the Y connection of the transformer or generator. The different states of connecting the neutral point of the transformer/generator to the earth are shown in Fig. 2.5. Also, Table 2.1 summarizes the basic features of these methods.

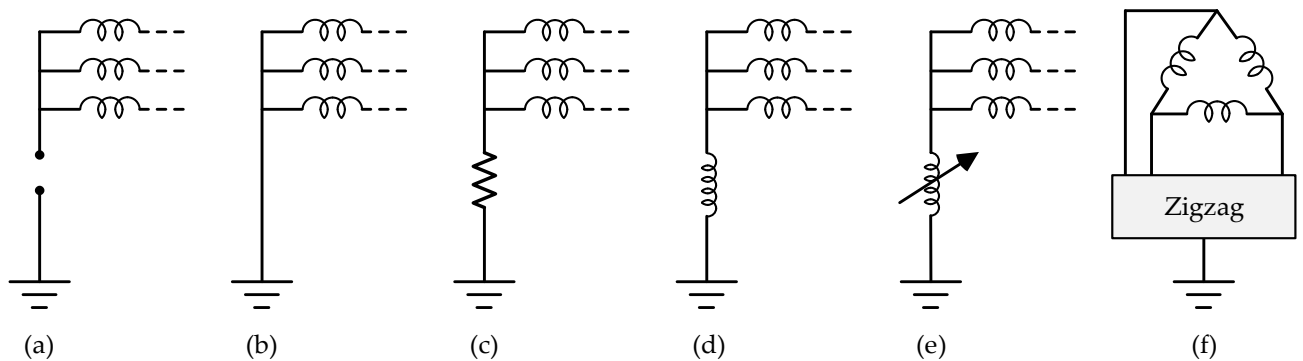


Fig. 2.5. Ac grid grounding type: (a) ungrounded; (b) solidly grounded; (c) resistance grounded; (d) reactance grounded; (e) adjustable reactance grounded; (f) zigzag connection grounded [124].

Table 2.1

Advantages and disadvantages of different grounding types in ac grids [125].

| Grounding device | Advantages and disadvantages |
|----------------------------|--|
| Ungrounded | - No cost - Continuity of operation in case of fault - Hard fault detection |
| Solidly grounded | -Simple grounding - No voltage fluctuation problem - High fault current - Easy fault detection |
| Resistance grounded | -Relatively simple - Limited fault current - Ability of continuity of operation in case of fault - Large installation area |
| Reactor grounded | - Absorbs reactive power and weakens ac voltage regulation ability - High cost - Large installation area - dc bias component in ac side voltage |
| Zigzag Grounded | - High reliability - Low reactive power consumption and small installation area |

2.4.2 Ac grounding configurations

In the distribution low-voltage grid, different configurations are provided according to the grounding of the neutral point of the transformer/generator and the way of grounding on the consumption (building) side. By considering different grounding types in Fig. 2.5 and whether there is an earth connection on the transformer/generator side or not, based on IEC 60364, various configurations can be defined as TN, TT, and IT [81], [126]. It should also be mentioned that in the protection and grounding system, the protective earth (PE) conductor is also considered to connect the enclosure of the equipment to the earth. In case the equipment is exposed to the electric potential for any reason, the PE conductor connects this potential to the ground and prevents shock to the human body.

In the TN mode, the neutral point of the transformer is connected directly to the earth. In the case of single-phase loads, the neutral conductor (N) and the protective earth conductor (PE), which is connected to the body of the equipment, are connected to the earth on the transformer side. In the case of TN-S, N and PE conductors are separately connected to the earth of the transformer. If a common conductor is used for the N and PE conductors, it is called the TN-C model. In some cases, on the load side, the PE and

N conductors are used separately, and on the transformer side, it is combined, which in this case is called TN-C-S. Fig. 2.6 shows different cases of TN configuration for ac systems.

In the TT connection, the neutral point in Y of the transformer is directly connected to the earth, and on the load side, the body of the equipment is connected to the ground through the local earth. In this case, the two grounds are independent of each other. This model of grounding is very suitable for eliminating EMC interference.

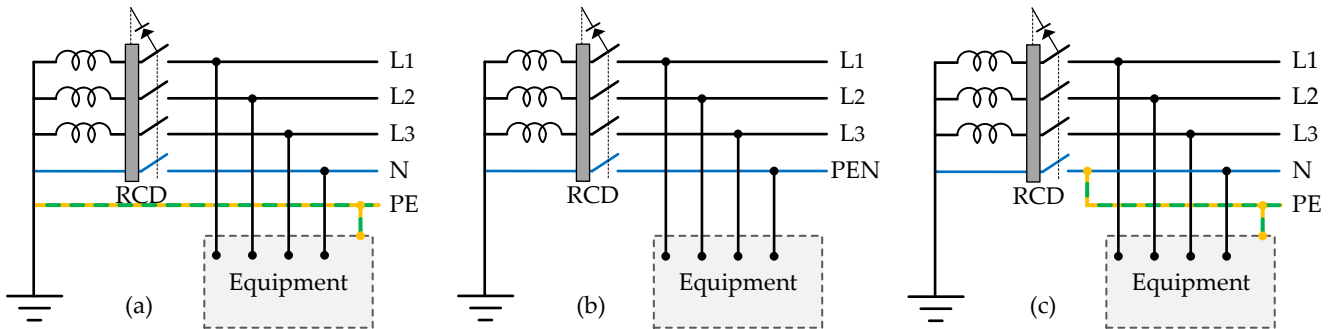


Fig. 2.6. Configuration of TN grounding schemes in the ac system: (a) TN-S; (b) TN-C; (c) TN-S-C.

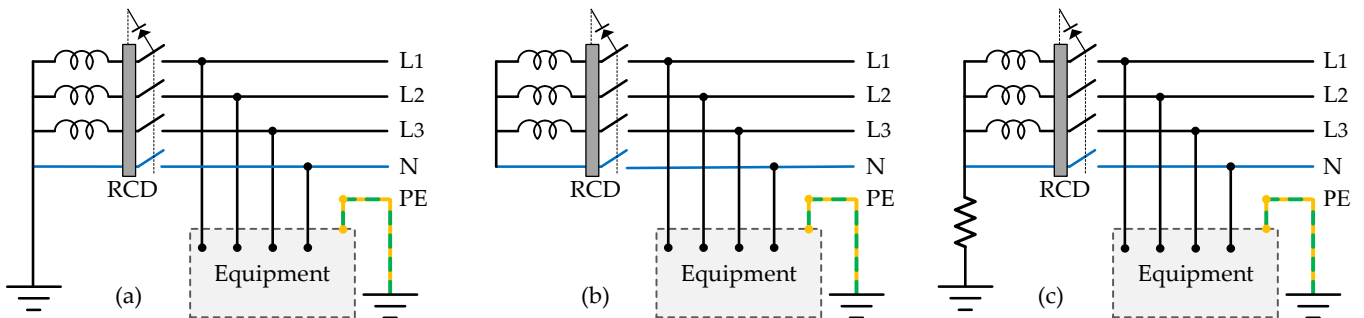


Fig. 2.7. Configuration of grounding schemes in the ac system: (a) TT; (b) IT; (c) HRG.

In the IT mode, the neutral point of the transformer is not connected to the earth, but only on the load side, the body of the equipment is connected to the local earth through the protective ground. In this method, in case of a fault, the system has a higher capacity and the relays do not work immediately.

High resistance grounding (HRG) can be considered another ac grounding configuration and when the resistance value is infinite, it is the same as in IT. As compared to the IT configuration, using the HRG method can reduce overvoltage caused

by faults and make fault detection easier. Also, in comparison to solidly grounded, the HRG method reduces high fault current and its damages [127].

Fig. 2.7 shows the configurations of TT, IT, and HRG. Table 2.2 compares the advantages and disadvantages of various types of grounding configurations in the ac system.

It is worth mentioning that the RCD protector shown in these figures consists of a core on which the phase and neutral conductors are wrapped and it works based on the magnetic field. If the system works properly and there is no leakage current, the phase and neutral currents are equal and opposite to each other. In such a case, the magnetic field produced by each conductor is equal and has opposite directions, and finally has zero output.

In case of current leakage due to any reason (for example, the contact of the human body with the phase), the neutral current will be lower than the phase current. In this case, the resulting field in the core will not be zero and it will generate a voltage in the existing coil in the core so that the command to disconnect the circuit is applied. It has the same function in the three-phase mode. The problem with RCD is that if there is a connection or leakage in the phase and neutral at the same time, it will not be able to detect the fault.

Table 2.2

Comparison of different configurations of ac grounding.

| Topology | Advantage | Disadvantage |
|----------|--|--|
| TN | <ul style="list-style-type: none"> - Effective for EMC - Fast fault detection | <ul style="list-style-type: none"> - Large fault current and inability to continue operation |
| TT | <ul style="list-style-type: none"> - Effective for EMC - Fast fault detection | <ul style="list-style-type: none"> - Large fault current and inability to continue operation |
| IT | <ul style="list-style-type: none"> - Availability under fault conditions | <ul style="list-style-type: none"> - Large transient voltage may occur during the ground fault |
| HRG | <ul style="list-style-type: none"> - Availability under fault conditions, Limited fault current, reduced overvoltage stress in TT | <ul style="list-style-type: none"> - It is difficult to determine the resistance value - Causes power losses |

2.5 Grounding in dc microgrids

Despite the advantages of dc microgrids, including flexibility in integration with renewable sources and higher efficiency, it requires high protection. The issue of protection in the dc system remains one of the challenges, and the grounding solution has a direct impact on protection aspects. In this regard, to solve the challenges of the dc system, it is important to provide proper grounding to be able to detect the fault in time and protect personnel and equipment, along with disconnection circuits to remove the fault. Therefore, grounding configuration plays an important role in protection systems. The purpose of grounding in microgrids is to protect personnel and equipment, detect ground faults, and reduce stray currents [99].

Before addressing the grounding in the dc systems, the general configuration of the dc system should be described; a dc system can be provided based on two conductors or three conductors. In a two-conductor structure with positive and negative poles, the negative line is usually connected to the earth. When there is a middle point (M), either in two or three-conductor cases, the middle line will be earthed. Fig. 2.8 shows these structures. It should be noted that although PEL and PEM carry current, they are not active conductors.

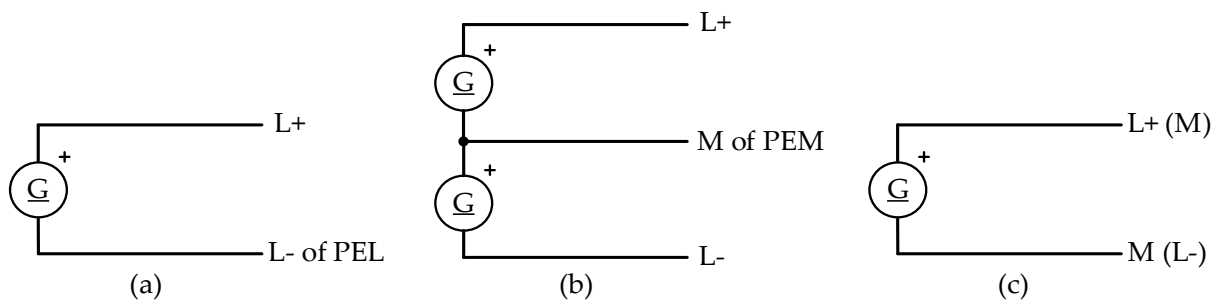


Fig. 2.8. Different configurations in dc systems: a) unipolar without middle point; b) bipolar, and c) unipolar.

In the case of using a three-conductor structure, line-to-line or line-to-ground with half voltage can be used to feed loads, and this gives redundancy and more flexibility to the configuration. However, in this structure, the voltage balance between the lines to the ground can be challenging, and it needs to be addressed [128].

2.5.1 Grounding type

Various methods have been proposed for grounding means in dc systems [100]. Fig. 2.9 shows the general connection states for a unipolar case. These methods include the following states: ungrounded (floating), solidly grounded, high-resistance grounded, diode grounded, and thyristor grounded. In the case of a bipolar configuration, these devices will be connected to the middle point.

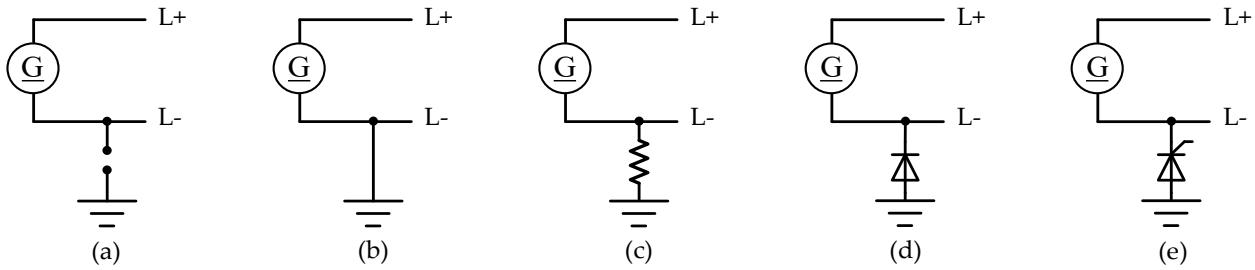


Fig. 2.9. Dc microgrid grounding devices: (a) ungrounded; (b) solidly grounded; (c) resistance grounded; (d) diode grounded; (e) thyristor grounded [100].

Each of these types of grounding gives a unique feature to the protection system. At low voltage levels, the ungrounded mode is usually recommended [101]. In this case, the common mode voltage cannot be too high to harm personnel or equipment. If a single line-to-ground (LG) fault occurs, the system can continue to operate without problems. But if a ground fault is the case in both lines, it will cause a line-to-line (LL) fault and will cause serious damage [129].

In the solid ground device, one of the conductors is connected to earth directly (in the unipolar case, it is usually the negative pole, and in the bipolar case, the middle point). The advantage of this method is the quick detection of the fault current. However, when a fault is detected, the system is unable to continue, and the functioning stops. Corrosion is also unavoidable due to the existence of stray currents in a path without impedance [130]. Other methods also have general features between these two modes. While in the ungrounded case, there is no path for current, and in the solidly grounded method, the ground current is high, the high resistance method can limit the fault current and subsequently, it will prevent the failure of equipment. On the other hand, the operation of the system does not stop during the fault [109].

In the diode ground type, the negative pole is connected to the ground using diode(s). Under normal operating conditions, the system will be ungrounded and this will reduce leakage currents. In case of a fault or transient condition, when the voltage applied to the diodes exceeds the permissible threshold, the diode conducts, and the system changes to the grounded type. Using a thyristor in the ground path also has the same function as the grounded diode type. The only difference is that by using a thyristor, there will be an active control on its conduction so that the system can be changed from ungrounded to grounded based on a pre-set threshold [99]. Table 2.3 summarizes the advantages and disadvantages of each method for grounding devices [99], [131], [132].

Table 2.3

Advantages and disadvantages of different grounding types in the dc microgrid [99].

| Grounding type | Advantage | Disadvantage |
|--------------------------|---|---|
| Ungrounded | <ul style="list-style-type: none"> - Low LG fault current - Power supply continuity at an LG fault - Minimized dc leakage current and corrosion - Simple implementation - No grounding power loss - No grounding cost | <ul style="list-style-type: none"> - Difficult to detect and locate LG faults - Possibility of significant system damage under LG fault evolving to LL fault - Sensitive to noise and disturbances - Small leakage currents cause large common mode voltage - Requires high insulation level |
| Solidly Grounded | <ul style="list-style-type: none"> - High safety due to low common mode voltage - Limited overvoltages - Low insulation level requirement - Low grounding cost - Easy to detect and clear LG faults - Absorbing and filtering disturbances | <ul style="list-style-type: none"> - High LG fault current - Lower power supply reliability - Risk of damage to equipment - Interference with communication systems due to larger LG fault currents |
| High-Resistance Grounded | <ul style="list-style-type: none"> - Limiting resonant overvoltages by absorbing the energy of the resonance - Low leakage current - Low LG fault current - Capability to operate under LG faults - Power supply continuity - High system reliability - Greater safety for equipment | <ul style="list-style-type: none"> - High overvoltage on the unfaulted line - Risk of damage to the system insulation - Power supply reliability due to the effects of faults - Difficult to detect LG faults - Susceptible to noise and disturbances - Considerable costs associated with the high-voltage grounding resistors |

| | | |
|-------------------------|---|--|
| Low-Resistance Grounded | <ul style="list-style-type: none"> - The leakage current and LG fault current levels are high and the common mode voltage is low - Reduced overvoltage at the unfaulted line during the LG fault and low-grounding cost - Absorbs and filters disturbances more easily than high-resistance-grounded systems | <ul style="list-style-type: none"> - Large LG fault current - Disturbances such as switching harmonics, nonlinear loads, and electromagnetic interference can inject currents into the dc system |
| Diode Grounded | <ul style="list-style-type: none"> - Under normal operating conditions, the system is ungrounded and leakage current is minimized - Both the leakage current concern and the common-mode voltage issue are addressed | <ul style="list-style-type: none"> - Requiring periodical maintenance as corrosion due to the leakage current is not eliminated |
| Thyristor Grounded | <ul style="list-style-type: none"> - Under normal operating conditions, the system is ungrounded and leakage current is minimized - Both the leakage current concern and the common-mode voltage issue are addressed - Active control based on preset value | <ul style="list-style-type: none"> - Requiring periodical maintenance as corrosion due to the leakage current is not eliminated |

Voltage level and grounding method have a direct impact on safety in the dc system [133]. The types of grounding devices presented for the unipolar structure can be applied to the bipolar structure and grounding is performed through the middle point. Grounding based on the middle point is a highly recommended solution in the dc system grounding [134]. By middle-point grounding at high-voltage levels, in case of a fault or electric shock on a person, the voltage on the body will be half of the nominal voltage [99], [135], [136]. This itself can be a form of protection.

2.5.2 Grounding configuration in dc microgrids

Similar to an ac power system, there are different configurations of earthing in the dc systems [107],[114],[136]. These configurations are TN, IT, and TT configurations. TN configuration can be divided into TN-S, TN-C, or a combination, as TN-S-C. TN systems are typically connected to earth through a low impedance path, and in this method, detection of the line fault is easy to implement.

While in TN configuration, there is one ground for the source side and load side, in TT systems, there are two separate earths for each side. Like TN, in the TT configuration, fault detection is easy, and this method is a good solution for EMC

mitigation. As different from TN systems, in IT systems, there is no earth on the source side. In this case, the fault current is very low, and fault detection is not an easy task. It requires separate measuring equipment, including measuring insulation conditions [112]. Fig. 2.10 to Fig. 2.13 show the different configurations of grounding for unipolar and bipolar modes in the dc system. Table 2.4 compares different features of these methods.

It should be added that the TN-S-C, which is the combination of TN-S and TN-C configurations, can also be considered, as in some parts, the PE wire is separate, and in other parts, it is implemented jointly.

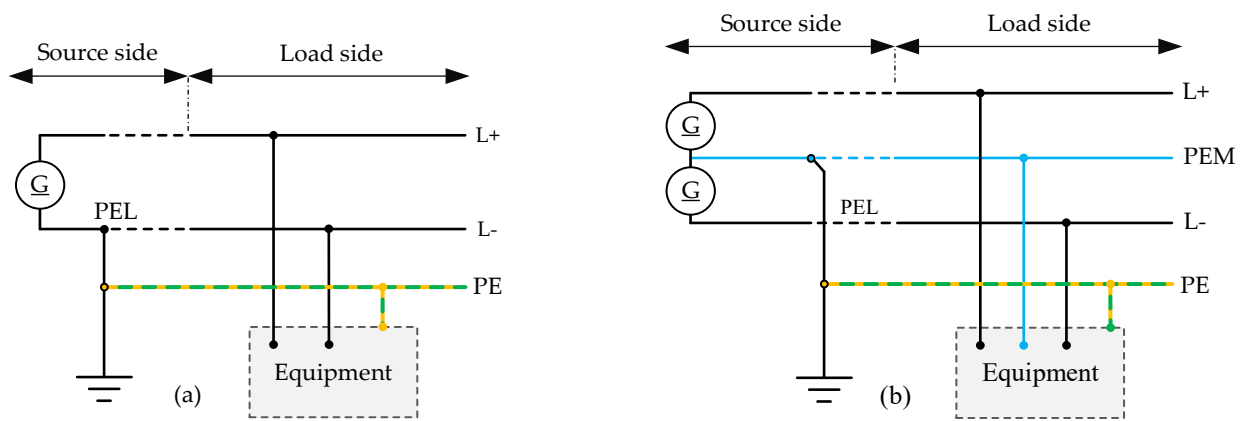


Fig. 2.10. TN-S grounding in the dc system with: (a) two conductors (unipolar); (b) three conductors (bipolar).

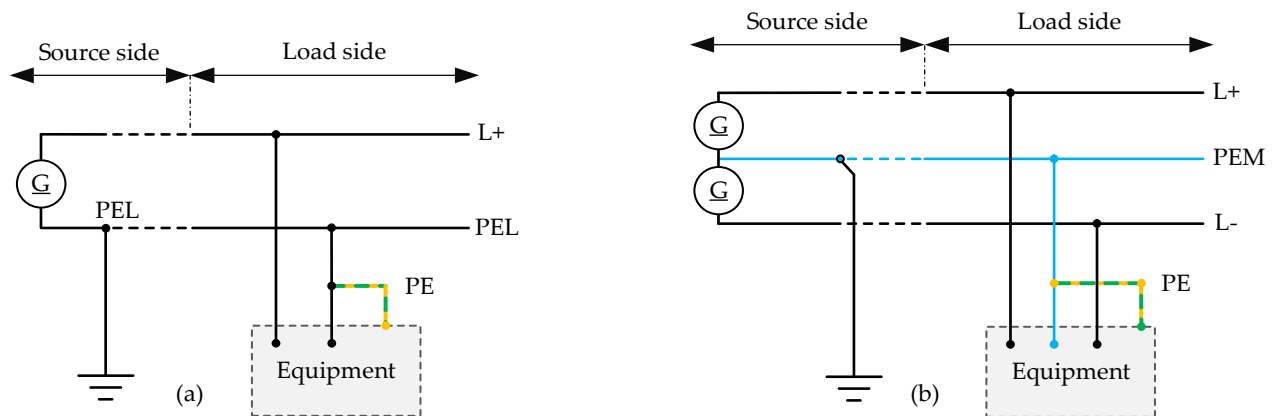


Fig. 2.11. TN-C grounding in the dc system with: (a) two conductors (unipolar); (b) three conductors (bipolar).

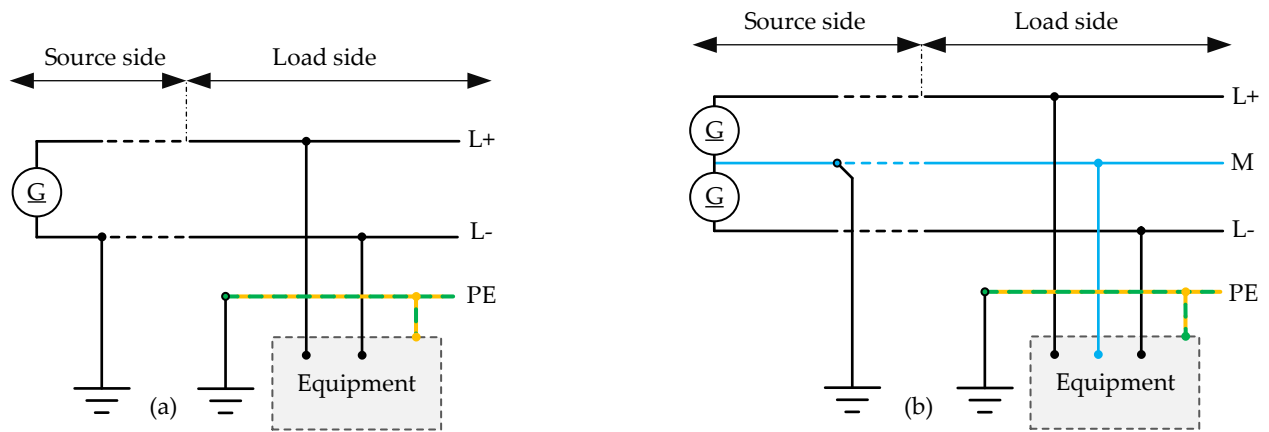


Fig. 2.12. TT grounding in the dc system with: (a) two conductors (unipolar); (b) three conductors (bipolar).

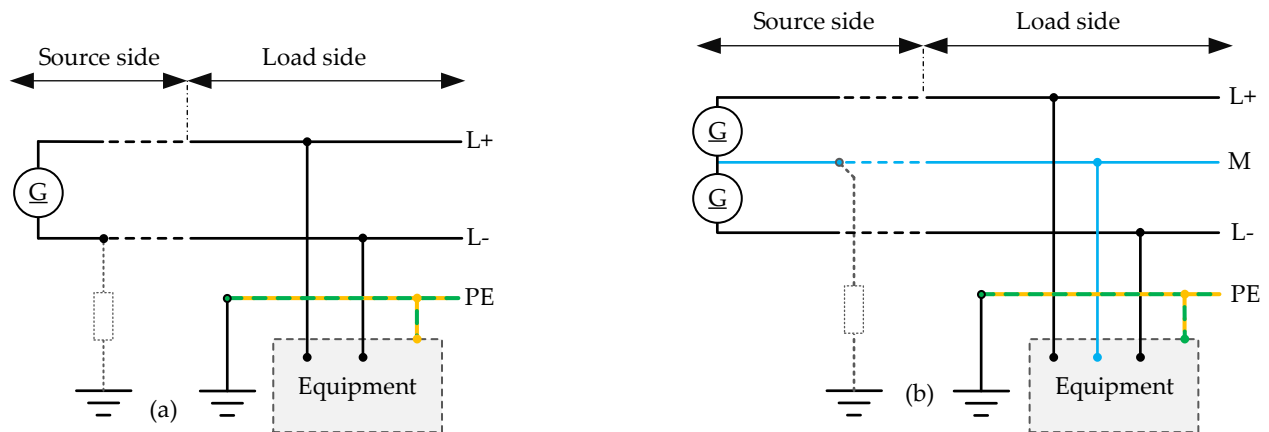


Fig. 2.13. IT grounding in the dc system with: (a) two conductors (unipolar); (b) unipolar three conductors (bipolar). (In this case, the system can be connected to earth via a sufficiently large resistance).

Table 2.4

Comparison of different grounding configurations in dc microgrids [102].

| Grounding configs | Safety of personnel | Safety of equipment | Continuity of service | Electromagnetic compatibility |
|-------------------|---------------------|--|-----------------------|---|
| TN-S | Good | <ul style="list-style-type: none"> · Poor · High fault current | Average | <ul style="list-style-type: none"> · Excellent · Less equipotential problems · Requirement to manage devices with high leakage currents · High fault current (transient disturbances) |
| TN-C | Good | <ul style="list-style-type: none"> · Poor · High fault current | Average | <ul style="list-style-type: none"> · Poor · High fault current (transient disturbances) |

| | | | | |
|-----------|------|--|-----------|---|
| TT | Good | <ul style="list-style-type: none"> · Good · Fault current less than a few dozen amperes | Average | <ul style="list-style-type: none"> · Good · Risk of overvoltage/voltage imbalance · Equipotential problems · Requirement to manage devices with high leakage currents |
| IT | Good | <ul style="list-style-type: none"> · Very good · Fault current less than a few dozen mA, but high for the second fault | Excellent | <ul style="list-style-type: none"> · Poor (to be avoided) · Risk of overvoltage |

Regarding these configurations and their general characteristics in the table, the following consideration can be made:

1. In the TN-C grounding mode, if the PEL or PEM wire is loose or has a weak connection, the body and metal parts of the equipment will be under line voltage. Therefore, regardless of the type of function, the TN-C structure should not be used in dc systems.
2. In the TT mode, the resistance of the two ground paths limits the fault current. Therefore, if the body comes to contact with the line with potential and electric shock, short-circuit protection cannot be used as protection against electric shock. Neither is overcurrent protection a suitable option for protection against electric shock due to its slow response time.
3. On the other hand, the use of the IT structure is usually preferred due to the continuity of operation in the event of a fault. This structure is suitable for skilled and trained personnel because it is not easy to detect and fix errors in this structure. The IT structure is also far from touch safety due to the presence of capacitors in EMC filters and existing cables and the creation of capacitive coupling with the ground.
4. Based on the above, on the risk classification in Fig. 2.2 and the types of ground structures, the TN-S grounding structure is preferred in zones 1 to 3 and 4a.
5. Systems in dc zone 4B are usually implemented as IT systems in practice because of the USB-C connection.

2.6 Impact of grounding on the dc leakage current

As discussed in the leakage current section, part of the leakage current is related to the dc leakage current. Using common grounding methods, this dc leakage current will flow, and it has adverse effects such as corrosion in metal and concrete parts or injection into the ac grid. In the case of solid ground, for instance, the voltage on the conductors will be fixed. In this case, due to the constant voltage on the ungrounded conductors, the dc leakage current can pass through the insulation resistance and the ground of the system. Also, as mentioned previously (Fig. 2.4(b)), when there are several sources and grounds in dc the system, the dc leakage current can flow between different grounds.

To solve this problem, several capacitive grounding methods have been proposed, which can greatly reduce or eliminate dc current despite the existence of low impedance grounding on the dc side.

The first solution, which is shown in Fig. 2.14(a), uses capacitors and anti-parallel diodes in the ground path [114]. The capacitor is like a short circuit for high-frequency components and it creates a low-impedance path and will be an open circuit for dc components. Passing the dc leakage current through the diodes also requires overcoming the forward voltage of the series diodes.

Another similar structure shown in Fig. 2.14(b) is the use of a capacitor in parallel with Zener diodes [137]. In this case, the Zener diodes are used to avoid a high number of diodes in series. Based on the predefined values, a Zener diode can be chosen. In this case, by creating a low-impedance path for high-frequency components, ac and transient current will pass, while there is no path in the ground structure for the dc component.

A similar solution to remove and limit the dc leakage current introduced in [138] is shown in Fig. 2.14(c). This grounding structure consists of an RL circuit parallel to the capacitor. This structure also has a capacitive path that has low impedance at high frequencies and a resistive path to prevent the dc current from passing through. This grounding network is also designed in a way to have a low equivalent impedance and subsequently a low voltage in a wide range.

In these capacitive solutions, the design of the components should be such that it prevents the passage of the dc leakage current. In Fig. 2.14(a) and Fig. 2.14(b), it should

be done through the design of the diode forward voltage value (Fig. 2.14(a)) and the Zener voltage value (Fig. 2.14(b)). For Fig. 2.14(c), it should also be done through the design of the resistance and an inductor.

The design of the capacitor should be such that it can have very low impedance for high-frequency components. Otherwise, the high-frequency components will pass through the diode or resistor/inductor path and due to the voltage drop in these paths, the voltage of the other conductor will fluctuate. This will create another path for the leakage current through the stray capacitor of the other conductor(s).

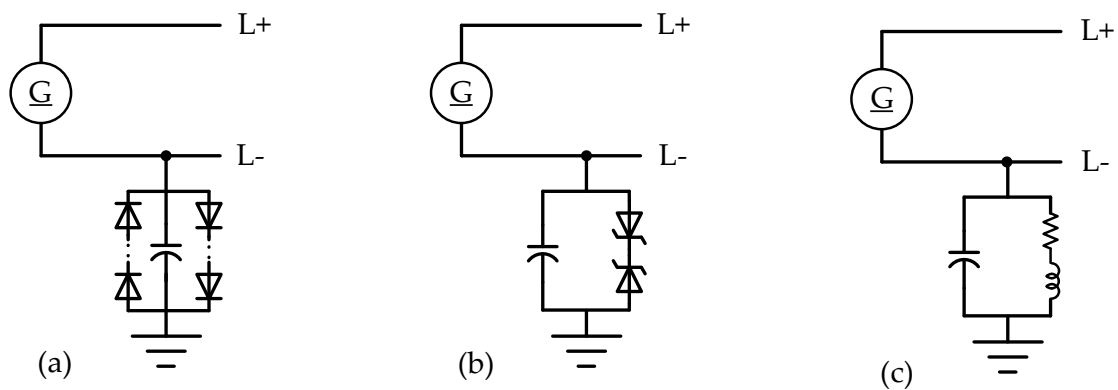


Fig. 2.14. Grounding solution for minimizing the dc leakage current: (a) anti-parallel diodes and capacitor solution in [114]; (b) Zener diode and capacitor solution in [137]; (c) RLC circuit solution in [138] (In the case of bipolar form, these grounding networks will be connected to the middle point).

2.7 Grounding configuration for several decentralized sources

Having several decentralized sources is one of the characteristics of the dc system. As mentioned previously, the use of a grounding TN-S configuration is preferred in the dc system. However, with several decentralized sources, the existence of one earth point cannot be enough due to a long distance and the resistance of the conductor, which affects the grounding system. In such cases, near any source, earthing will be implemented. Again, according to Fig. 2.4(b), having several grounds will cause the dc leakage current due to the voltage drop on the conductor. On the other hand, a solid grounding in different

points would result in dc ground currents flowing due to the difference in the neutral potential. This can cause corrosion and problems associated to the dc leakage current.

To solve this problem, grounding with capacitor networks is used as described earlier (Fig. 2.14) [132],[137]. In this grounding network, due to the very low impedance of the capacitor for high-frequency elements, high-frequency and transient elements pass through the capacitor and act like solid ground. Meanwhile, dc currents cannot pass through this grounding network. It should also be added that in the case of the presence of several grounds, only one of the sources can have a solid ground, and the rest of the sources should use capacitive grounding to prevent the leakage of dc currents through the grounds.

Regarding Fig. 2.14, one method is to use anti-parallel diodes and capacitors in the ground connection path of the sources [114]. As long as the voltage applied to them is low, these diodes prevent leakage current, and in case of a fault, show normal behaviour. Therefore, in this case, two modes, TN-S-CD and TN-S-CDD, are proposed. Fig. 2.15 shows this solution.

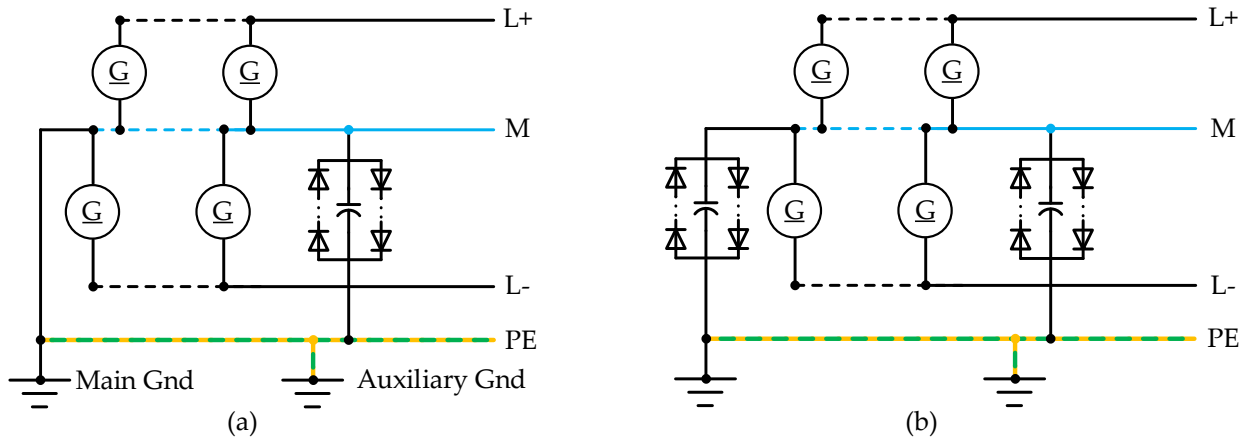


Fig. 2.15. Grounding multiple sources in the bipolar dc system: (a) TN-S-CD; (b) TN-S-CDD.

In the first case, one source is directly connected to the ground and the other through the diode-capacitor network. In the second case, all sources are connected to the ground through the diode-capacitor network. The use of these modes is applicable for zones 2 and 3 in Fig. 2.2, where the current of resources is limited. In this case, the

components should be designed according to the maximum fault current. Using this mode for zones 0 and 1 requires a lot of accurate calculations to determine the maximum fault current for component design.

2.8 Grounding in the connection point of the dc microgrid to the ac grid

Although in some cases, dc micro/nanogrids can be designed for the off-grid mode in relation to the ac grid, in most cases, they should be connected to the main ac grid to improve the reliability of the electricity supply. Regarding the dominance of the ac grid from the generation, transmission, and distribution sector, dc microgrids should be connected to the existing ac grid and should interact with power from that for self-balancing. In this connection, protection, safety, and grounding methods should be considered on both sides [125],[139]. Different configurations of grounding for pure ac and pure dc systems were discussed in previous parts. But at the point where the dc system is connected to the ac system, some aspects should be considered and the protection method should be designed according to the grounding structure on both sides. At high power and voltage levels, using isolation between dc and ac is mandatory to guarantee reliability and safety. In the LVdc, galvanic isolation is supposed to be recruited, but it is not obligatory. In the isolated mode, the grounding method on each side is independent of the other side and the type of grounding is selected according to the above-mentioned configurations in the ac and dc system grounding.

Fig. 2.16 shows a simplified connection point in the isolated case, while both sides have grounding near the connection point as dc and ac sources.

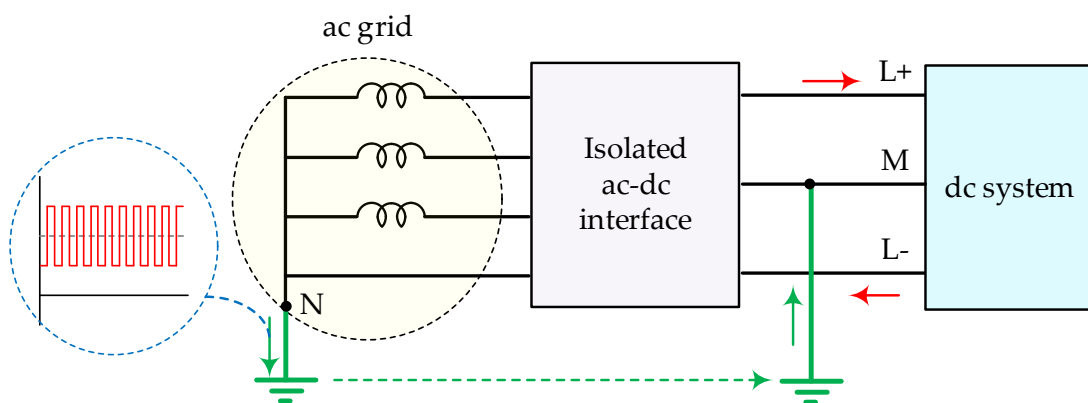


Fig. 2.16. When both ac and dc sides have grounding, there will be a direct electric path for current to pass between sides.

The way of grounding has a direct effect on the leakage current. Due to the use of an ac-dc interface converter in all situations, leakage currents can be seen passing through different paths. In this section, the aim is to investigate the path of the possible leakage current in different states of connecting the dc system to the ac grid.

2.8.1 Isolated case

In the case of high-frequency isolation, the important point is the existence of a stray parasitic capacitor between the primary and secondary of the high-frequency transformer C_{iw} (interwinding capacitor). In different studies, different methods have been presented to model this capacitor, which is in the picofarad range [140], [141]. Stray capacitors in parallel to insulation resistance are used here for a high-frequency transformer.

Two cases for grounding a dc microgrid are considered. The leakage current can flow between the ac grid and the dc system through the stray capacitor and the insulation resistance of the primary and secondary transformer, as demonstrated in Fig. 2.17 and Fig. 2.18.

Fig. 2.17(a) shows the first condition when the dc microgrid is grounded at a negative point. For this configuration, since the ground on the dc side is at the negative point, a bias voltage proportional to the dc side voltage will be added to the equivalent circuit. Therefore, in this case, leakage current may have a dc component. Fig. 2.17(b) shows the equivalent circuit for the leakage current paths in this connection type.

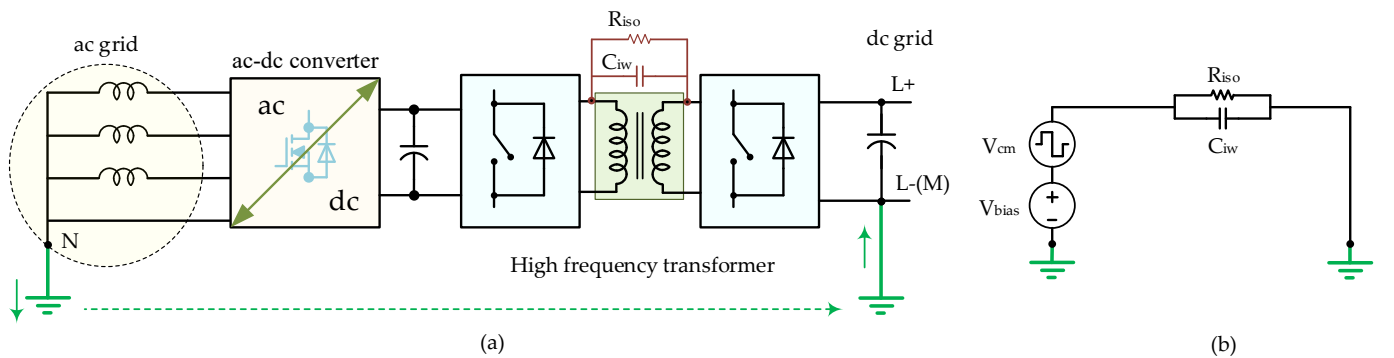


Fig. 2.17. Leakage current path of high-frequency isolated connection for the unipolar dc system: (a) general circuit; (b) simplified equivalent common-mode circuit.

Fig. 2.18(a) shows the case where the dc microgrid has middle-point grounding. Fig. 2.18(b) shows the simplified equivalent common-mode circuit. Due to the middle-point grounding in the dc side, there will be no bias voltage in the equivalent circuit (bias voltage sources will cancel each other). In this case, there is only a common-mode voltage source, which can lead to high-frequency ac leakage current in this case.

In the case of using a low-frequency transformer, the ac grid is completely isolated and there is no significant ac leakage current component between dc and ac grids.

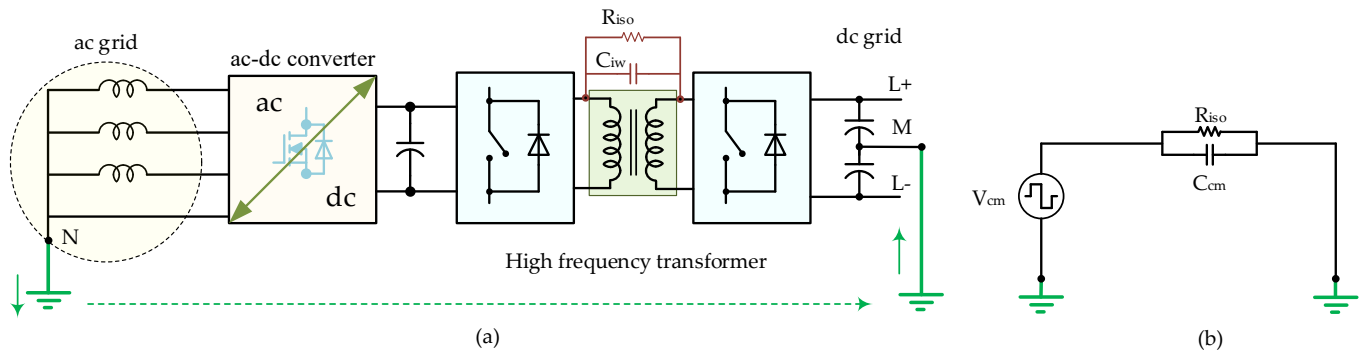


Fig. 2.18. Leakage current path of high-frequency isolated connection for the bipolar dc system (grounded at the middle point): (a) general circuit; (b) simplified equivalent common-mode circuit.

The path of the dc leakage current is the same due to the theoretical presence of an insulation resistance in parallel to this inter-winding capacitor. At the middle-point grounding in the dc side, the insulation resistance will not have a significant impact on the dc leakage current. But at the negative-point grounding in the dc side, insulation resistance in the ac side causes a dc component in the total leakage current.

If the secondary side of the transformer and the dc system are both without grounding (or IT grounding), then there will be no path for the leakage current due to the absence of ground. Although in this case the leakage current is eliminated, this method is not recommended because of protection and fault detection problems.

2.8.2 Non-isolated case

To increase efficiency and reduce the cost, volume, and weight, the connection without isolation and solving the issues related to safety and protection in this connection point can be a focus of future research and engineering considerations.

At the same time, the absence of isolation applies a significant limitation on the grounding possibilities on both sides. Depending on the condition of the switches, a direct electrical path can be created through the grounds on both sides. Although the presence of filters in the current path prevents short circuits, high-amplitude high-frequency current can pass through two grounds.

The obvious solution in the case of a non-isolated connection is that only one side should be grounded. This means having an IT configuration on the ac side in case the dc side should be grounded, or if grounding in the ac side is mandatory, the dc side should be ungrounded [81],[142]-[144]. Table 2.5 shows different possible solutions for grounding at the connection point in non-isolated cases. As can be seen in this table, when there is grounding on the ac side (TN and TT), the only possible solution on the dc side is an ungrounded case. On the other hand, for the IT case, the dc side can be grounded at the negative or middle point or even remain ungrounded.

Table 2.5

Different solutions for grounding at the connection point.

| ac GND \ dc GND | TN (any kind) | TT | IT |
|-------------------------|---------------|-----------|----------|
| Negative point grounded | Forbidden | Forbidden | Possible |
| Middle point grounded | Forbidden | Forbidden | Possible |
| Ungrounded | Possible | Possible | Possible |

The best solution for the non-isolated connection of dc microgrids to the ac grids can be the use of common-ground structures [116], [145]-[151]. In this case, considering that the negative pole of the dc system and the neutral of the ac grid are directly connected to each other, a similar or even an asymmetrical grounding method can be used for both sides. In the common-ground structure, the common-mode voltage on the dc negative and the ac neutral is clamped to zero and their stray capacitors are bypassed. Therefore, ac leakage current can be eliminated. The dc leakage current can also pass through the

insulation resistance, ground on the dc side of the system. To solve this, a TN-S-CD type of connection (Fig.2.15) should be used on the dc side. Fig.2.19 shows the general view of this solution.

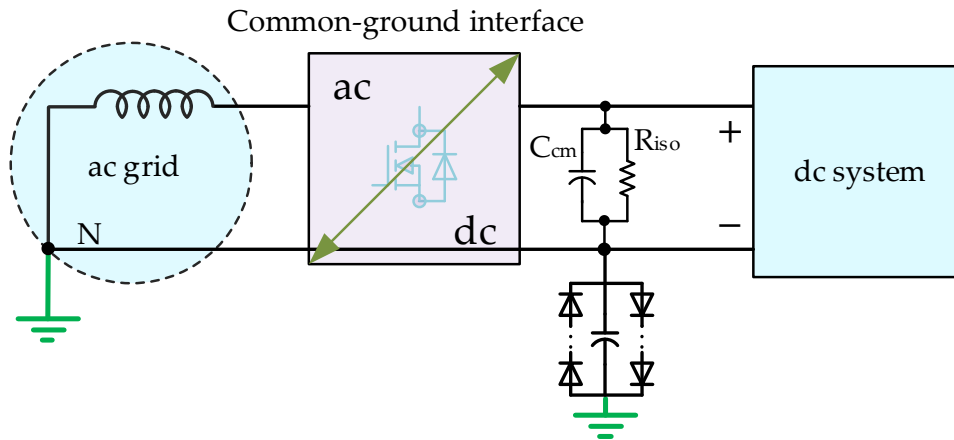


Fig. 2.19. Connection through a common-grounded inverter and elimination of the leakage current path.

2.9 Conclusion

LVdc is increasing and developing in the distribution sector; however, as it was shown in Chapter 1, there are still no sufficient standards and studies in the field of dc system protection and grounding. To solve the issue of the improvement of the safety in dc systems, all types of grounding methods in the dc system and at the connection point of the dc to the ac grid were examined. Based on their comprehensive analysis, the dc and the ac leakage current paths were identified, and finally, the advantages and disadvantages of all possible grounding techniques were articulated. The following conclusions of findings can be highlighted:

1. Even in the presence of galvanic isolation by means of high-frequency transformer, leakage current can't be eliminated due to the stray inter-winding parasitic capacitance between primary and secondary sides. In case of grounding on ac side (TN or TT configurations), leakage current originated from dc side will be injected into the ac side via mentioned stray capacitance. Low-frequency transformer eliminates this pass completely and can be considered as a solution for leakage current elimination.

2. Even in presence of high-frequency and low-frequency isolation, a dc component in the leakage current can be originated by dc voltage bias between the middle (or negative) point of the dc system and the neutral point of the ac system. In order to eliminate this component, the configurations where there is no voltage bias between the neutral point of the ac system and the middle point of the dc system are recommended.
3. Grounding based on the middle point based on the TN-S-CD type is a highly recommended solution in the dc system grounding. In addition to fault or minimization of electric shock, it eliminates the dc leakage current between the ac and the dc system.
4. Non-isolated common-ground solution for interlinking dc and ac grids can be recommended as an alternative, cost-effective solution where the leakage current between the ac and the dc grid can be completely eliminated.

Provided in the chapter analysis and conclusions create the foundation for further research with the focus on the analysis of common-ground structures that have higher capabilities, such as a high-power range, higher output quality in bi-directional operation, and can be used at the connection point. In addition, practical solutions to reduce or eliminate the leakage current at the connection point, as well as methods for fault detection according to these grounding configurations, can be further analyzed.

3 PROPOSED HYBRID ENERGY ROUTER

As it was mentioned in the first chapter, the increasing integration of PV systems and BSSs in residential buildings, coupled with the new trends in PV-integrated energy communities, has led to the development of various power electronics devices and EMSs, such as Energy Router. This chapter introduces the general structure of the proposed multiport ER structure and analyzes different parts of the ER, including inverter modulation techniques and component design. Regarding the proposed structure, safety, protection, and DCCB are also presented in the chapter.

3.1 Proposed structure

Based on the results of the analysis in previous chapters, the proposed topology for an SC-TP multiport ER, as a new solution for the integration of PV systems and BSS in residential buildings, is illustrated in Fig. 3.1. On the grid side, the single-stage common-ground inverter (SSCG-Inv) is an inverter with a single-stage design, which is capable of both voltage step-up and step-down operations [31]. A central dc bus (highlighted in orange) acts as the system backbone, interconnecting all power sources, inverters, and dc loads. This bus also facilitates potential interconnection with other nanogrids, thereby enhancing system scalability. For load management, ac loads are positioned between the inverter and the grid, enabling seamless operation in both grid-connected and islanded modes. Relays are deployed on the grid, inverter, and load sides to dynamically connect the inverter to the appropriate phase and supply ac loads accordingly. In this setup, the dc bus can interact with all three ac phases via the ER, though not simultaneously. Phase balancing is achieved by identifying and limiting power flow in the most heavily loaded phase. In typical three-phase residential or commercial buildings, the power drawn from each phase often varies significantly. The proposed approach helps mitigate this imbalance, offering economic advantages by eliminating the need for two additional conversion cells. This supports the adoption of a Single-Cell (SC) architecture over traditional three-phase conversion systems. On the source side, both the PV system and BSS are interfaced with the dc bus through dedicated dc-dc converters. The PV converter operates in buck and boost modes, depending on the panel's output voltage, while the

BSS is connected via a bidirectional interleaved dc-dc converter that efficiently manages high charging/discharging currents. The common-ground inverter structure not only addresses leakage current issues but also unifies the ac and dc ground references, enhancing system safety and protection [30]. Additionally, a Solid-State Circuit Breaker (SSCB) is integrated into the system to provide rapid fault isolation in the event of a short circuit [22].

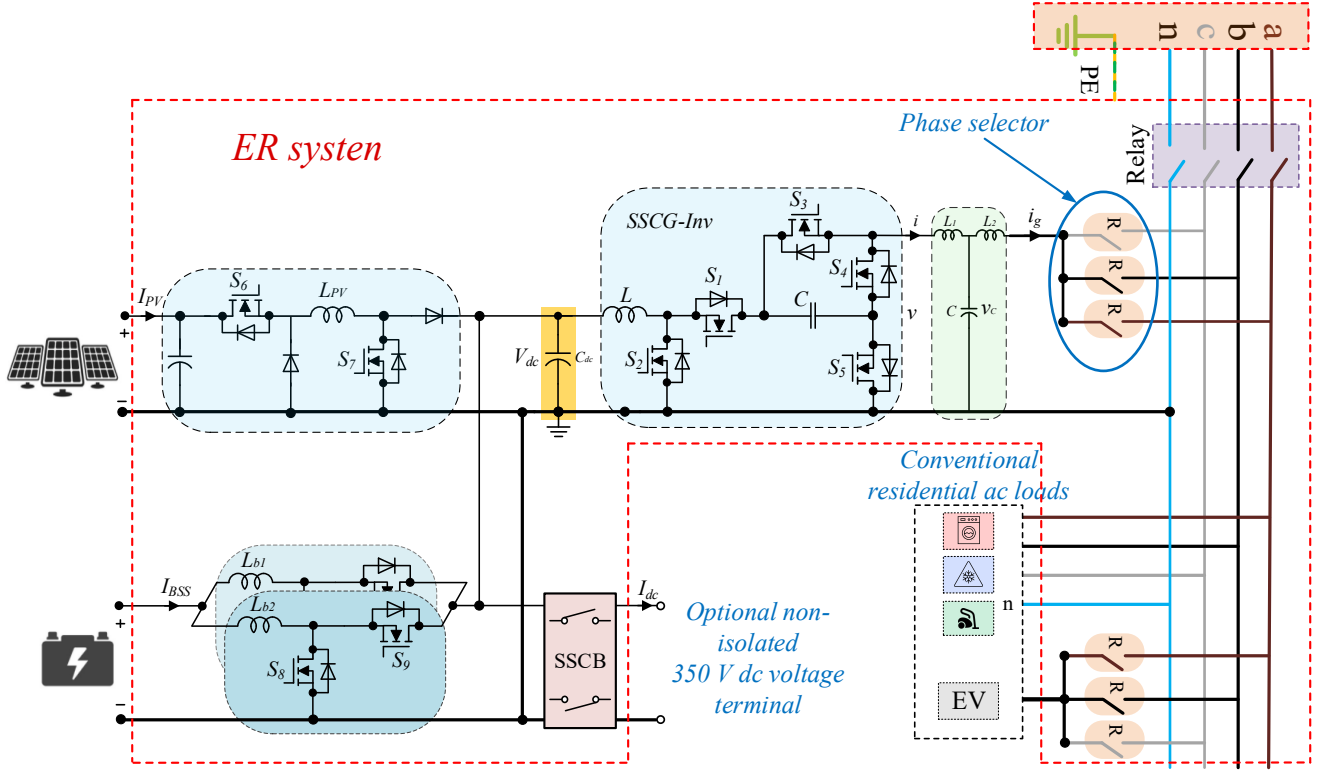


Fig. 3.1. Concept of proposed SC-TP multiport ER.

The rationale for adopting the SC topology over the Three-Cell (TC) ER is thoroughly discussed in [152]. It has been shown that the proposed SC-TP configuration not only enhances PV self-consumption and reduces phase unbalance compared to single-phase systems but also offers significant cost advantages relative to the TC-TP architecture. These benefits position the SC-TP topology as a compelling alternative to conventional single-phase approaches. By providing improved phase balancing, the SC-TP system effectively mitigates the adverse impacts of behind-the-meter distributed PV installations, enhances grid reliability and resilience, and enables more uniform load distribution across the three phases. These attributes collectively contribute to increased grid stability and reduced operational complexity for utility operators.

To realize these advantages, the deployment of a Smart Energy Management Algorithm (SEMA), operating alongside a fundamental low-level control algorithm, is essential. This SEMA is responsible for detecting, managing, and compensating for phase imbalances. However, the development of such an algorithm lies beyond the scope of this work. Instead, the present study focuses on the proposed hardware architecture and its associated low-level control layer, which is responsible for current control and regulating a stable dc-link voltage through appropriate control strategies.

3.2 Inverter, modulation, and designing the passive element

As previously mentioned, the common-ground inverter is used in the ER structure to eliminate leakage current and provide grounding in both ac and dc sides. This section focuses particularly on the common-ground inverter, its modulation, and the design of passive elements.

3.2.1 Single-stage common-ground inverter

Fig. 3.2 shows the structure of the common-ground inverter used in the ER. This structure has five switches, a capacitor, and an inductor. This topology was introduced in [31]. For this converter to be able to produce a sinusoidal output from the input dc voltage, it is necessary to have the ability to operate in three different conditions as boost, buck, and buck-boost [147]. Fig. 3.3 shows the desired sinusoidal output voltage curve and dc input voltage. According to this diagram, in the positive half cycle, when the output voltage is lower than the dc voltage, the converter should work in buck mode, and when the output voltage is higher, in boost mode. In the negative half cycle, the situation is completely different. In this case, this structure should work like a buck-boost converter because the polarity of its output voltage is negative. Each of these situations is examined below.

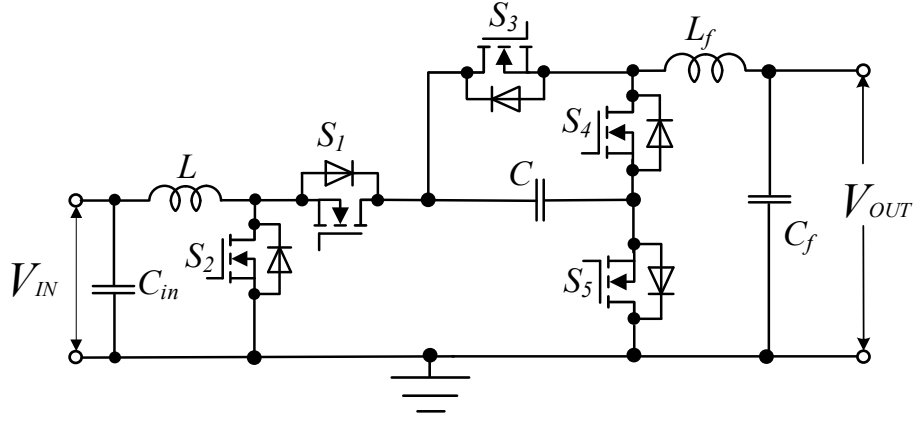


Fig. 3.2. The topology of the common-ground inverter used in ER.

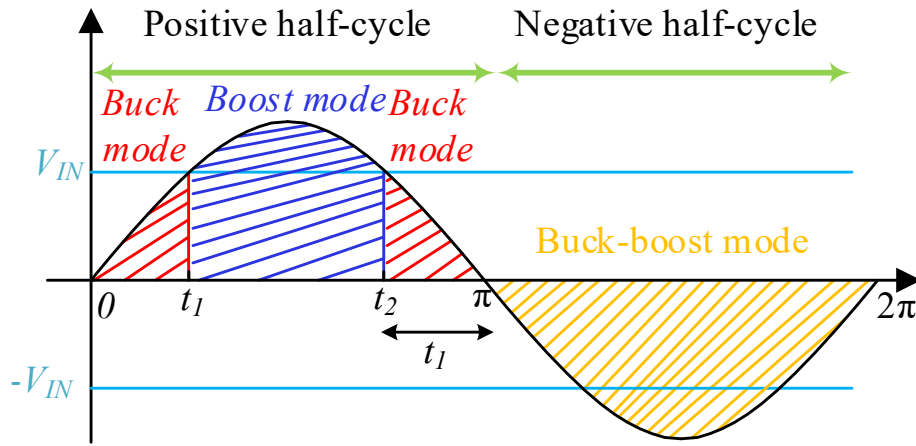


Fig. 3.3. Different operating modes of the common-ground inverter.

3.2.1.1 Boost operation

In the boost function, the switches in this structure must act in a way that increases the output voltage, similar to a boost converter. For this operation, S_3 and S_5 are always on, while S_4 is always off. S_1 and S_2 work in complementary mode. Fig. 3.4(a) and (b) show this function. In case A, the inductor is charged first and the output voltage is equal to the voltage of the intermediate capacitor. In state B, the inductor is discharged into the intermediate capacitor. The equations of this state are also in the following form. The duty cycle of the boost operation is controlled by S_2 . By extracting the equation of voltage across inductors in a period, we can write:

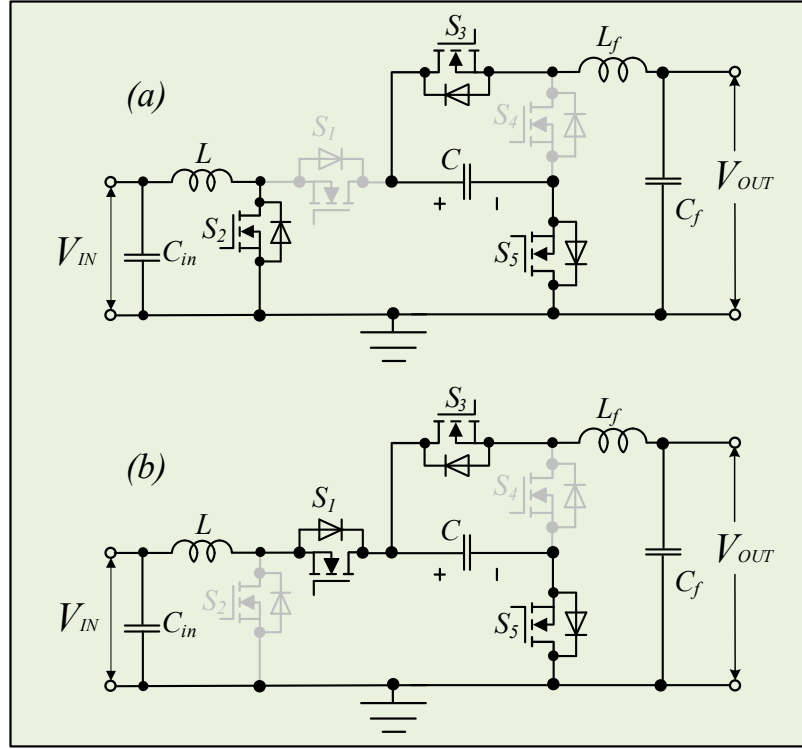


Fig. 3.4. Operating mode under dc-dc positive boosted output voltage (a): first state, (b): second state.

$$\langle V_L \rangle = \frac{1}{T_s} \int_0^{D_1 T_s} (V_{IN}) dt + \frac{1}{T_s} \int_{D_1 T_s}^{T_s} (V_{IN} - V_C) dt. \quad (3.1)$$

$$D_1 = 1 - \frac{\langle V_{IN} \rangle}{\langle V_C \rangle}. \quad (3.2)$$

$$\langle V_{L_f} \rangle = \frac{1}{T_s} \int_0^{T_s} (V_C - V_{OUT}) dt. \quad (3.3)$$

$$\langle V_C \rangle = \langle V_{OUT} \rangle. \quad (3.4)$$

$$D_1 = 1 - \frac{\langle V_{IN} \rangle}{\langle V_{OUT} \rangle}. \quad (3.5)$$

while in these equations, V_L is the voltage across the input-side inductor, V_C is the voltage across the inverter capacitor and V_{L_f} is the voltage across the output filter inductor. D_1 refers to the duty cycle of S_2 , which is responsible for the boost operation and T_s is the switching period. Values in $\langle \cdot \rangle$ refers to averaged value of the voltage.

3.2.1.2 Buck operation

Fig. 3.5 illustrates this operation. In this case, S_1 and S_5 are always on, and S_2 is off. S_3 and S_4 work in a complementary condition and perform the buck operation. The input source feeds the intermediate capacitor. Then this capacitor will be like a source for a simple buck converter. The filter inductor also stores energy and transfers it to the output. D_2 refers to the duty cycle of S_3 , which is responsible for the buck operation. The equations of this function are as follows.

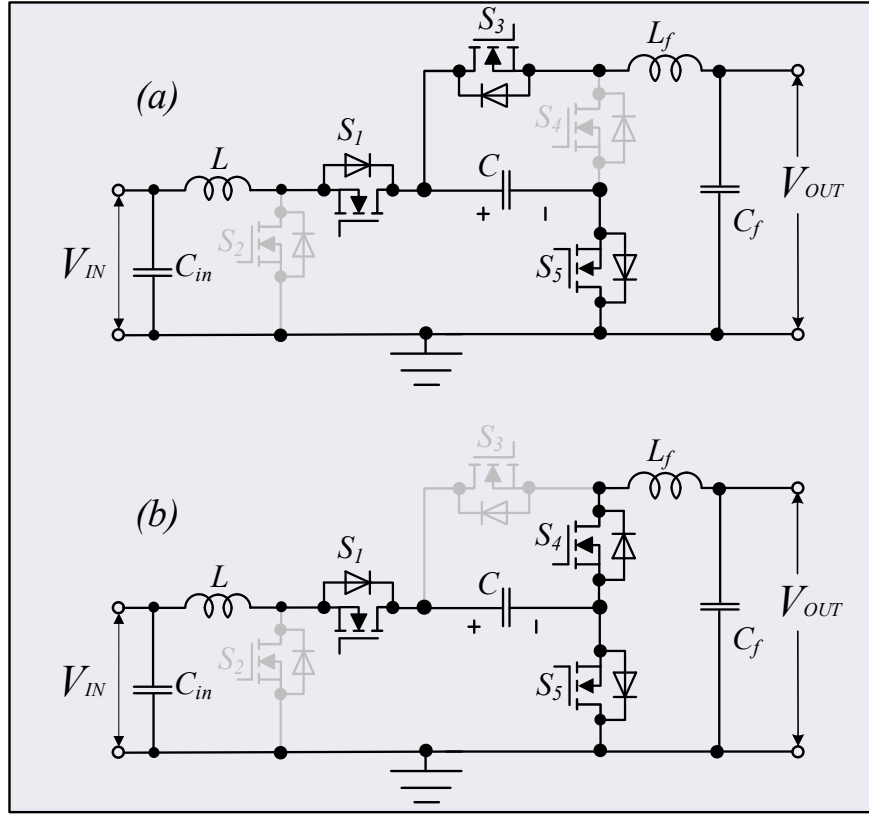


Fig. 3.5. Operating mode under dc-dc positive stepped down output voltage (a): first state, (b): second state.

$$\langle V_L \rangle = \frac{1}{T_s} \int_0^{T_s} (V_{IN} - V_C) dt. \quad (3.6)$$

$$\langle V_{IN} \rangle = \langle V_C \rangle. \quad (3.7)$$

$$\langle V_{L_f} \rangle = \frac{1}{T_s} \int_0^{D_2 T_s} (V_C - V_{OUT}) dt + \frac{1}{T_s} \int_{D_2 T_s}^{T_s} (-V_{OUT}) dt. \quad (3.8)$$

$$D_2 = \frac{\langle V_{OUT} \rangle}{\langle V_C \rangle}. \quad (3.9)$$

$$D_2 = \frac{\langle V_{OUT} \rangle}{\langle V_{IN} \rangle}. \quad (3.10)$$

3.2.1.3 Buck-boost operation

In this case (Fig. 3.6), for having a negative output voltage, this structure should act like a buck-boost converter. S_1 and S_4 are always on, and S_3 is always off for this operation. S_2 and S_5 work in complementary mode, and the duty cycle value of S_2 (D_3) determines the buck or boost gain. The output equations in this case are as follows.

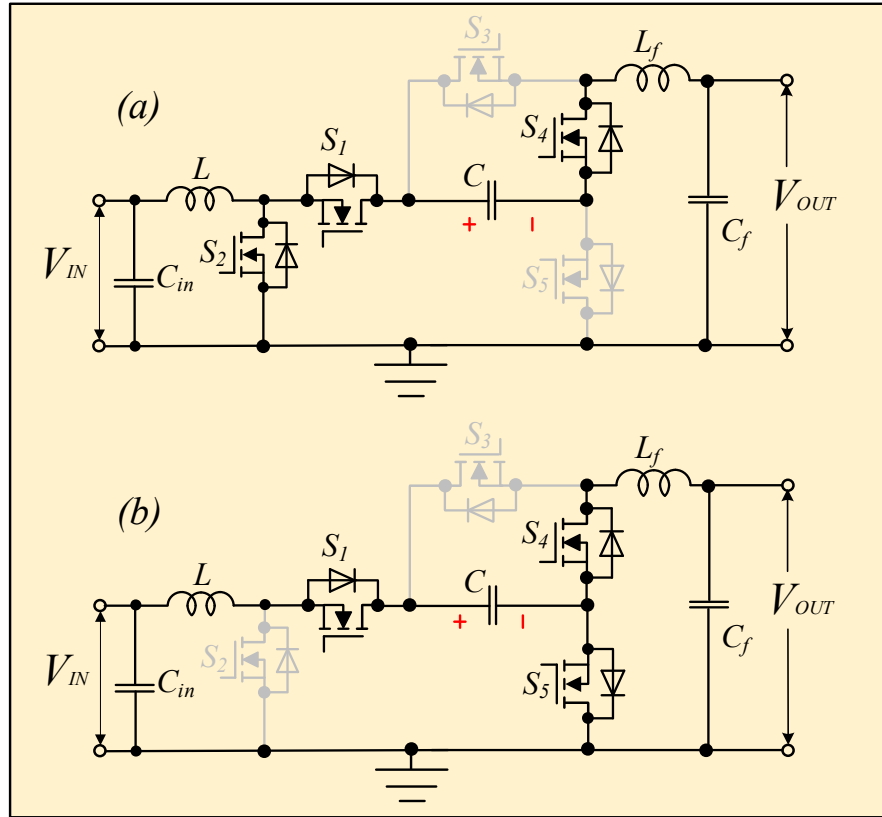


Fig. 3.6. Operating mode under dc-dc negative buck-boost mode (a): first state, (b): second state.

$$\langle V_L \rangle = \frac{1}{T_s} \int_0^{D_3 T_s} (V_{IN}) dt + \frac{1}{T_s} \int_{D_3 T_s}^{T_s} (V_{IN} - V_C) dt. \quad (3.11)$$

$$D_3 = 1 - \frac{\langle V_{IN} \rangle}{\langle V_C \rangle}. \quad (3.12)$$

$$\langle V_{L_f} \rangle = \frac{1}{T_s} \int_0^{D_3 T_s} (V_C - V_{OUT}) dt + \frac{1}{T_s} \int_{D_3 T_s}^{T_s} (-V_{OUT}) dt. \quad (3.13)$$

$$\langle V_C \rangle = \frac{\langle V_{OUT} \rangle}{D_3}. \quad (3.14)$$

$$D_3 = \frac{\langle V_{OUT} \rangle}{\langle V_{OUT} \rangle + \langle V_{IN} \rangle}. \quad (3.15)$$

Therefore, the modulation of this inverter will be in such a way that, according to Fig. 3.3, one of the above functional states is selected and the desired sinusoidal output is produced. Table 3.1 shows the switching table for each of the cases, and Table 3.2 also shows the voltage stress on the switches in each of the cases. The way to implement this modulation can also be implemented by comparing the reference sinusoidal value with the dc voltage and finally applying equations 3.5, 3.10, and 3.15.

Table 3.1

Inverter switching pattern.

| | Positive half cycle | | | Negative half cycle |
|----------------------|----------------------------|--------------------------------------|--------------------------|----------------------------|
| Switches | [0-t₁] | [t₁-t₂] | [t₂-π] | [π-2π] |
| S₁ | 1 | 1-D ₁ | 1 | 1 |
| S₂ | 0 | D ₁ | 0 | D ₃ |
| S₃ | D ₂ | 1 | D ₂ | 0 |
| S₄ | 1-D ₂ | 0 | 1-D ₂ | 1 |
| S₅ | 1 | 1 | 1 | 1-D ₃ |

Table 3.2

Inverter voltage stress.

| Mode | S₁ | S₂ | S₃ | S₄ | S₅ | Capacitor |
|-------------------|--------------------------------------|--------------------------------------|--------------------------------------|--------------------------------------|--------------------------------------|--------------------------------------|
| Buck | 0 | V _{IN} | V _{IN} | V _{IN} | 0 | V _{IN} |
| Boost | V _{IN} /(1-D ₁) | V _{IN} /(1-D ₁) | 0 | V _{IN} /(1-D ₁) | 0 | V _{IN} /(1-D ₁) |
| Buck-boost | 0 | V _{IN} /(1-D ₃) | V _{IN} /(1-D ₃) | 0 | V _{IN} /(1-D ₃) | V _{IN} /(1-D ₃) |

3.2.2 Inverter component design

For the design of the passive components of the common ground inverter, the inverter parameter values are given in Table 3.3. As can be found in the table, the permissible voltage ripple across the capacitor is 10% and the inductor current ripple is 20% of the input current. Using general equations 16 and 17, the inductor and capacitor in this inverter can be designed. In equation 3.16, I_C , f_{SW} , ΔV_C , and D stand for the capacitor current, switching frequency, voltage ripple over the capacitor and the duty cycle, respectively. Also, in equation 3.17, V_L , f_{SW} , ΔI_L , and D stand for the voltage across L , the switching frequency, the current ripple of the inductor, and the duty cycle.

Table 3.3

Design parameter

| | |
|-----------------------------------|---------------------------|
| Peak value of grid voltage | 325 Vac |
| Maximum output power | 7000 W |
| Input voltage range | 320 – 380 V |
| Voltage ripple across C | 0.1 V_C |
| Current ripple of L | 0.2 I_{IN} |
| Switching frequency | 65kHz |

$$C = \frac{D \times I_C}{f_{SW} \times \Delta V_C}. \quad (3.16)$$

$$L = \frac{D \times V_L}{f_{SW} \times \Delta I_L}. \quad (3.17)$$

Given that the inverter in question operates in three modes: buck, boost, and buck-boost, the corresponding duty cycle (equations 3.5, 3.10, and 3.15), capacitor current for capacitor design, and inductor voltage for inductor design for each mode are substituted into equations 3.16 and 3.17. The inductor and capacitor values are obtained for each

mode. In equations 3.18-3.20, input and output current can be calculated through the input and output voltage and the power of the inverter. In equation 3.21 also it should be mentioned that the input voltage and the capacitor voltage are equal and therefore the required inductor in this case is zero, and the buck operation is done through the inductor filter. Finally, the largest value for the capacitor in equations 3.18-3.20 and the largest value for the inductor in equations 3.21-3.23, or in other words, the worst case, are considered for the inductor and capacitor.

$$C_{Buck} = \frac{|\langle I_{IN} \rangle - \langle I_{OUT} \rangle|}{f_{SW} \times \Delta V_C} \times \left(\frac{\langle V_{OUT} \rangle}{\langle V_{IN} \rangle} \right). \quad (3.18)$$

$$C_{Boost} = \frac{\langle I_{OUT} \rangle}{f_{SW} \times \Delta V_C} \times \left(1 - \frac{\langle V_{IN} \rangle}{\langle V_{OUT} \rangle} \right). \quad (3.19)$$

$$C_{Buck-Boost} = \frac{\langle I_{OUT} \rangle}{f_{SW} \times \Delta V_C} \times \left(\frac{\langle V_{OUT} \rangle}{\langle V_{OUT} \rangle + \langle V_{IN} \rangle} \right). \quad (3.20)$$

$$L_{Buck} = \frac{\langle V_{IN} \rangle - \langle V_C \rangle}{f_{SW} \times \Delta I_L} \times \left(\frac{\langle V_{OUT} \rangle}{\langle V_{IN} \rangle} \right). \quad (3.21)$$

$$L_{Boost} = \frac{\langle V_{IN} \rangle}{f_{SW} \times \Delta I_L} \times \left(1 - \frac{\langle V_{IN} \rangle}{\langle V_{OUT} \rangle} \right). \quad (3.22)$$

$$L_{Buck-Boost} = \frac{\langle V_{IN} \rangle}{f_{SW} \times \Delta I_L} \times \left(\frac{\langle V_{OUT} \rangle}{\langle V_{OUT} \rangle + \langle V_{IN} \rangle} \right). \quad (3.23)$$

3.2.3 dc-dc converters component design

For the PV converter in Fig. 3.1, there are two operation modes: simple buck while S_7 is off and S_6 is switching with buck mode duty cycle (D_{buck}), and boost operation while S_6 is on and S_7 is switching with boost mode duty cycle (D_{boost}). In buck mode, the required inductor can be calculated as in 3.24, and for boost mode as in 3.25.

$$L_{PV} = \frac{V_{dc} \times (1 - D_{buck})}{f_{SW} \times \Delta I_L}, \quad (3.24)$$

$$L_{PV} = \frac{V_{PV} \times D_{boost}}{f_{SW} \times \Delta I_L}, \quad (3.25)$$

while V_{dc} is the dc-link voltage, V_{PV} is the PV voltage, f_{SW} is the switching frequency and ΔI_L is the inductor current ripple.

Replacing the duty cycle in each case equations 3.26 and 3.27 will be driven. Finally larger value will be chosen as the worst case. It should also be mentioned that for this calculation, the upper and lower PV voltage should be tested to find the worst case.

$$L_{PV-Buck} = \frac{V_{dc} \times (V_{PV} - V_{dc})}{f_{SW} \times \Delta I_L \times V_{PV}}. \quad (3.26)$$

$$L_{PV-Boost} = \frac{V_{PV} \times (V_{dc} - V_{PV})}{f_{SW} \times \Delta I_L \times V_{PV}}. \quad (3.27)$$

To calculate the inductors of the BSS interleaved dc-dc converter in Fig. 3.1 for the boost case or discharging mode, the same equations as 3.25 and 3.27 can be used. Reminding that the current ripple will be half, and the battery voltage (V_{BSS}) will be used instead of the PV voltage. As below:

$$L_{BSS-Boost} = \frac{V_{BSS} \times (V_{dc} - V_{BSS})}{f_{SW} \times \Delta I_L / 2 \times V_{BSS}}. \quad (3.28)$$

In charging or buck mode of BSS, the buck equations 3.24 and 3.26 can also be used, considering that the current ripple will be half, the input voltage will be the dc link voltage, and the output voltage will be the battery voltage. As below:

$$L_{BSS-Buck} = \frac{V_{BSS} \times (V_{dc} - V_{BSS})}{f_{SW} \times \Delta I_L / 2 \times V_{dc}}. \quad (3.29)$$

It should be mentioned that in interleave mode, the values of inductors are equal and equations 3.28 and 3.29 are the values of each one. Finally, by calculating equations 3.28 and 3.29, the larger value will be chosen for the inductors of the battery side converter.

3.3 Safety and protection

As discussed in previous parts, common-ground structures can be a reliable solution to mitigate leakage currents. At the same time, to protect personnel and equipment, RCD is installed in the grid-side input. Fig. 3.7(a) shows a simple schematic of grounding on both sides of the common-ground inverter. The neutral point of ac grid is solidly grounded, which is also connected to the M point in dc part, eliminating leakage

current paths. As can be seen, bodies of loads, inverter, etc., are connected to the ground through the ground impedance Z_{gDC} . Fig. 3.7(b) shows the case when a person touches the hot line (L+) and the residual current path. In this case, the residual current will pass through the capacitors in the inverter structure and the neutral wire of ac side. Therefore, the RCD will trip and disconnect the grid.

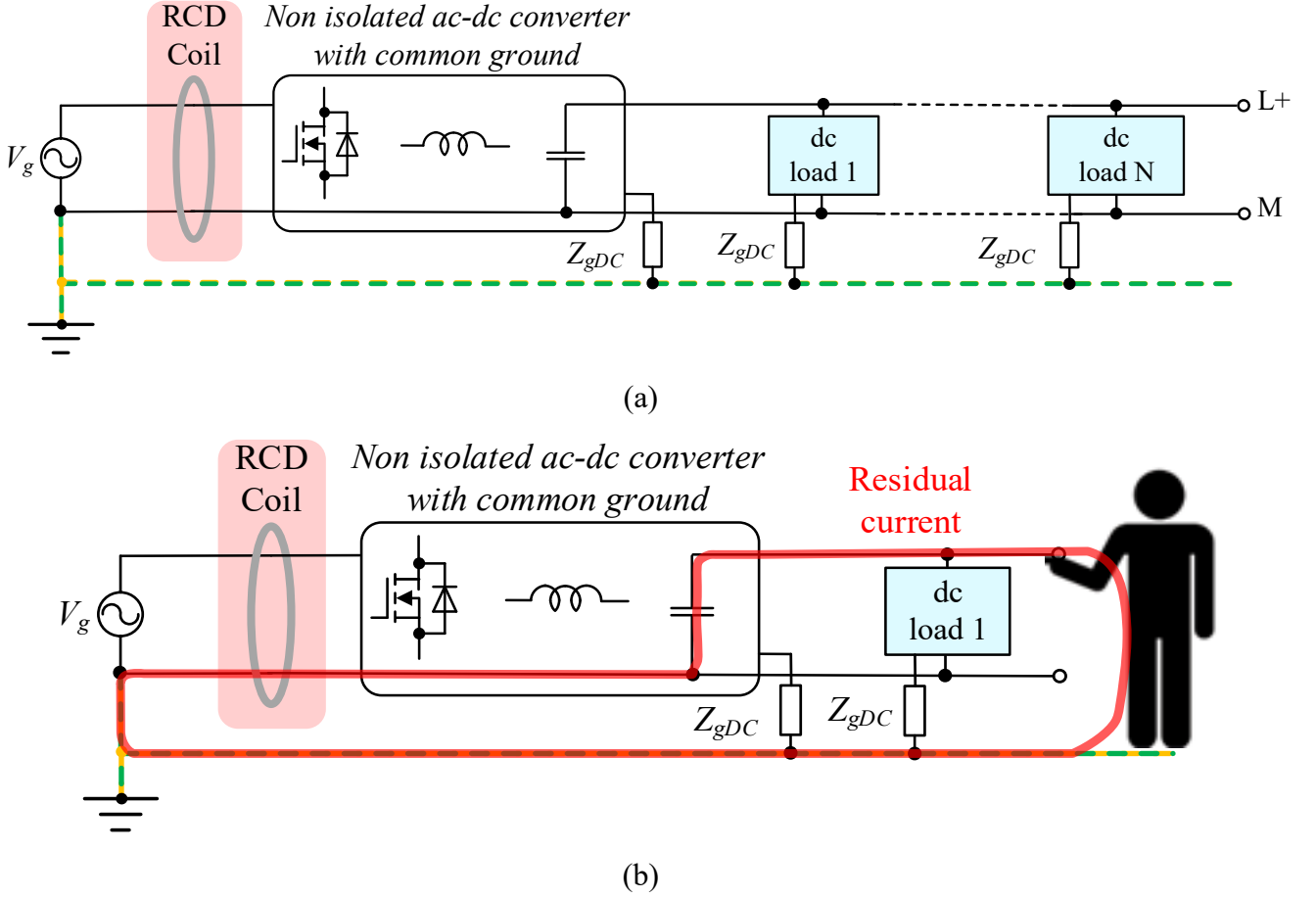


Fig. 3.7. Protection and grounding for the proposed ER (a), residual current path in case of touching the hot line.

3.4 Solid-state circuit breaker

The proposed ER in this work employs a dc link to supply loads or connect with other nanogrids, requiring protection against short circuits and fast fault interruption. Since dc system lacks a zero-crossing point and fault currents rise rapidly, a reliable protection structure is essential. Various dc circuit breaker (DCCB) technologies have been developed, generally classified as electromechanical, solid-state, and hybrid. Electromechanical breakers suffer from arcing, slow operation, and component damage.

Solid-state DCCBs, using devices such as SCRs, IGBTs, or MOSFETs, offer faster performance, while hybrid designs combine electromechanical and solid-state features, reducing losses but at a higher cost and with limited speed. In this work, a solid-state DCCB, as presented in [22], is adopted for the ER. This structure is shown in Fig. 3.8. As can be seen, three MOSFETs, four diodes, and a snubber are used in this structure.

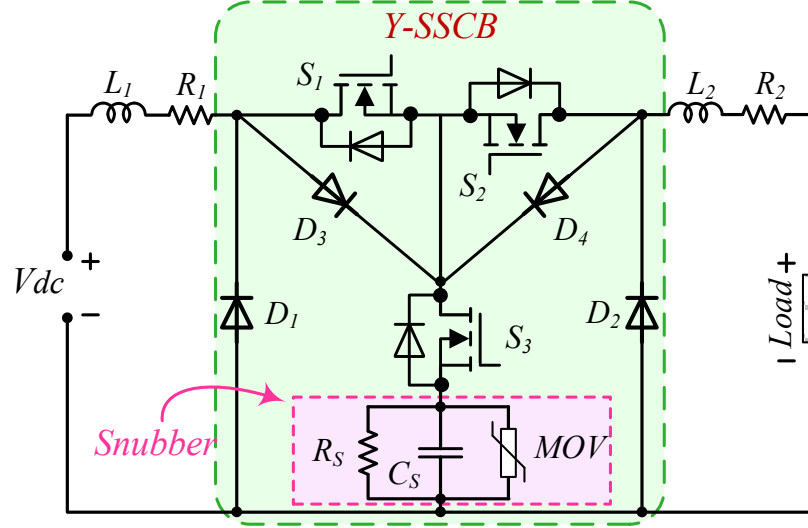


Fig. 3.8. Topology of the SSCB used in ER structure [22].

In normal operation, the dc load is supplied through the MOSFETs S_1 and S_2 path, and in the event of a short circuit, the MOSFET S_3 turns on and the short-circuit path is disconnected from the dc link. The current in the inductors L_1 and L_2 also continues through the diodes D_3 and D_2 path. The snubber circuit also reduces di/dt due to S_3 switching.

This topology has the following characteristics:

1. Total input and output isolation both during and after the outage, improving the safety level.
2. By removing the snubber from the main switch and power line, the leakage current from the MOV is minimized, increasing the switches' voltage usage and dependability.
3. This design avoids using the main path switches for fault clearance, increasing reliability.
4. The snubber capacitor is quickly and completely discharged before reclosing.

5. High modularity and higher power density as a result of the switches' enhanced voltage utilization rate.
6. Reduced switch voltage overshoot.

Considering the above-mentioned features, using this DCCB, which has a relatively low number of components at a reasonable cost, seems to be a logical choice for ER structure.

3.5 Conclusion

This chapter presented the proposed SC-TP hybrid ER and described the benefits of the SC-TP topology. Focusing on the common-ground inverter, its modulation was analyzed for different modes to produce a sinusoidal voltage waveform. Besides the component design for different parts, it was shown that using a common-ground inverter not only eliminates leakage current paths, but also provides grounding for both sides without isolation and subsequently lowers the weight and cost. Regarding the protection, and RCD protection and DCCB were described. It was demonstrated that RCD will trip in the event of leakage current on both dc and ac sides, ensuring safety. The used DCCB also protected against short circuits with minimum components and reliable operation.

4 CONTROL SYSTEM

Along with the structural layout, the control system of ER at different levels is also a topic of much research. As it was described in the first chapter, in low and mid-level control, classical control strategies are primarily used and designed to regulate the dc link and manage power exchange with the grid. While these methods demonstrate acceptable performance, they often exhibit relatively slow dynamic responses [32]. To enhance the system response in dynamic conditions, other solutions have been proposed in various studies.

Among the control methods suitable for dynamic conditions and nonlinear systems, FBC theory has been introduced as a fast and reliable solution in dynamic conditions [39]. This control method, initially introduced by M. Fliess, demonstrates excellent performance in managing nonlinear systems and provides robust capabilities for systems with multiple state variables and inputs. Therefore, it can be a promising control solution for ER where there are multiple power sources and sinks.

In this chapter, an FBC strategy is designed and used for the proposed ER to regulate the dc link voltage and to control the grid-side current with a cascade dual-loop structure. This solution is proposed to handle dynamic conditions in ERs, where conventional methods may fail. In addition to FBC, the PR method has also been investigated as a reliable alternative to control grid current due to its inherent capability to achieve zero steady-state error for sinusoidal signals and its robustness in eliminating higher-order harmonics.

4.1 Proposed solution in low-level control

Given the complex structure of the ER, where multiple sources and loads are interconnected through a common dc link, implementing a control strategy that ensures fast and accurate dynamic response is crucial. FBC can be a promising solution for dynamic conditions in the power electronics field [153]-[156]. Among the available control methods, FBC offers distinct advantages. This method, which is used for nonlinear and multivariable systems, has a fast and accurate response in dynamic conditions. This approach aims to extract an equivalent model of a system that satisfies

the flat system requirement. In the FBC method, knowing the algebraic relations of the system is enough, and with the algebraic and analytical relations, the system can be controlled effectively. Therefore, the volume of system calculations is reduced and, unlike the MPC method, it does not require solving the optimization problem at each time step. However, this method also has limitations. The most important limitation is that the system should have a flat output, or in other words, system variables should be defined in such a way that the overall conditions of the flat system can be met. Like the MPC method, this method also requires a mathematical model of the system, and if the parameters change drastically, the controller's performance decreases.

Considering the above, FBC can be a promising option for a multi-port ER in low-level control. To use this control method, the system should meet flat conditions. In the following, the flat system is first defined, and then FBC is applied in the low-level control of ER. Since the FBC control on the grid side is in the dq reference frame and the ER structure is single-phase, first, how to apply dq transmission in the single-phase system is investigated.

4.1.1 Theoretical foundation of the single-phase rotating dq reference frame transformation

As is known, the conventional dq transformation derived from the abc frame (time-domain variables) applies only to three-phase systems. This method has been extensively employed in applications such as active power filters and reactive power compensation, since it converts the fundamental frequency components into dc quantities [157157]. The linear mapping from abc signals in the time domain to synchronous dq reference components is expressed in (4.1):

$$\begin{bmatrix} v_d \\ v_q \\ v_0 \end{bmatrix} = \frac{2}{3} \begin{bmatrix} \sin \omega t & \sin (\theta - 2\pi/3) & \sin (\theta + 2\pi/3) \\ \cos \omega t & \cos (\theta - 2\pi/3) & \cos (\theta + 2\pi/3) \\ 1/2 & 1/2 & 1/2 \end{bmatrix} \begin{bmatrix} v_a \\ v_b \\ v_c \end{bmatrix}. \quad (4.1)$$

Here, θ is the ωt and ω denotes the electrical angular frequency. The three-phase abc variables (currents or voltages) can also be projected onto the rotating dq frame by first applying the Clarke transformation to obtain the orthogonal stationary $\alpha\beta$

components (equation (4.2)), followed by the Park transformation into the synchronous dq frame using expression (4.3):

$$\begin{bmatrix} v_\alpha \\ v_\beta \end{bmatrix} = \frac{\sqrt{2}}{3} \begin{bmatrix} 1 & -1/2 & 1/2 \\ 0 & \sqrt{3}/2 & -\sqrt{3}/2 \end{bmatrix} \begin{bmatrix} v_a \\ v_b \\ v_c \end{bmatrix}, \quad (4.2)$$

$$\begin{bmatrix} v_d \\ v_q \end{bmatrix} = \begin{bmatrix} \sin\omega t & -\cos\omega t \\ \cos\omega t & \sin\omega t \end{bmatrix} \begin{bmatrix} v_\alpha \\ v_\beta \end{bmatrix}. \quad (4.3)$$

Expression (4.3) is derived by rotating the stationary $\alpha\beta$ frame at the fundamental frequency, which requires two orthogonal components to obtain the corresponding dq values. This becomes a challenge in single-phase circuits, where only one signal (voltage or current) is available. To address this, several methods have been developed to generate the missing orthogonal component, thereby enabling the application of dq theory in single-phase systems.

In [158], [159], the concept of an orthogonal imaginary circuit is introduced, where two signals are defined: the real component (measured voltage or current) and an imaginary one, having the same properties but shifted by a quarter of the fundamental period.

From a practical standpoint, if the real signal is measured, the orthogonal component can be obtained using a simple time-delay approach (storing the signal value). In this way, the measured signal represents the α component, while its delayed version represents the β component, as illustrated in Fig. 4.1(a).

The mathematical foundation for this method, assuming the real signal is sinusoidal, is presented below (example for a voltage signal):

$$\begin{cases} v_r = v_\alpha = V \sin(\omega t + \varphi) \\ v_i = v_\beta = V \sin(\omega t + \varphi - \pi/2) = -V \cos(\omega t + \varphi) \end{cases}, \quad (4.4)$$

where v_r and v_i are the real and imaginary signals corresponding to v_α and v_β . In order to extract the dc values in the dq rotating frame from ac signals (Fig. 4.1(b)), it is necessary to apply the linear transformation given in (4.4):

$$\begin{bmatrix} v_d \\ v_q \end{bmatrix} = \begin{bmatrix} \sin\omega t & -\cos\omega t \\ \cos\omega t & \sin\omega t \end{bmatrix} \begin{bmatrix} v_\alpha \\ v_\beta \end{bmatrix}. \quad (4.5)$$

Finally, the inverse transformation from dq signals to $\alpha\beta$ is given by (4.8):

$$\begin{bmatrix} v_\alpha \\ v_\beta \end{bmatrix} = \begin{bmatrix} \sin \omega t & \cos \omega t \\ \cos \omega t & -\sin \omega t \end{bmatrix} \begin{bmatrix} v_d \\ v_q \end{bmatrix}. \quad (4.6)$$

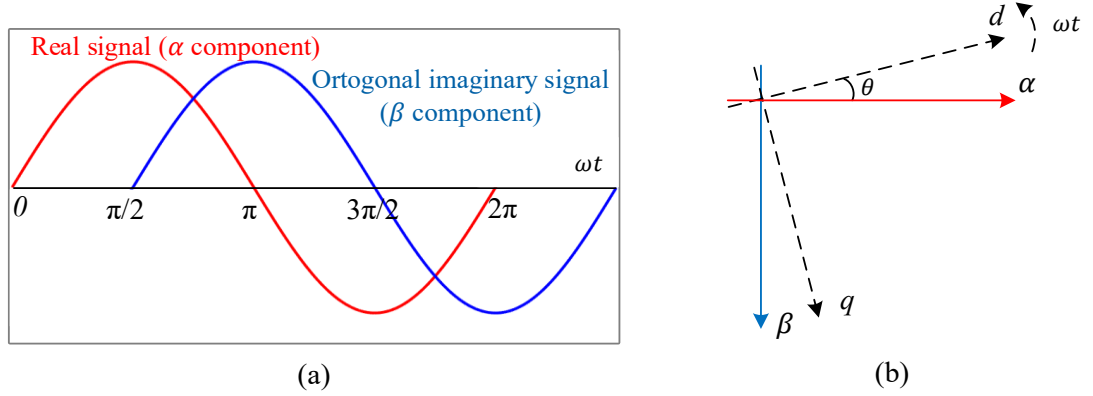


Fig. 4.1. Real and imaginary signals (a), $\alpha\beta$ to rotating dq reference frame transformation (b).

4.1.2 Flat system

By definition, a flat system is a system for which a set of flat outputs can be found such that the control variable and the control input can be written in terms of those outputs and their derivatives. From a mathematical point of view, if the system $\dot{x} = f(x, u)$ has a state $x \in R^n$, and an input $u \in R^m$, then the system is differentially flat if an output $y \in R^m$, can be found in the form:

$$y = \phi(x, u, \dot{u}, \dots, u^{(l)}), \quad (4.7)$$

when,

$$x = \varphi(y, \dot{y}, \dots, y^{(r)}), \quad (4.8)$$

And,

$$u = \psi(y, \dot{y}, \dots, y^{(r+1)}), \quad (4.9)$$

Which means this system is differentially flat, and the mapping of (φ, ψ) is called Lie-Backlund isomorphism and defines a flat system. l and r are also the number of time derivatives. Fig. 4.2 shows a system model in both normal and corresponding flat models. This method transforms a system defined in a complex space with integral curves into a simpler space characterized by simple trajectories, without relying on differential equations or imposing constraints on the variables. Consequently, system control in this transformed space is expected to yield faster and more precise responses.

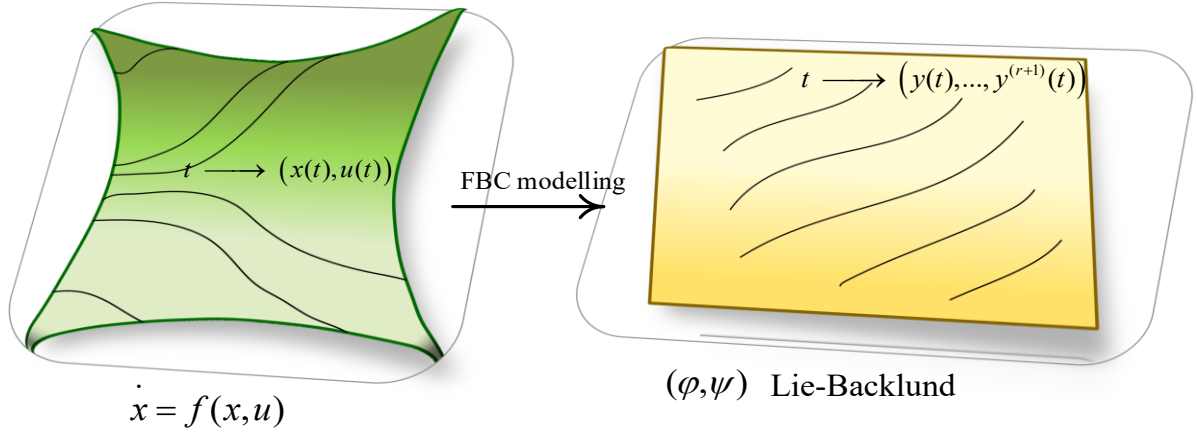


Fig. 4.2. System modelling and its control trajectories.

Considering control levels in the first chapter, the ER low-level controller in grid-connected mode employs a dual-loop control structure: an outer loop regulates the dc-link voltage, while an inner loop tracks the inverter's reference current. Consequently, FBC should be implemented in a cascaded configuration. Once it is applied to the dc-link subsystem to establish the inverter reference current, it is then utilized at the inverter's output side to ensure precise tracking and regulation of the inverter reference current. System modelling.

Before formulating and developing the FBC control laws, it is essential to derive the fundamental equations governing the ER. By applying Kirchhoff's voltage law (KVL) and Kirchhoff's current law (KCL) to the inverter output and the LCL filter in the grid side of the inverter (Fig. 4.3), the mathematical model governing the inverter-side dynamics can be expressed as follows:

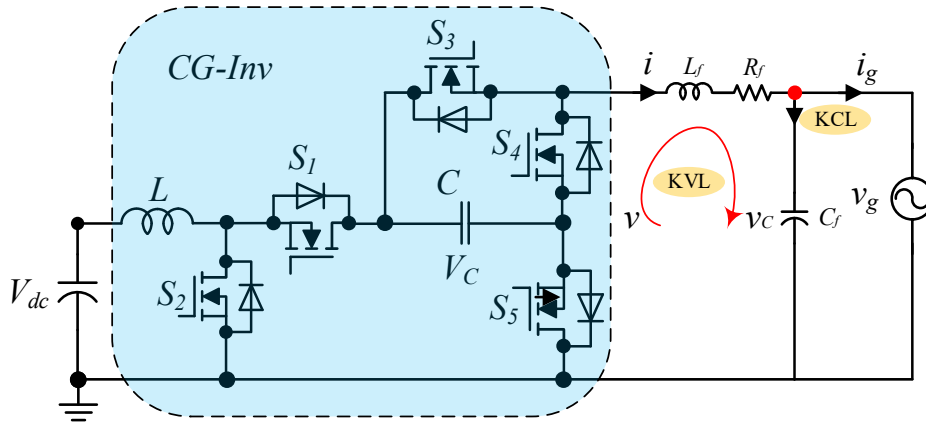


Fig. 4.3. ER inverter and its LC filter.

$$\frac{di}{dt} = \frac{1}{L_1}(v - R_1 i - v_C), \quad (4.9)$$

$$\frac{di_g}{dt} = \frac{1}{L_2}(v_C - R_2 i_g - v_g), \quad (4.10)$$

$$\frac{dv_C}{dt} = \frac{1}{C}(i - i_g), \quad (4.11)$$

where L_1 , L_2 , and C are the LCL filter inductors and capacitors, respectively. R_1 and R_2 are the internal resistance of the inductors in the LCL filter.

In the dq frame, these equations will be written as:

$$\frac{di_d}{dt} = \frac{1}{L_1}(v_d - R_1 i_d - v_{Cd}) + \omega i_q, \quad (4.12)$$

$$\frac{di_q}{dt} = \frac{1}{L_1}(v_q - R_1 i_q - v_{Cq}) - \omega i_d, \quad (4.13)$$

$$\frac{di_{gd}}{dt} = \frac{1}{L_2}(v_{Cd} - R_2 i_{gd} - v_{gd}) + \omega i_{gq}, \quad (4.14)$$

$$\frac{di_{gq}}{dt} = \frac{1}{L_2}(v_{Cq} - R_2 i_{gq} - v_{gq}) - \omega i_{gd}, \quad (4.15)$$

$$\frac{dv_{Cd}}{dt} = \frac{1}{C}(i_d - i_{gd}) + \omega v_{Cq}, \quad (4.16)$$

$$\frac{dv_{Cq}}{dt} = \frac{1}{C}(i_q - i_{gq}) - \omega v_{Cd}, \quad (4.17)$$

where i_d , i_q , are dq components of the inverter side current, and v_d and v_q are the dq components of the inverter output voltage. i_{gd} , i_{gq} , v_{Cd} , and v_{Cq} are also the dq components of the grid side current and the voltage across the filter capacitor, respectively. Finally, ω is the angular frequency.

The mathematical equation governing the dc link should also be considered. It is evident that the power in the dc link is equal to the sum of the input and output powers to the dc link. It means the sum of the input and output powers in the dc link is equal to the power available in the dc link as follows:

$$\text{Total power in dc lin} = P_{PV} + P_{BSS} + P_{dc} + P_{Inv}, \quad (4.18)$$

where P_{PV} is the PV power, P_{BSS} is the BSS power, P_{dc} is the power of dc loads, and P_{Inv} is the inverter power. For input power to dc link, it is considered positive, and for output power, the sign of power should be negative. Accordingly, the dc load power (P_{dc}) is always negative, and P_{PV} is always positive.

4.1.3 Dc-link voltage regulation

The dc-link voltage in grid-connected mode is controlled by the inverter reference current. To apply FBC in dc link, the energy available in the dc link is considered as the flat output (e_{dc}), the dc voltage as the control variable (V_{dc}), and the inverter power as the control input (P_{Inv}) with the following definitions:

$$\begin{cases} y = e_{dc} \\ x = V_{dc} \\ u = P_{Inv} \end{cases} \quad (4.19)$$

With these conditions, the system can be differentially flat, and the V_{dc} can be controlled through the P_{Inv} and subsequently the inverter current. In this regard, the energy in the dc link is estimated by the following equation:

$$e_{dc} = \frac{1}{2} C_{dc} V_{dc}^2, \quad (4.20)$$

where e_{dc} is the energy in the link, C_{dc} is the capacitance value of the dc-link capacitor, and V_{dc} is the dc-link voltage. From the power point of view, the power in the dc-link is the derivative of energy, which is the total power in the dc link:

$$\dot{e}_{dc} = P_{PV} \pm P_{BSS} - P_{dc} \pm P_{Inv}. \quad (4.21)$$

It should be mentioned that the EMS set the P_{PV} and P_{BSS} . P_{dc} can also be measured through the dc-load current. The power direction should also be considered by the corresponding signs as previously mentioned. Then, rewriting (4.20) to obtain V_{dc} :

$$V_{dc} = \sqrt{\frac{2e_{dc}}{C_{dc}}} \Rightarrow x = \varphi(y). \quad (4.22)$$

Therefore, the state variable (V_{dc}) is a function of flat output (e_{dc}). Also, from (4.21) and considering positive signs for P_{Inv} and P_{BSS} , and rewriting P_{dc} in terms of V_{dc} :

$$\begin{aligned} P_{Inv} = P_{PV} + P_{BSS} - \frac{V_{dc}^2}{R_{dc}} - \dot{e}_{dc} &= P_{PV} + P_{Bat} - \frac{2e_{dc}}{C_{dc}R_{dc}} - \dot{e}_{dc} \Rightarrow \\ u = \psi(y, \dot{y}), \end{aligned} \quad (4.23)$$

which proves that the input variable is a function of flat output and its derivative. Considering the flat system criteria, it can be concluded that this system is differentially flat.

4.1.4 Inverter current control

The second FBC is considered for the inner control loop, and it works based on the dq components of the inverter voltage and current. Considering the mathematical modeling equations of the inverter output filter in dq coordinates, the flat output and control variable are considered the same as i_d and i_q , and the control inputs are considered as v_d and v_q . The following equations show these assumptions to reach the conditions of the flat system:

$$y = \begin{bmatrix} i_d \\ i_q \end{bmatrix}, \quad x = \begin{bmatrix} i_d \\ i_q \end{bmatrix}, \quad u = \begin{bmatrix} v_d \\ v_q \end{bmatrix}. \quad (4.24)$$

From (4.24), it is clear that $x=y$, and then $x=\phi(y)$, which means the control variable is a function of flat output. Then, from (4.12), it can be written,

$$v_d = L_1 \dot{i}_d + R_1 i_d - \omega L_f i_q + v_{cd} \Rightarrow u_1 = \psi(y_1, \dot{y}_1, y_2), \quad (4.25)$$

and from (4.13):

$$v_q = L_1 \dot{i}_q + R_1 i_q + \omega L_f i_d + v_{cq} \Rightarrow u_2 = \psi(y_2, \dot{y}_2, y_1). \quad (4.26)$$

Therefore, the input variables can also be expressed in terms of flat outputs and their derivatives, meaning the considered system is differentially flat.

4.1.5 Design process

The control system works based on the control inputs “ u ” in equations (4.23), (4.25), and (4.26). In these equations, other terms are available, and just the derivative of the control output “ \dot{y} ” should be obtained. For this purpose, using a linear feedback control law with the following equation \dot{y} can also be obtained [160], [161]:

$$(\dot{y} - \dot{y}_{Ref}) + K_{11}(y - y_{Ref}) + K_{12} \int_0^t (y - y_{Ref}) d\tau = 0, \quad (4.27)$$

while y_{Ref} is the reference value of the control output. Also, K_{11} and K_{12} are the coefficients and must comply with the following polynomial:

$$p(s) = s^2 + 2\zeta\omega_n s + \omega_n^2, \quad (4.28)$$

which K_{11} and K_{12} are defined as follows:

$$K_{11} = 2\zeta\omega_n, \quad K_{12} = \omega_n^2, \quad (4.29)$$

while ζ and ω_n are the desired dominant damping ratio and natural frequency, respectively. These parameters are set knowing the switching frequency f_{sw} of the system.

In the outer control loop, P_{Inv} , is obtained by using equation (4.23). Obtained P_{Inv} by any control solution, the inverter reference current can be computed. Considering the power expressions in the dq frame, the current can be obtained as follows:

$$\begin{bmatrix} i_d \\ i_q \end{bmatrix} = \frac{1}{(v_d^2 + v_q^2)} \begin{bmatrix} v_{gd} & v_{gq} \\ v_{gq} & -v_{gd} \end{bmatrix} \cdot \begin{bmatrix} P_{Inv} \\ Q_{Inv} \end{bmatrix}, \quad (4.30)$$

The inner control loop works based on the control inputs (v_d, v_q) in equations (4.25) and (4.26). To calculate control inputs, the derivative of the flat output (\dot{i}_d, \dot{i}_q) in equations (4.25) and (4.26) should be obtained based on the control feedback law as in the previous FBC. Other terms of these two equations are available, and finally, the control input can be calculated. In the end, by using the dq to $\alpha\beta$ conversion, the reference modulating signal is generated.

According to the above explanations, the cascade control block diagram of the inverter in the grid-connected state is shown in Fig. 4.4. The detailed implementation process of the single-phase $\alpha\beta$ to dq conversion and vice versa is described in previous parts. Also, for simplicity in implementation and reducing the number of voltage sensors, the capacitor voltage in (4.25) and (4.26) (v_{Cd}, v_{Cq}) can be considered approximately equivalent to the grid voltage in the case of using an LCL filter.

It should also be mentioned that in FBC, trajectory planning plays a key role in ensuring that the system follows a desired evolution of states while respecting physical constraints. The main objective is to design smooth reference trajectories for flat outputs and limit the derivative terms. Proper trajectory planning not only improves the transient response and reduces overshoot but also guarantees feasibility by limiting the rate of change and avoiding abrupt setpoint variations. As a result, it bridges the gap between the theoretical flatness property and practical implementation under dynamic operating conditions. To plan a desired trajectory for the flat output components, a low-pass second-order filter can be used as follows:

$$\frac{y'_{ref}(s)}{y_{ref}(s)} = \frac{1}{\left(\frac{s}{\omega_{n2}}\right)^2 + \frac{2\zeta_2}{\omega_{n2}}s + 1}, \quad (4.31)$$

where $y'_{ref}(s)$ is the reference value of the flat output after passing the filter, and ζ_2 and ω_{n2} are also the desired dominant damping ratio and natural frequency, respectively.

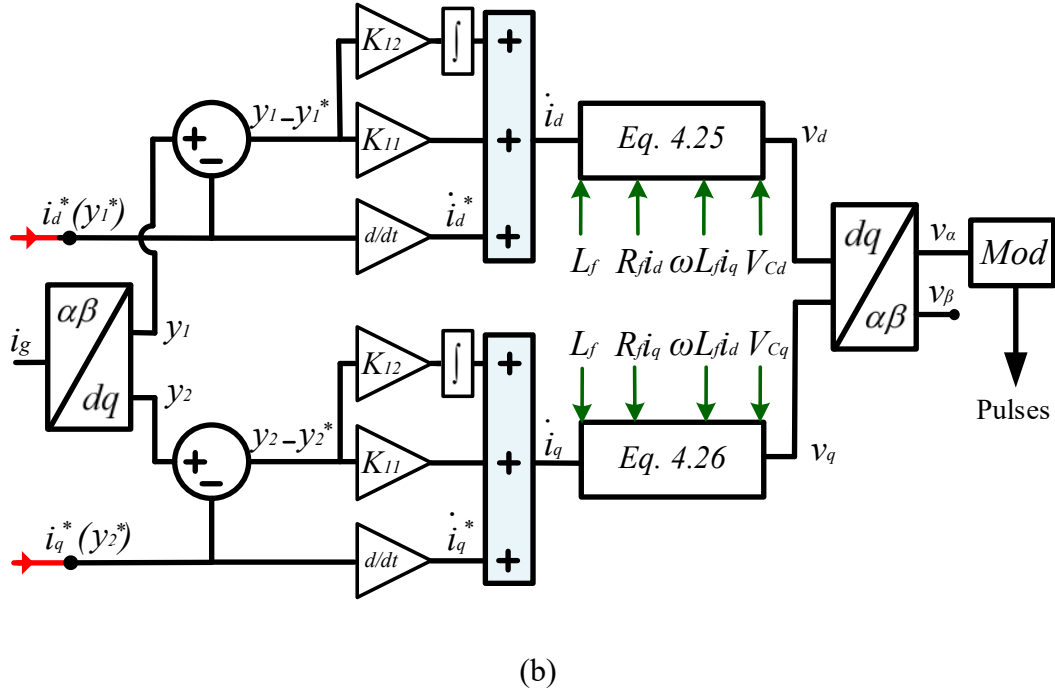
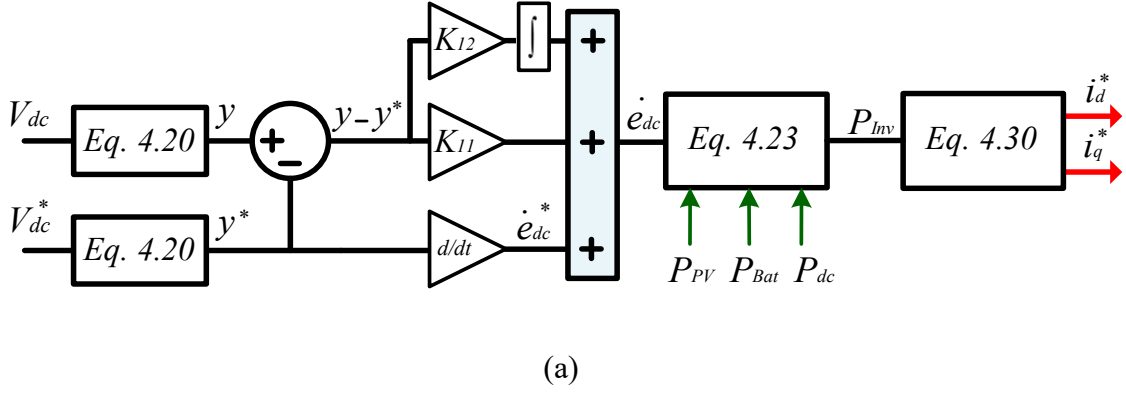


Fig. 4.4. New proposed comprehensive FBC control scheme. (a). FBC outer control loop for the dc-link voltage regulation. (b). FBC inner control loop for the inverter current control.

4.1.6 PR controller as an alternative for the grid current controller

Although FBC was successfully applied in simulations for both dc-link regulation and grid current control, the experimental implementation focused on dc-link voltage regulation only. For the inner current control loop, a PR controller was adopted. The

choice of PR control is justified by its well-established reliability in grid-connected applications, its inherent capability to achieve zero steady-state error for sinusoidal signals, and its robustness in eliminating higher-order harmonics [162]. These properties make the PR controller particularly attractive for practical implementation, where computational simplicity, robustness, and compliance with grid standards are of primary importance.

The PR controller is widely used in ac current control applications, especially for grid-connected converters. The PR controller combines a proportional term with one or more resonant terms to achieve both fast dynamic response and high steady-state accuracy. The proportional gain K_p improves transient performance and stabilizes the system, while the resonant term introduces infinite gain at the fundamental grid frequency ω_0 , ensuring zero steady-state error for sinusoidal references. To further improve power quality, additional resonant terms can be tuned at selected harmonic frequencies ($\omega_h, h=3, 5, \dots$), effectively suppressing grid distortions and reducing total harmonic distortion (THD). This combination makes the PR controller an effective and reliable solution for achieving high-quality sinusoidal current injection into the grid.

Fig. 4.5 shows the general block diagram of an ideal PR controller form with an infinite gain (K_{rh}) at ω_h . The transfer function of this controller is also written in (4.32).

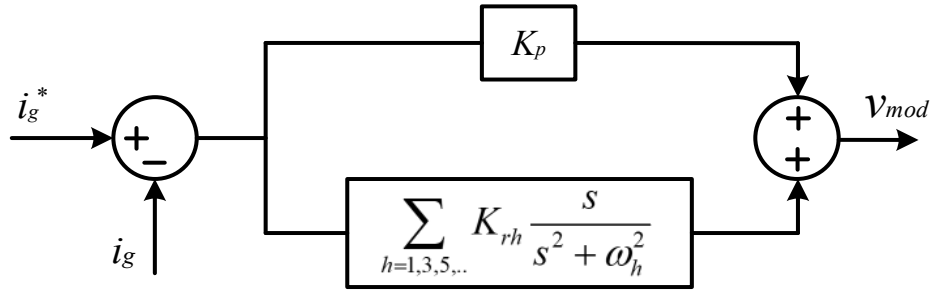


Fig. 4.5. Block diagram of an ideal PR controller.

$$G_{PR}^{id}(s) = K_p + \sum_{h=1,3,5,\dots} K_{rh} \frac{s}{s^2 + \omega_h^2}. \quad (4.32)$$

where K_p is the proportional gain, K_{rh} is the resonant gain and ω_h harmonic frequencies at harmonic h .

The resonant section of the PR controller can be realized using two cascaded integrators, allowing control at a single frequency at ω_0 .

In practice, the real implementation of the PR controller often employs a finite gain, which helps minimize steady-state error and extend the controller's bandwidth by properly selecting the cutoff frequency ω_c [163], [164]. This adjustment also reduces sensitivity to grid frequency deviations and therefore improves robustness. Equation (4.33) is an expression for this solution [165]:

$$G_{PR}^{id}(s) = K_p + \sum_{h=1,3,5,\dots} K_{rh} \frac{2\omega_c s}{s^2 + 2\omega_c s + \omega_h^2} \quad (4.33)$$

Lastly, some researchers suggest the following equation as a phase-compensation method to reduce the effect of processing delays [166].

$$G_{PR}^{id}(s) = K_p + \sum_{h=1,3,5,\dots} K_{rh} \frac{s \cdot \cos(\phi_h) - \omega_h \cdot \sin(\phi_h)}{s^2 + \omega_h^2}. \quad (4.34)$$

where the angle ϕ_h is a phase delay for each harmonic and is calculated in (4.34):

$$\phi_h = N \cdot 360^\circ \cdot \frac{\omega_h}{2\pi} \cdot \frac{1}{f_s}, \quad (4.35)$$

which f_s stands for switching frequency, and N is the number of harmonics. Regarding the above equations and explanations, Fig. 4.6 shows the PR controller with phase delay consideration, which is used in this work for simulation comparison and experimental test.

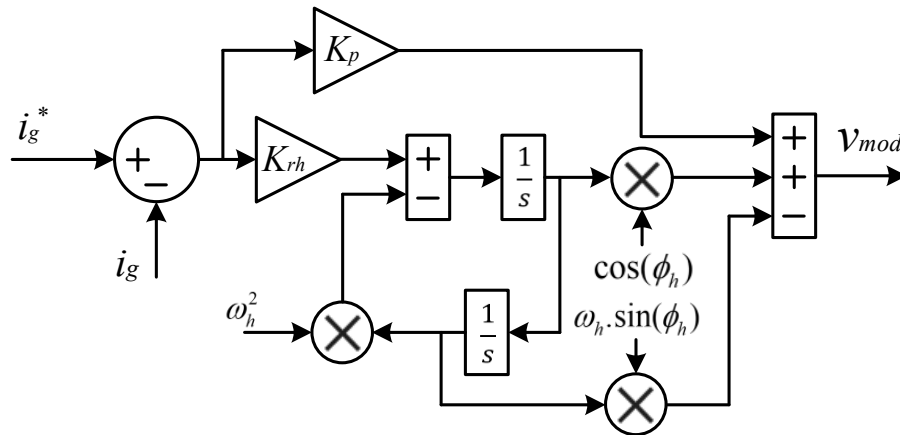


Fig. 4.6. Block diagram of PR controller considering phase delay.

4.2 Possible high-level control and EMS

As previously mentioned, the control system consists of different levels. In high-level control, an EMS sets the reference currents for different parts based on some simple rules or a developed EMS based on the latest optimization solutions. In the following, simple internal EMS and digitalized solutions are discussed.

4.2.1 Simple local EMS

Energy management algorithms for various operation modes include two general conditions: grid-connected mode and off-grid mode. The EMS has different operations. In each of these cases, the presence of PV and BSS can introduce different modes and scenarios. Fig. 4.7 shows the general flowchart for a simple internal EMS and different possible modes. In the off-grid state, the battery should always be connected to the dc link to guarantee dc link stability. In a grid-connected mode, the inverter controls dc link voltage and operates in grid-following mode, while in dc link, the BSS and PV can be connected. The energy management algorithm finally determines the reference current values for PV and BSS for each mode. Regarding the different operation modes in grid-connected or off-grid conditions, reference signals are sent to the control system of each converter. As can be seen in this flowchart SoC of the BSS and the battery charging or discharging mode are determining factors to set the reference currents. It should also be mentioned that this charging and discharging mode can be set externally or by other optimization algorithms. Therefore, modes 1 to 4 are related to different grid-following cases, while modes 5 and 6 can be grid-forming or dc-mode, based on the ac or dc load type connection.

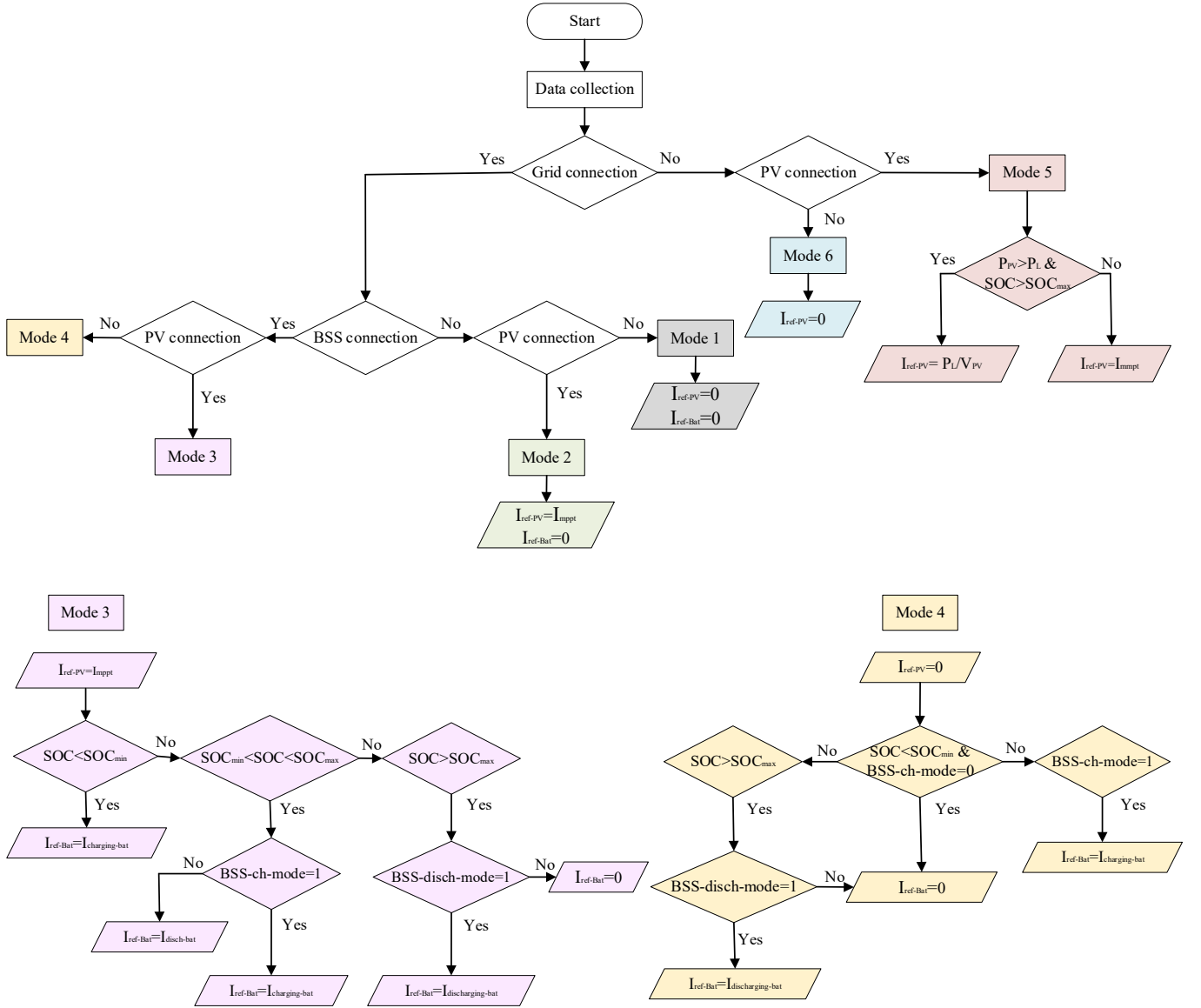


Fig. 4.7. Simple internal energy management flowchart for different operating modes.

4.2.2 From distributed control to full Digitalization of EMS

Nowadays, the IoT is present in the daily operation of many industries; applications include but are not limited to smart cities, smart grids, and smart homes. IoT collects, processes, analyzes, and uses data for management and optimization in various cases to answer substantial requirements in terms of comfort, usability, security, and energy management [167]. New buildings make no exception and the use of digitalization under the title of smart buildings has been emerging in recent years. IoT provides remote

monitoring, temperature and lighting control, building efficiency improvement, and consequently money saving while increasing user comfort [168].

In response to the increase in the electrical power demand, the installation of distributed generation units, in particular PVs, along with energy storage systems in buildings have been gaining interest in the last decades. This gave way to new considerations regarding the EMS within these buildings in terms of monitoring the production, storage, and consumption. The goal is to migrate toward modern ZEBs. This challenge was possible due to the advancement in power converters and microcontrollers.

Different strategies can be applied in EMS, with droop control being the most common for power sharing in microgrids. It offers a reliable, low-cost, and communication-free plug-and-play solution, though it suffers from impedance dependency, inaccurate sharing, and slow dynamics. To overcome these issues, variants such as adaptive, robust, and neural network-based droop control have been introduced, as well as hybrid schemes combining droop with secondary communication-based control.

For broader objectives, distributed hierarchical control with two or three levels is often adopted, combining local droop at the primary level with higher-level controllers that use low-bandwidth communication, consensus algorithms, and optimization at the tertiary level. However, distributed methods cannot fully optimize power flow economically, which requires centralized EMS. With increasing digitalization, cloud-based EMS has become practical, offering scalable computation, storage, and data analysis, as well as predictive and machine-learning capabilities, making it an efficient and cost-effective solution for smart buildings and microgrids. However, as with all centralized systems, the main drawback is the single-point failure problem and consequently, the reliability in case of communication loss. In addition, the communication cost can be a burden [169].

In order to overcome these issues, new paradigms are emerging, combining the cloud-based EMS with an edge-computing device at the ER level [169]. Most computation tasks are done at the Cloud-Computing Platform (CCP). With an optimization objective, long-term prediction using all the available resources at the cloud

are performed. This leaves simple calculation tasks to the local level that can be handled by the computing resources of the inverters. In fact, all that is needed is to adapt or fine-tune the strategy sent by the CCP based on local information and measurements related to the storage devices, the generation, consumption, and switchable loads. Thus, the maintenance needed at the edge level is reduced. In addition, the edge computing device does not rely on instantaneous communication with the cloud and can work as a standalone for short-term control; consequently, the communication burden is lightened.

In addition, the computing programs at the CCP can be easily modified, which makes the approach flexible and expandable. Finally, the CCP can be shared by many independent buildings, which reduces the cost.

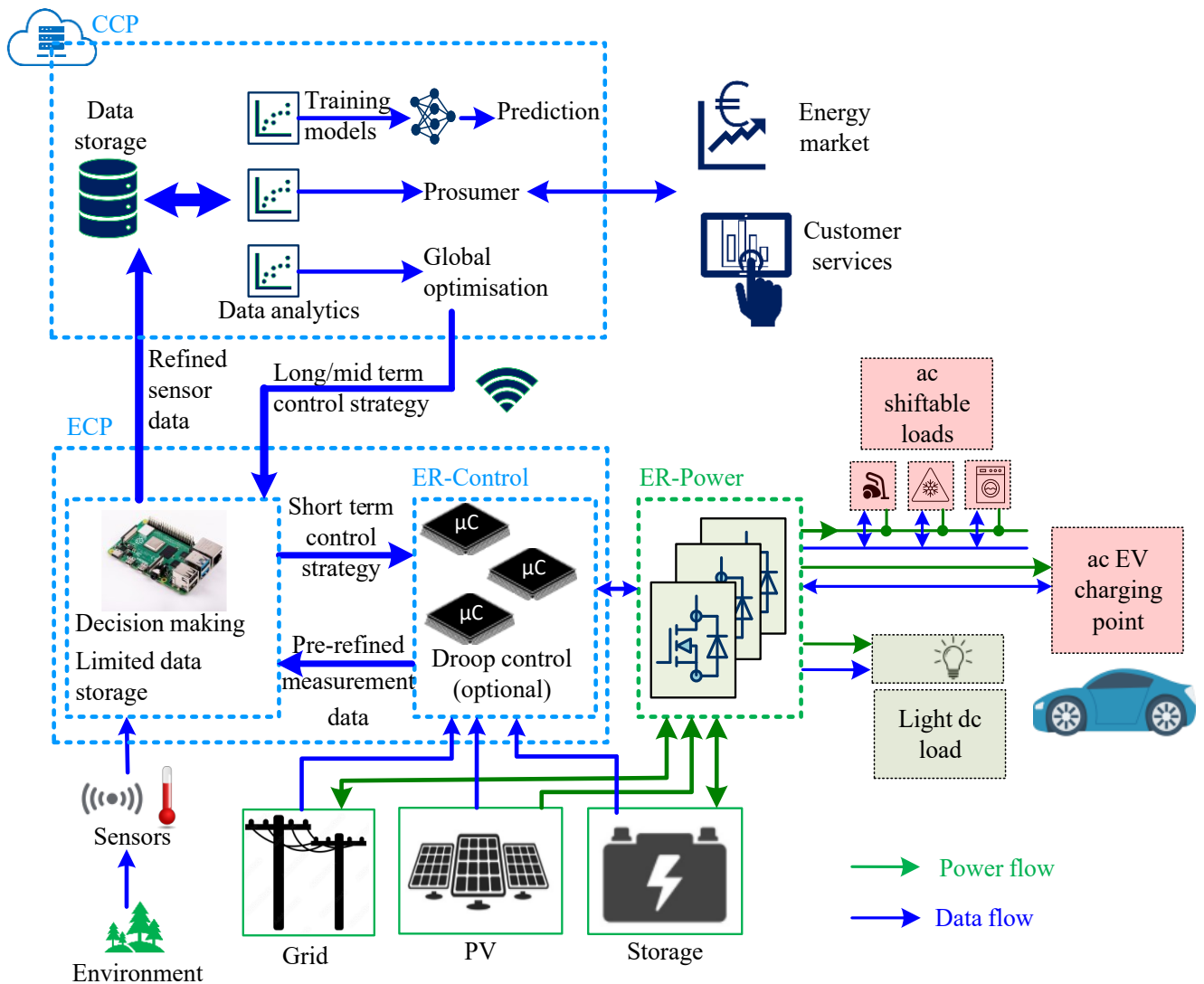


Fig. 4.8. Hybrid CCP/ ECP for high-level ER control.

To summarize, combining CCP with the edge computing platform (ECP) gives a flexible, expandable, cost-effective solution that performs overall economic optimization based on collected data and prediction, which is not possible with decentralized EMS. In addition, it is always possible to maintain a droop control at local level as a backup option in case of communication loss in order to improve the reliability. This hybrid solution, illustrated in Fig. 4.8, provides for autonomous operation when needed, so the single-point failure problem is avoided and the communication cost is reduced when compared to centralized EMS.

4.3 Conclusion

This chapter focused on low-level control of ER and then proposed FBC as an effective approach to enhance the dynamic performance of the ER control system. The FBC theory was described in detail. Since for FBC on the grid side, the dq transfer is used, it was described how to implement the dq transfer for single-phase systems. After deriving the ER modeling equations, the system's differential flatness conditions were rigorously examined. FBC was implemented in two key aspects of the control system: first, at the dc link to regulate energy flow and stabilize the dc-link voltage, and second, at the inverter output filter to generate the reference voltage for inverter modulation. Although FBC can be used for both dc-link and grid current, the PR controller was also described as a reliable alternative solution for grid current, which can effectively eliminate different harmonics. At the end, in high-level control, a simple local EMS and a high-tech EMS based on CCP and ECP was described to reach the most optimized energy management conditions.

In this chapter, control system of the energy router was deeply analyzed in various levels of hierarchy and following results and findings were drawn:

1. Two conceptual high-level ER control were proposed: local energy management system and its extension with the edge computing platform and cloud computing platform, providing extended possibilities for the energy management.
2. A new flatness-theory based controller for dc-link voltage regulation in an energy router was proposed, including structure, derivations and design considerations.

3. As grid current controller, it was proposed to use a classical proportional-resonant controller, which ensure fast and robust grid current control.

5 SIMULATION AND EXPERIMENTAL VERIFICATION OF PROPOSED ENERGY ROUTER SOLUTION

In this chapter, verification of the proposed energy router will be provided. The first part presents simulation results regarding the proposed FBC method for the ER system in low-level control. Simulation results examine the FBC solution for both the dc-link voltage and grid current control, and then the performance of FBC is compared with the conventional methods.

The second part of the verification procedures lies in the experimental tests, where experimental results are presented in different operating conditions. For experimental, FBC is used in the dc-link, while for the grid current, the PR method is used. Results validate the proposed ER and its control system in different operating modes and dynamic conditions.

To better understand the different simulation scenarios and experimental tests, Fig. 5.1 illustrates a simplified block diagram of the ER system along with the direction of power flow in different parts. In our case, programmable DC-voltage power supplies. ITECH IT6000C was used as an emulation of battery and PV modules in the experiment, whereas computer models of battery and PV were used in verification by simulation.

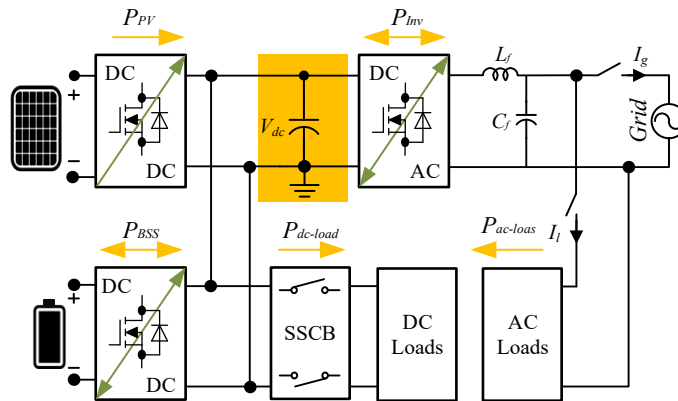


Fig. 5.1. Simplified block diagram of the ER system with power flow direction in different parts.

5.1 Simulation results for the FBC solution in dynamic conditions

To evaluate the adequate performance of the utilized FBC approach applied to the ER structure (depicted in Fig. 5.1), a comprehensive simulation study in the PLECS software is carried out. In the simulation parts, FBC theory is applied to regulate dc-link voltage in an outer control loop and then the grid current in an inner loop. The main simulation parameters are collected in Table 5.1. Under various dynamic conditions, the FBC performance in stabilizing the dc-link and controlling the grid current has been examined and compared with the traditional controller. In dc-link control, FBC performance is compared with a PI controller. For the PI controller, the transfer function of the structure for different modes is extracted, and then, using the PID tuner in MATLAB, suitable PI coefficients are chosen. The selected scenario for this evaluation includes step changes in different subsystems in off-grid and grid-connected cases. For instance, a step change in loads or in PV production, a sudden shift in the battery current, or a change mode from charging to discharging mode (or vice versa), or a step change in the direction of the grid-side current to inject or receive power to/from the grid.

Table 5.1

Simulation parameters

| Parameter's name | Value | Units |
|---------------------------------|-------|---------------|
| Grid voltage, v_g | 230 | V |
| Dc-link voltage, V_{dc} | 350 | V |
| Battery storage nominal voltage | 250 | V |
| Dc-link capacitor | 4760 | μF |
| LC filter inductance, L_f | 0.8 | mH |
| LC filter capacitance, C_f | 3.3 | μF |
| LC filter resistance | 0.1 | Ω |
| Switching frequency, f_{sw} | 62.5 | kHz |

5.1.1 Step change in ac load (grid-forming)

In the grid-forming mode, the BSS is responsible for controlling the dc-link voltage. To test the performance of the applied FBC method on ER in this case, the BSS is discharging and feeding a dc load with a power of 630 W, while PV is not connected. Then, at $t = 0.7$ s, a resistive ac load (59Ω) is added to the output side of the inverter. Fig. 5.2(a) shows the responses of the controller using FBC and PI solutions. As can be seen in this case, the BSS reference currents for FBS is slightly faster. Fig. 5.2(b) shows the dc-link voltage for this case, using FBC and PI approaches. As a result, the dc-link voltage level is better maintained using FBC, and the step change in ac load will result in 3 V undershoot and 50 ms settling time. However, with the PI control, the dc-link has almost 5 V undershoot, and it takes nearly 150 ms to reach its reference value.

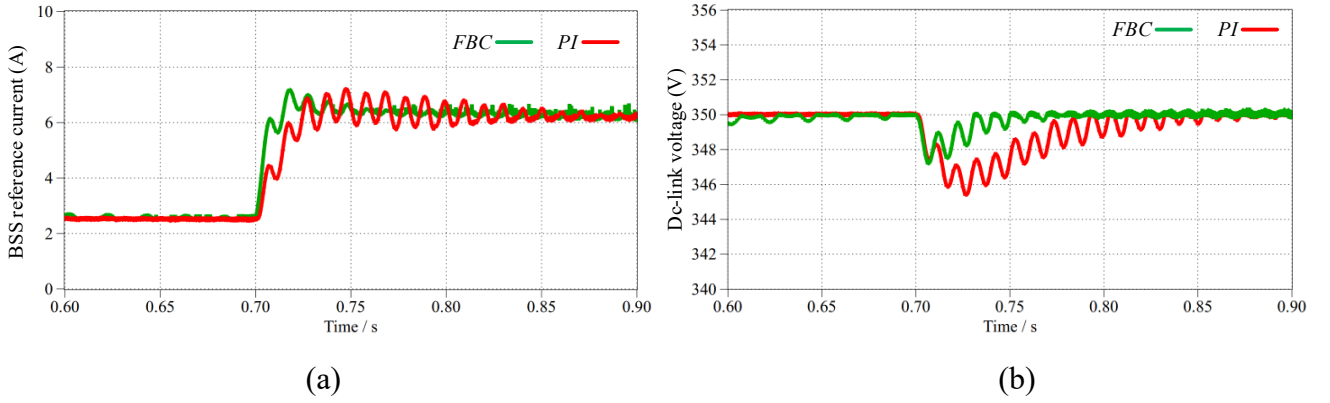


Fig. 5.2. (a). BSS reference current (control response) for a step change in ac load (grid-forming mode) using FBC and PI, (b). Dc-link voltage and its behavior for the ac load step change.

5.1.2 Step change in dc load (grid-following)

In this grid-following mode, it is assumed that initially, the BSS is discharging with a power of 500 W, and PV is also working with a power of 520 W. Dc-link is feeding a 1000 W load. Then, at $t = 0.3$ s, the dc load increases to 2000 W. Fig. 5.3(a) shows the responses of the control system using FBC and PI solutions. The reference current for the injected ac currents in FBC reacts faster against the step change, and also it has a lower ripple compared to the PI control-based implementation. Fig. 5.3(b) shows the dc-link voltage for this case, using FBC and PI approaches. As a result, the dc-link voltage level

is much better maintained using FBC, and the step change in load has almost no impact on the dc-link voltage. However, with the PI control, the dc-link voltage drops, and due to the slow response and high capacitance in the dc link, it takes a much longer time (nearly 1 s) to reach its reference.

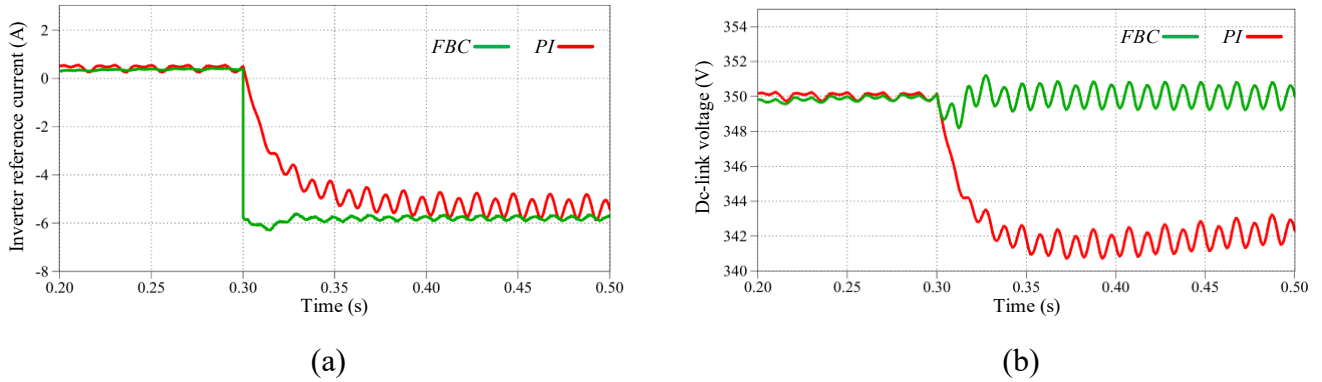


Fig. 5.3. (a). Inverter reference current (control response) for a step change in dc load using FBC and PI, (b). Dc-link voltage and its behavior for dc load step change. In the PI case, it takes almost 1 second to reach its reference.

5.1.3 Step changes in PV (grid-following)

The third case study is related to a step change in PV power in grid-following mode. At $t = 0.3$ s, PV power increases from 520 W to 1020 W. Fig. 5.4 shows the inverter reference current and the dc-link voltage, respectively. In this case, it is also clear that FBC is faster and the dc-link is much more stable. In the PI case, the dc-link voltage increases at the step change time, and again it needs a long time to reach its reference value.

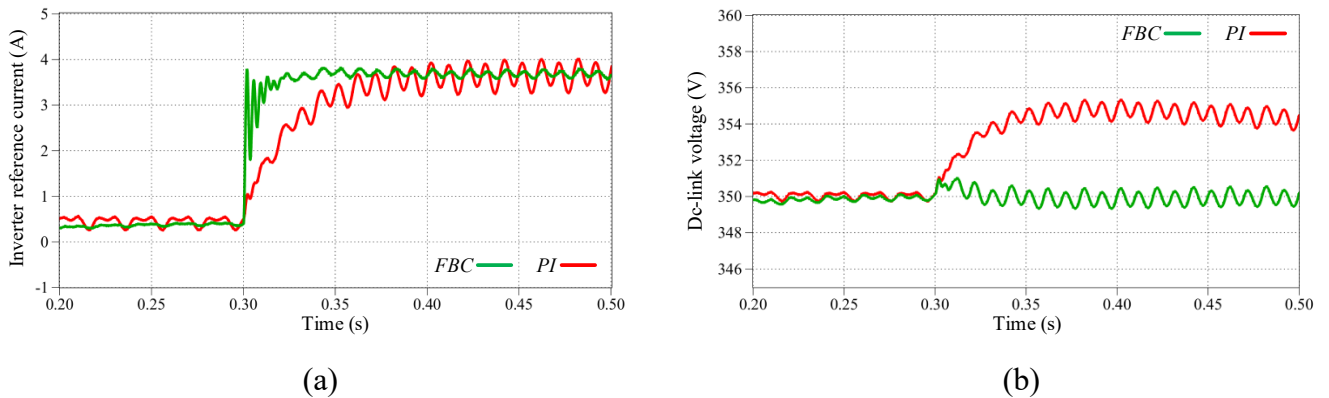


Fig. 5.4. (a) Inverter reference current for a step change in PV using FBC and PI, (b) Dc-link voltage and its behaviour for a step change in PV.

5.1.4 Step change in the BSS reference current (grid-following)

The fourth case is during the night without PV power. The BSS is discharging at 1000 W and there is a dc load of 1000 W. At $t = 0.3$ s, the BSS reference current changes and it shifts from discharging mode to charging mode, receiving 1000 W from the grid. In this situation, the inverter reference current changes and it demands power from the grid. Fig. 5.5 shows the inverter reference current and dc-link voltage. It is also evident that FBC is much faster than PI and the dc-link voltage for FBS doesn't drop as in the PI case. After applying this step change, as shown, the dc link voltage for the PI case starts to track the reference very slowly, and it takes almost 1 second to reach its reference value.

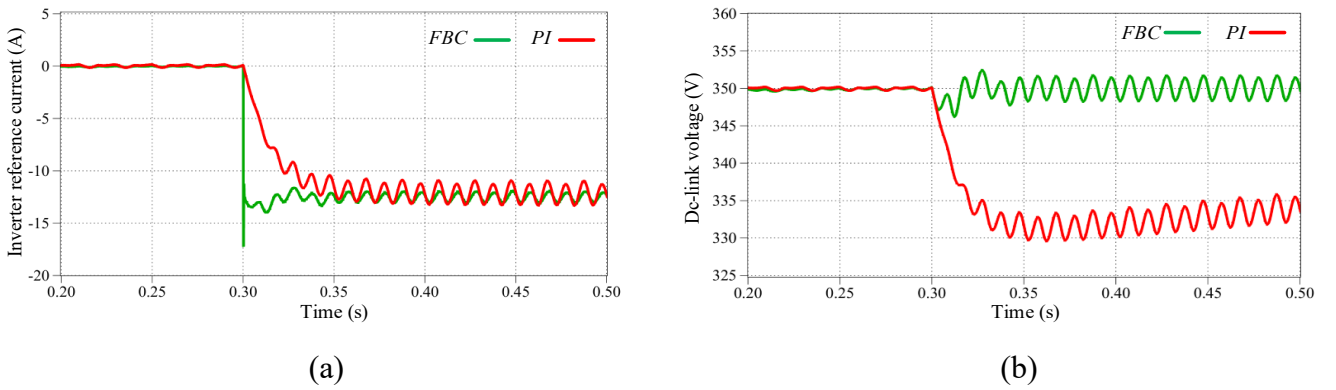


Fig. 5.5. (a) Inverter reference current for step in the battery using FBC and PI, (b) Dc-link voltage behavior for a step change in battery power.

5.1.5 Grid-side evaluation with FBC

To evaluate the performance of FBC on controlling the injected current of the inverter into the grid, it is assumed that there will be dynamic conditions for load, PV, and BSS. First, the BSS discharges 1000 W, and PV outputs 570 W. At $t = 0.3$ s, the PV power increases to 1600 W at $t = 0.5$ s, the BSS mode changes to charging mode with 1000W, and finally, at $t = 0.7$ s, a dc load of 1500 W is added.

Fig.5.6(a) shows the d component of the inverter reference current, which is the FBC response to the corresponding dynamic conditions. Dc-link voltage evolution can be seen in Fig.5.6(b). As seen, these dynamic conditions have little effect on the dc-link voltage and it oscillates around its reference, while in the case of using PI, voltage

drop/swell is inevitable. Finally, grid-side voltage and current ($\times 10$) along with grid current frequency spectrum are shown in Fig.5.6(c). The voltage and current are in phase, and the amplitude of the grid current properly tracks the inverter reference current. It is also worth mentioning that at $t = 0.7$ s, the reference current changes from a positive to a negative value, thus the power flow direction changes rapidly and receives power from the grid, which all proves the reliability and fast response of the FBC solution to control both the dc-link voltage and the grid current. However, as can be seen in the frequency spectrum of the grid current, the current waveform has a relatively high 3rd harmonic, resulting in 11.5% THD.

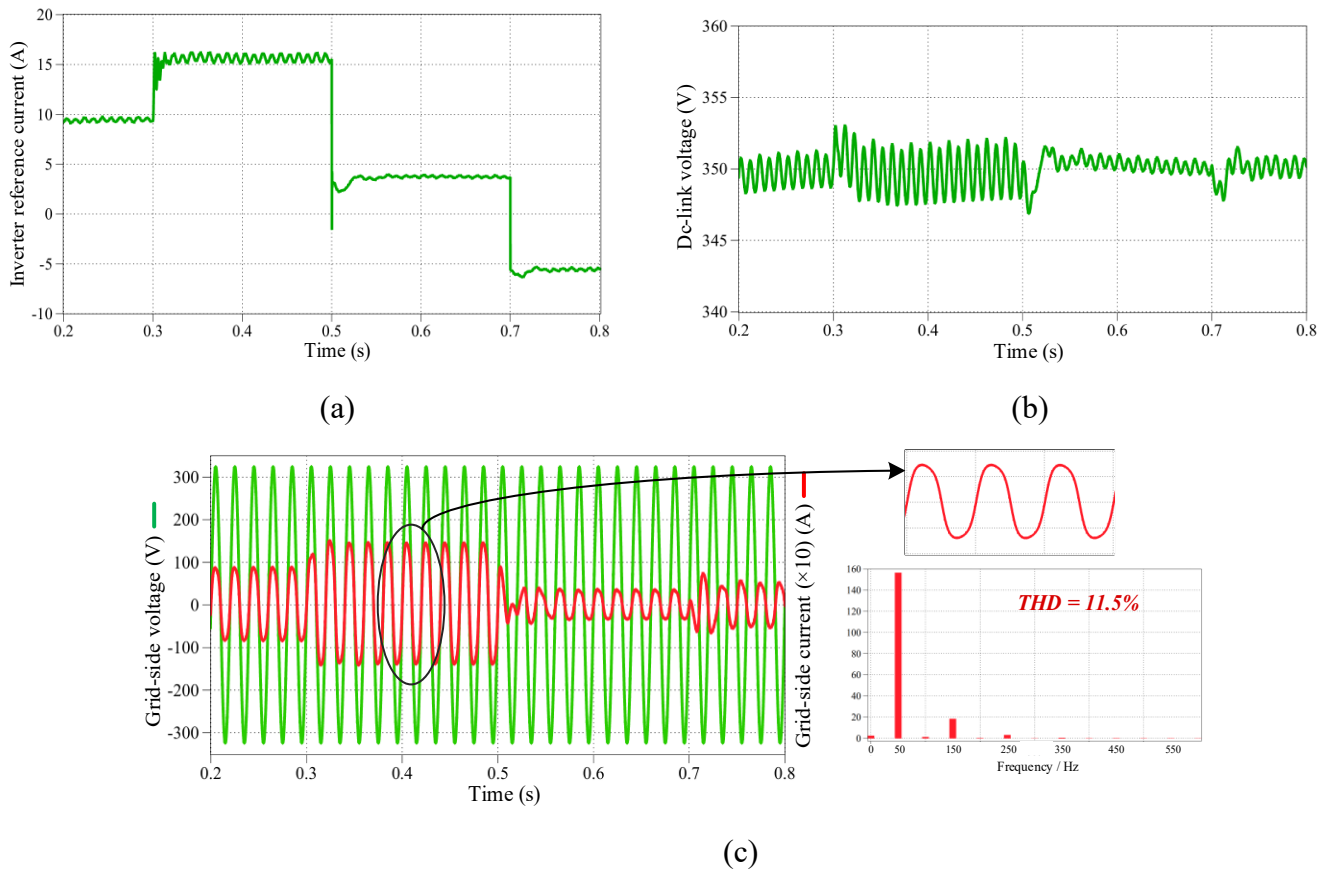


Fig. 5.6. Results for several different dynamic conditions using FBC (a) Inverter reference current, (b) Dc-link voltage, (c) Grid-side voltage and current, along with current frequency spectrum.

5.1.6 Grid-side evaluation with PR controller

As seen in the previous section, using FBC to control the dc-link voltage is associated with a very fast and accurate response and consequently results in a stable dc-

link voltage around the reference value. However, for grid current control, the grid current has relatively high harmonics. In this section, the conditions are examined to control the dc link voltage through FBC and the grid current in the inner control loop through PR to eliminate all types of higher-order harmonics. The same condition as Fig.5.6 is considered to examine the performance of the PR controller. Fig. 5.7 shows the grid-side voltage and current ($\times 10$) along with the frequency spectrum of grid current while using PR method to control grid current. As can be seen in this figure, PR response to dynamic conditions is slower compared to FBC, while PR performance in eliminating harmonics is superior, resulting in 3.3% THD. Taking into account this benefit, for the grid current control in the experimental setup, a PR-controller is used to reach lower harmonic components.

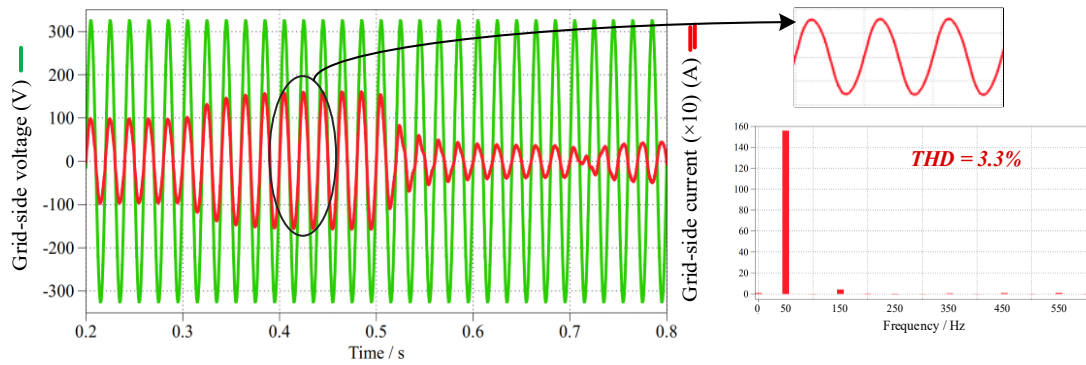


Fig. 5.7. Grid-side voltage and current (along with current frequency spectrum) under dynamic conditions using PR to control grid current.

5.2 Experimental verification

Table 5.2 lists the specifications of the experimental prototype. The experimental realization of the ER structure and its different parts is illustrated in Fig. 5.8, while Fig. 5.9 shows the laboratory setup, including supplies and loads. The processor used in this work is a Texas Instruments TMS320F28379D, and the power switches are SiC-type MOSFETs. ITECH IT6000C bi-directional power supplies are used as a battery and PV emulator. Considering the presence of grid, PV, BSS, and dc/ac loads, experiments have been performed for different operating modes and scenarios, including grid-forming or grid-following conditions. In this part, different tests have been conducted to validate the general operating modes and the control system in dynamic conditions.

Table 5.2

Laboratory prototype specifications

| Components Characteristics | |
|----------------------------|---------------------------|
| Switching frequency | 62.5 kHz |
| Sampling time | 32 μ s |
| Dc-link capacitor | 4760 μ F |
| Inverter inductor | 850 μ H |
| LCL filters inductors | 680 μ H & 320 μ H |
| LCL filter capacitor | 3.3 μ F |
| PV inductor | 1.8 mH |
| Battery inductors | 500 μ H |
| Operating points | |
| Grid voltage | -400-400 V |
| dc-link voltage | 280-380 V |
| Battery voltage | 250-360 V |
| PV voltage | 200-450 V |
| Semiconductor elements | |
| Inverter MOSFETs | C3M0021120K |
| Battery converter MOSFETs | C3M0025065K |
| PV converter MOSFETs | C3M0025065K |
| SSCB MOSFETs | C3M0025065K |

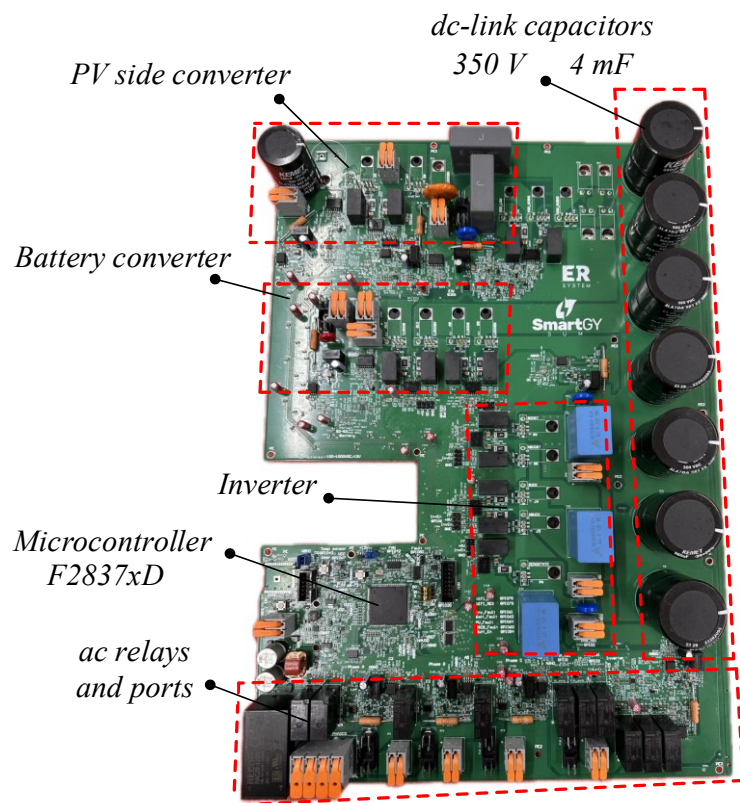


Fig. 5.8. Experimental prototype of multiport ER.

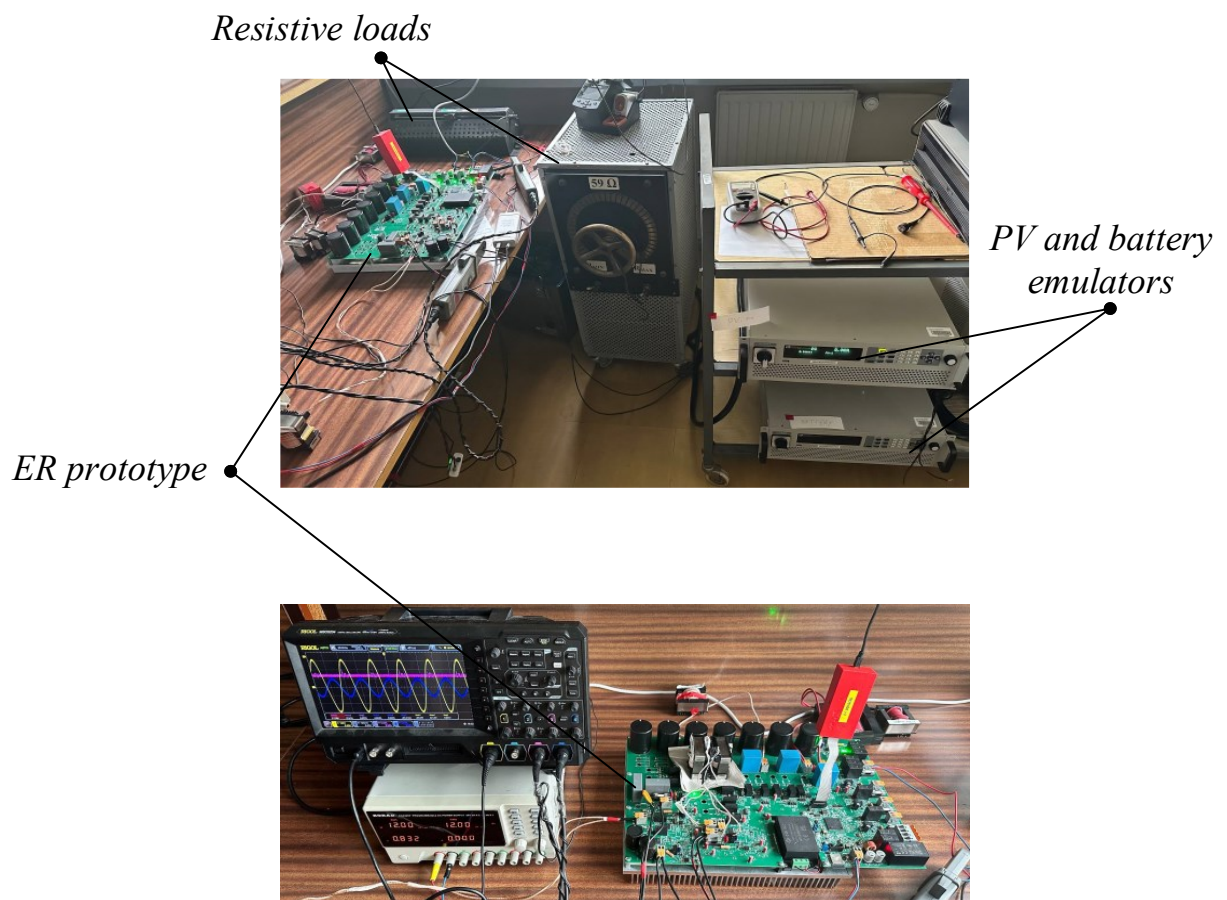
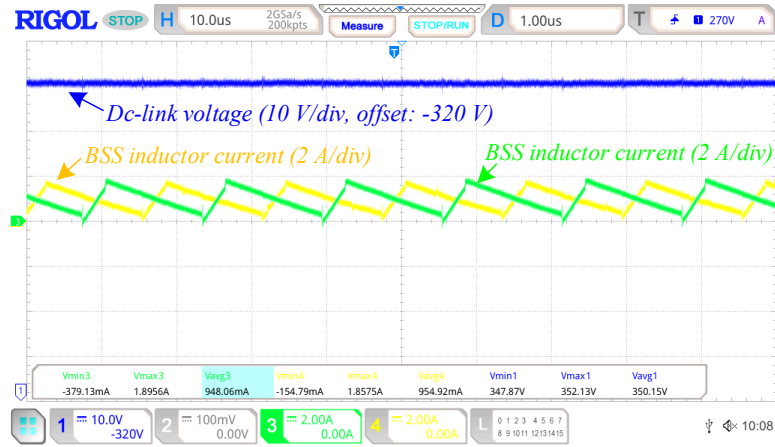


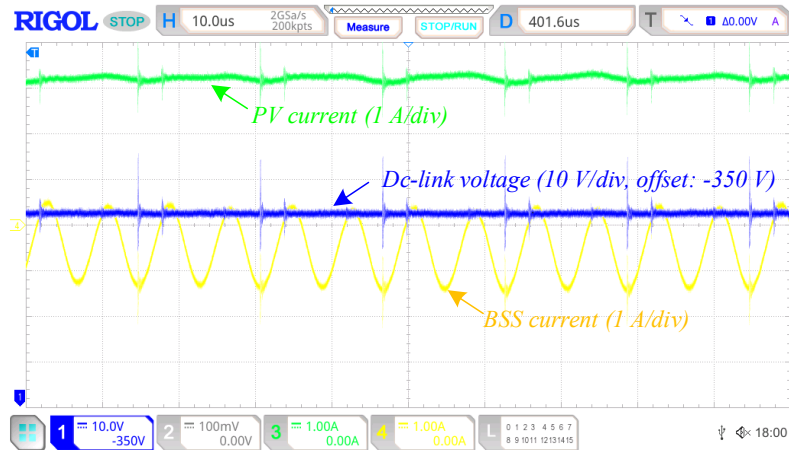
Fig. 5.9. Laboratory setup.

5.2.1 Dc-mode

This mode operates when supplying a dc load or connecting to other dc nanogrids. It is activated once the BSS or PV voltage reaches the operating level, and grid-forming and following permission is inactive. Fig. 5.10(a) and Fig. 5.10(b) illustrate two scenarios of this mode. Fig. 5.10(a) corresponds to the dc mode with the BSS, showing inductor currents of the interleaved BSS converter and the dc-link voltage supplying a 194 Ω resistive dc load. Fig. 5.10(b) shows the case where PV power exceeds the load demand, resulting in BSS charging and receiving current. As shown, the dc-link voltage is regulated at its reference; the PV current is positive, while the BSS current is negative, indicating charging.



(a)

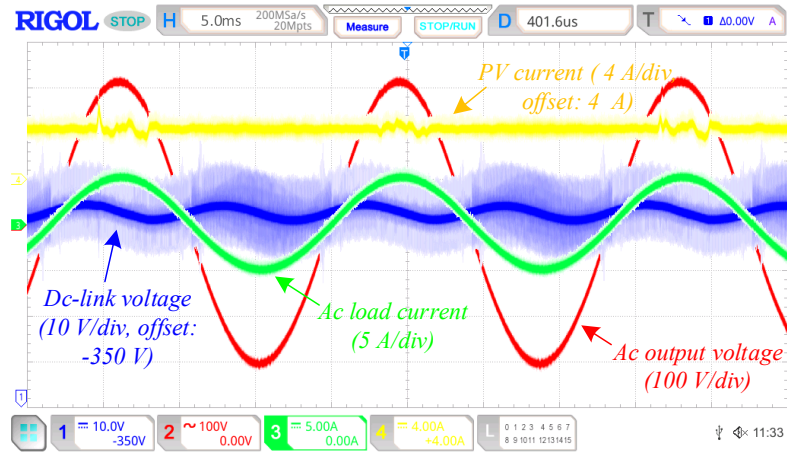


(b)

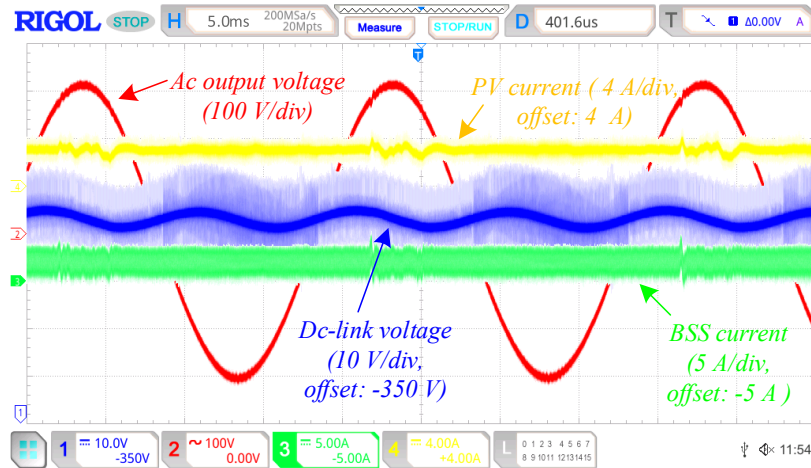
Fig. 5.10. Experimental results for different operating modes. (a) dc-mode with BSS. (b) dc-mode with PV and BSS.

5.2.2 Grid-forming mode

This mode is activated when the PV or BSS voltage reaches the operating level, grid-forming permission is active, while grid-following is inactive. Ac loads are powered via their respective relays, while dc load supply is optional. Fig. 5.11(a) and Fig. 5.11(b) correspond to this case. In Fig. 5.11(a), the PV supplies both dc and ac load of $194\ \Omega$ and $59\ \Omega$, respectively. Fig. 5.11(b) presents the case where both PV and BSS operate in grid-forming mode, supplying the same dc and ac loads. It displays the PV and BSS currents, dc-link voltage, and ac output voltage. As observed, the dc-link voltage is regulated at 350 V and includes double-frequency components of the ac output.



(a)

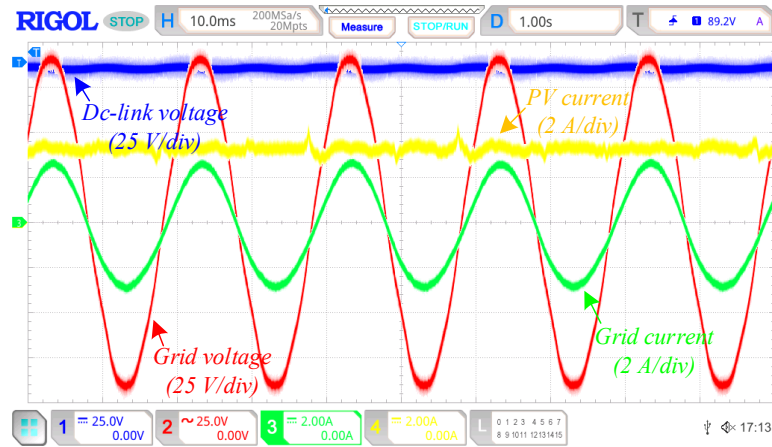


(b)

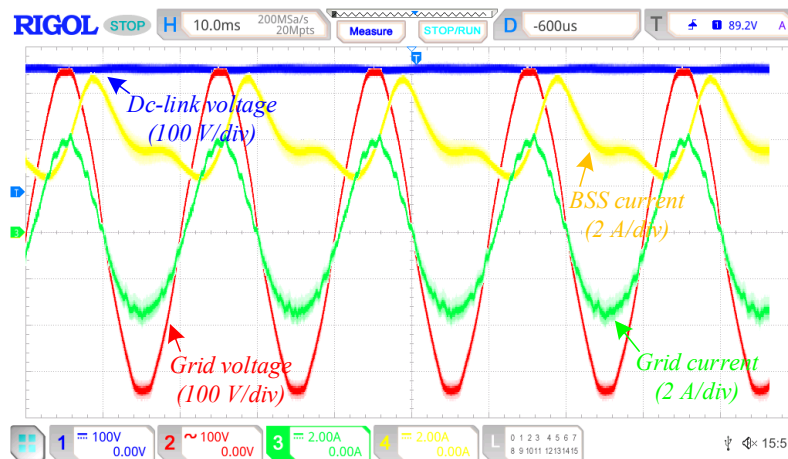
Fig. 5.11. Experimental results for (a) Grid-forming with PV. (b) Grid-forming with PV and BSS.

5.2.3 Grid-following mode

When grid-following permission is active and PV or BSS voltage reaches the operating range, this mode is initiated, allowing power exchange with the grid. Fig. 5.12(a) and Fig. 5.12(b) illustrate this case. In Fig. 5.12(a), a grid-following test is performed with the PV operating at 25% of the nominal voltage for both the grid and dc link. In the second case, the BSS voltage is set to 350 V, injecting 400 W into the grid according to the predefined inverter current in the control algorithm. Fig. 5.12(b) displays the grid voltage and current, the dc-link voltage, and the BSS current. As can be seen, the injected current is in phase with the grid voltage, resulting in a unity power factor.



(a)



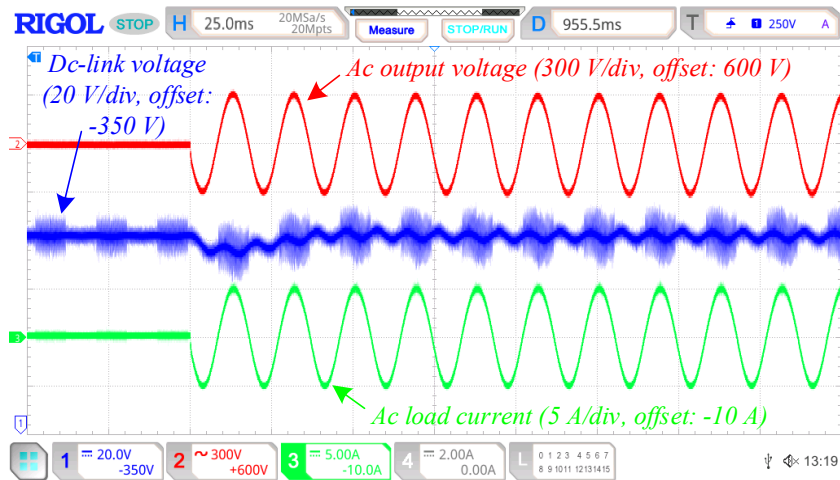
(b)

Fig. 5.12. Experimental results for (a) Grid-following with PV at 25% of the nominal voltage, (b) Grid-following with BSS, the nominal voltage.

It should be mentioned that for these tests, FBC has been used to regulate dc-link voltage and produce the grid current reference, and then the PR controller is used to control the grid current.

5.2.4 Dynamic conditions

To evaluate control performance under dynamic conditions, a $59\ \Omega$ resistive load is connected and disconnected at the ac output while the system continues supplying dc loads. This test is examined in grid-forming mode and it is in the same condition as in the simulation part 5.1.1. Fig. 5.13(a) and Fig. 5.13(b) present the dc-link voltage alongside the ac voltage and load current. Fig. 5.13(a) captures the moment when a $59\ \Omega$ load ($820\ \text{W}$) is connected. The controller responds effectively, with minimal dc-link voltage disturbance, approximately $5\ \text{V}$ undershoot and a settling time around $40\ \text{ms}$. Fig. 5.13(b) illustrates the load disconnection, where the controller responds with minimal overshoot and rapid stabilization. Notably, with conventional controllers, such step changes result in significantly slower responses and larger undershoots/overshoots in the dc-link voltage. Fig. 5.14 shows the same dynamic condition using a PI controller. As can be seen in this figure, there is around $35\ \text{V}$ undershoot, and the settling time is almost $500\ \text{ms}$. However, by changing PI coefficients, the response might be faster, but undershoot/overshoot will increase, resulting in reaching voltage protection thresholds and subsequently triggering system protection shutdown.



(a)

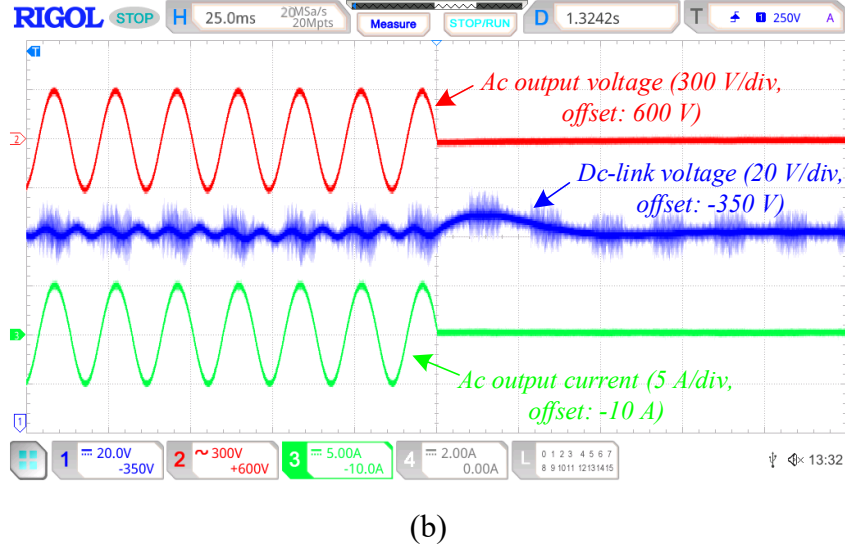


Fig. 5.13. Dc-link voltage behaviour under dynamic conditions with FBC (a) adding 820 W ($59\ \Omega$) ac load, (b) disconnecting the same ac load.

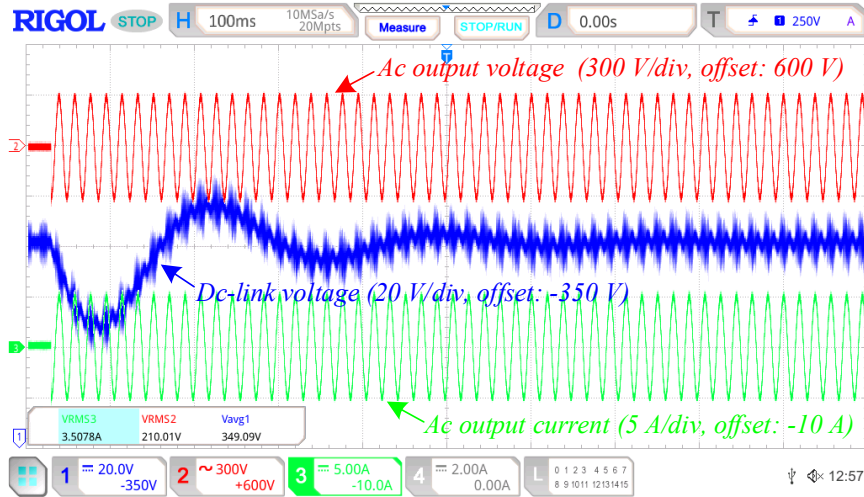


Fig. 5.14. Dc-link voltage behaviour under dynamic conditions with PI controller when adding 820 W ($59\ \Omega$) ac load.

Table 5.3 summarizes the comparison of dynamic performance for dc-link voltage control based on the simulations presented in Section 5.1.1 and the corresponding experimental results. As observed, in the case of the FBC method, the simulation results show 3 V undershoot and 50 ms settling time, while in the experimental implementation, these values slightly increase, with a voltage drop of about 5 V and a settling time of approximately 40 ms.

A closer examination of the table also reveals that for the PI controller, both the voltage undershoot and the settling time are smaller in the simulations compared to the

experimental results. Nonetheless, despite the differences between simulation and hardware implementation, the FBC method consistently demonstrates superior performance. Specifically, it achieves faster response and significantly smaller voltage undershoot compared to the PI controller, highlighting its robustness and effectiveness in practical applications.

It should also be noted that regarding simulation results, when only the BSS is connected (5.1.1), the PI response is faster, whereas in cases where all parts are connected to the dc link (sections 5.1.2 to 5.1.4), the PI response is significantly slower due to the slower dynamics of the total structure.

Table 5.3

Simulation and experimental comparison

| | Simulations | | Experiments | |
|------------|---------------|------------|---------------|------------|
| | Settling time | Undershoot | Settling time | Undershoot |
| PI method | 150 ms | 5 V | 500 ms | 35 V |
| FBC method | 50 ms | 3 V | 40 ms | 5 V |

5.3 Conclusion

This chapter evaluates the performance of the proposed ER and control system using simulations and experimental tests. In simulation parts, step changes were applied to different parts of the ER in a simulation environment, and the results were compared with conventional control methods. The findings confirmed that FBC offers superior dynamic performance, achieving faster response and greater accuracy for dc-link voltage control. FBC was also compared with PR controller for grid current. It was also shown that although FBC has a faster speed in dynamic conditions, but the grid current contains harmonic components and subsequently higher THD.

Experimental tests were also conducted under general operating modes and dynamic conditions of step changes in load. FBC was used to control dc-link and the grid current was controlled through the PR method. The results validated the effectiveness of both the proposed structure and the control methods, confirming valid general performance and a robust and fast control response in dynamic operating environments.

It was shown that FBC in dynamic conditions has a robust and fast response for the dc-link in comparison to a conventional PI controller. While in FBC, the dc-link undershoot is almost 5 V and the settling time is around 40 ms, in PI method, there is a near 35 V undershoot and a settling time of near 500 ms.

6 CONCLUSION

Rising electric energy consumption requires a completely new approach to electric energy supply and management. In the case of increasing the percentage of renewable energy generation along with the implementation of the concept of ZEB, load-shifting demand and battery storage are unavoidable components in future residential buildings. At the same time, there are not many power electronics solutions on the market that correspond to future challenges.

The possible architectures of the future ER are being discussed. One of the important factors of any future ER structure is the ability to connect to future LVdc microgrids. It is well known that LVdc distribution systems are emerging as an attractive future solution to improve efficiency and increase system flexibility due to the initial dc nature of all appliances. However, safety issues should be addressed as a priority, along control strategy at different control levels.

The following conclusions were obtained in this thesis:

1. While ensuring the required safety and protection, a non-isolated structure was proposed, which offers reduced volume, weight, and cost by eliminating the isolation transformer.
2. Although using isolation between the ac grid and the dc nanogrid does not completely suppress leakage currents, the proposed structure based on a common-ground inverter effectively eliminates leakage current paths by establishing a common ground for both ac and dc sides.
3. Although the pure dc system in the integration of ZEB to the grid has higher efficiency, due to the current dominance of ac system, a hybrid structure is a promising solution with relatively high efficiency.
4. Considering the growing expansion of dc nano/microgrids, the implementation of appropriate grounding systems is essential to ensure the protection of both personnel and equipment. Unlike previous studies and conventional structures, which often overlook comprehensive protection strategies in the dc link, this study investigated and applied effective grounding techniques. Various

connection scenarios were analyzed, and tailored grounding methods were proposed to provide reliable protection on both the ac and dc sides.

5. In both high-frequency and low-frequency isolation, a dc component in the leakage current can be created by dc voltage bias between the middle (or negative) point of the dc system and the neutral point of the ac system. In order to eliminate dc components, special grounding configurations and types were proposed to cancel the voltage bias between the neutral point of the ac system and the middle point of the dc system.
6. Unlike conventional architectures that employ a single-cell configuration for single-phase systems and a three-cell design for three-phase systems, the proposed structure adopts a single-cell approach for three-phase operation. This configuration enables dynamic phase selection, contributing to grid balancing and offering considerable economic advantages by reducing hardware complexity and cost.
7. In this thesis, the FBC method is employed to enhance dynamic performance. Despite requiring relatively low computational effort, the proposed approach demonstrated notable improvements in dynamic response and significantly enhanced the overall reliability of the system. FBC solution was used as a promising control method to reach a fast a robust control response.
8. For dc-link voltage regulation under dynamic conditions, the FBC demonstrates a much faster and more robust response compared to the conventional PI controller. However, while FBC also provides a fast response in grid current control, the resulting current exhibits higher harmonic content and greater THD compared to the PR method.
9. It was demonstrated that for a significant step change in load with FBC, the dc-link undershoot is less than 10 V and the settling time is approximately 40 ms. While with PI, there is a near 35V undershoot and a settling time of near 500 ms.

10. A possible higher control level, as the energy management layer, that integrates droop control as a feedback mechanism alongside cloud and edge platforms, is disclosed.
11. The simulation and experimental results validated the effectiveness of both the proposed structure and the control method, confirming their robustness for dynamic operating environments.

7 REFERENCES

1. Council of the European Union, "How is EU electricity produced and sold," Consilium.europa.eu. [Online]. Available: <https://www.consilium.europa.eu/en/infographics/how-is-eu-electricity-produced-and-sold>.
2. SolarPower Europe, "New report: EU solar reaches record heights of 56 GW in 2023 but warns of clouds on the horizon," SolarPowerEurope.org. [Online]. Available: <https://www.solarpowereurope.org/press-releases/new-report-eu-solar-reaches-record-heights-of-56-gw-in-2023-but-warns-of-clouds-on-the-horizon>.
3. SolarPower Europe, "New analysis reveals European solar battery storage market increased by 94% in 2023," SolarPowerEurope.org. [Online]. Available: <https://www.solarpowereurope.org/press-releases/new-analysis-reveals-european-solar-battery-storage-market-increased-by-94-in-2023>.
4. European Commission, "REPowerEU Plan," Energy.ec.europa.eu, COM(2022) 221 final, May 2022. [Online]. Available: https://energy.ec.europa.eu/system/files/2022-05/COM_2022_221_2_EN_ACT_part1_v7.pdf.
5. E. Tsioumas, N. Jabbour, M. Koseoglou, D. Papagiannis and C. Mademlis, "Enhanced Sizing Methodology for the Renewable Energy Sources and the Battery Storage System in a Nearly Zero Energy Building," in IEEE Trans. on Power Electron., vol. 36, no. 9, pp. 10142-10156, Sept. 2021, doi: 10.1109/TPEL.2021.3058395.
6. European Commission, "Fit for 55: Delivering the EU's 2030 Climate Target on the Way to Climate Neutrality," Press Corner – European Commission. [Online]. Available: https://ec.europa.eu/commission/presscorner/detail/en/ip_21_6683.
7. S. Kouro, J. I. Leon, D. Vinnikov and L. G. Franquelo, "Grid-Connected Photovoltaic Systems: An Overview of Recent Research and Emerging PV

- Converter Technology," in *IEEE Ind. Electron. Magazine*, vol. 9, no. 1, pp. 47-61, March 2015.
8. E. González-Romera, M. Ruiz-Cortés, M.-I. Milanés-Montero, F. Barrero-González, E. Romero-Cadaval, and R. A. Lopes, "Advantages of minimizing energy exchange instead of energy cost in prosumer microgrids," *Energies*, vol. 12, no. 719, pp. 1–15, 2019, doi: 10.3390/en12040719.
 9. C. Roncero-Clemente, N. Vilhena, V. Delgado-Gomes, E. Romero-Cadaval, and J. F. Martins, "Control and operation of a three-phase local energy router for prosumers in a smart community," *IET Renewable Power Generation*, vol. 14, no. 4, pp. 560–570, 2020, doi: 10.1049/iet-rpg.2019.0771.
 10. R. Wang, S. Jiang, D. Ma, Q. Sun, H. Zhang and P. Wang, "The Energy Management of Multiport Energy Router in Smart Home," in *IEEE Transactions on Consumer Electronics*, vol. 68, no. 4, pp. 344-353, Nov. 2022.
 11. B. Liu, Y. Peng, J. Xu, C. Mao, D. Wang and Q. Duan, "Design and Implementation of Multiport Energy Routers Toward Future Energy Internet," in *IEEE Transactions on Industry Applications*, vol. 57, no. 3, pp. 1945-1957, May-June 2021.
 12. Y. Liu, J. Li, Y. Wu, and F. Zhou, "Coordinated control of the energy router-based smart home energy management system," *Applied Sciences*, vol. 7, no. 9, p. 943, 2017, doi: 10.3390/app7090943.
 13. W. Guedes, C. Oliveira, T. A. Soares, B. H. Dias and M. Matos, "Collective Asset Sharing Mechanisms for PV and BESS in Renewable Energy Communities," in *IEEE Transactions on Smart Grid*, vol. 15, no. 1, pp. 607-616, Jan. 2024.
 14. M. Azizi, O. Husev, R. Mbayed, E. Monmasson, J. Martins and O. Veligorskyi, "Energy Router: A Sustainable Solution for Future Residential Buildings," in *IEEE Power Electronics Magazine*, vol. 12, no. 1, pp. 75-86, March 2025.
 15. J. Gutiérrez-Escalona, C. Roncero-Clemente, O. Husev, O. Matiushkin and F. Blaabjerg, "Artificial Intelligence in the Hierarchical Control of AC, DC, and Hybrid AC/DC Microgrids: A Review," in *IEEE Access*, vol. 12, pp. 157227-157246, 2024.

- 16.C. Roncero-Clemente, J. -G. Escalona, V. F. Pires, O. Matiushkin, M. I. Milanés-Montero and E. Romero-Cadaval, "Dead-Beat-based Model Predictive Current Control for the Dual-Purpose dc-dc/ac PWM Modular Power Converter," 2024 IEEE 18th International Conference on Compatibility, Power Electronics and Power Engineering (CPEPOWERENG), Gdynia, Poland, 2024, pp. 1-6.
- 17.I. Roasto, A. Rosin and T. Jalakas, "Power electronic interface converter for resource efficient buildings," IECON 2017 - 43rd Annual Conference of the IEEE Industrial Electronics Society, Beijing, China, 2017, pp. 3638-3643.
- 18.B. Liu et al., "An AC–DC Hybrid Multi-Port Energy Router With Coordinated Control and Energy Management Strategies," in IEEE Access, vol. 7, pp. 109069-109082, 2019.
- 19.X. Sun et al., "A Cascaded Multilevel Modular Energy Router Hybrid Photovoltaic and Energy Storage With Improved Power Balance Capability," in IEEE Transactions on Power Electronics, vol. 39, no. 3, pp. 3637-3654, March 2024.
- 20.H. E. Gelani, F. Dastgeer, M. Nasir, S. Khan, and J. M. Guerrero, "AC vs. DC distribution efficiency: Are we on the right path?," Energies, vol. 14, no. 13, p. 4039, 2021, doi: 10.3390/en14134039.
- 21.M. Azizi et al., "Grounding and isolation requirements in DC microgrids: Overview and critical analysis," Energies, vol. 16, no. 23, p. 7747, Nov. 2023, doi: 10.3390/en16237747.
- 22.S. Rahimpour, O. Husev and D. Vinnikov, "A Family of Bidirectional Solid-State Circuit Breakers with Increased Safety in DC Microgrids," in IEEE Transactions on Industrial Electronics, vol. 71, no. 9, pp. 10919 10929, Sept. 2024.
- 23.F. Mohammadi et al., "HVDC Circuit Breakers: A Comprehensive Review," in IEEE Transactions on Power Electronics, vol. 36, no. 12, pp. 13726-13739, Dec. 2021, doi: 10.1109/TPEL.2021.3073895.
- 24.A. Raza et al., "HVdc circuit breakers: Prospects and challenges," Appl. Sci., vol. 11, no. 11, 2021, Art. no. 5047, doi: 10.3390/app11115047.
- 25.X. Xu, J. Ye, Y. Wang, X. Xu, Z. Lai and X. Wei, "Design of a Reliable Bidirectional Solid-State Circuit Breaker for DC Microgrids," in IEEE

- Transactions on Power Electronics, vol. 37, no. 6, pp. 7200-7208, June 2022, doi: 10.1109/TPEL.2021.3139110.
- 26.S. Rahimpour, O. Husev, and D. Vinnikov, "Impedance-source DC solid-state circuit breakers: An overview," in Proc. Int. Symp. Power Power Electron., Elect. Drives, Automat. Motion, 2022, pp. 186–191.
 - 27.C. E. Ugalde-Loo, Y. Wang, S. Wang, W. Ming, J. Liang, and W. Li, "A review on Z-source solid state circuit breakers for DC distribution networks," CSEE J. Power Energy Syst., vol. 9, no. 1, pp. 15–27, Jan. 2023, doi: 10.17775/CSEEJPES.2022.04320.
 - 28.X. Song, P. Cairoli, Y. Du, and A. Antoniazzi, "A review of thyristor-based DC solid-state circuit breakers," IEEE Open J. Power Electron., vol. 2, pp. 659–672, 2021, doi: 10.1109/ojpe.2021.3134640.
 - 29.G. P. Adam, T. K. Vrana, R. Li, P. Li, G. Burt, and S. Finney, "Review of technologies for DC grids–Power conversion, flow control and protection," Inst. Eng. Technol. Power Electron., vol. 1212, no. 8, pp. 1851–1867, 2019,doi: 10.1049/iet-pel.2018.5719.
 - 30.O. Husev, N.V. Kurdkandi, M.G. Marangalu, D. Vinnikov and S. H. Hosseini, "A New Single-Phase Flying Inductor-Based Common Grounded Converter for Dual-Purpose Application," in IEEE Trans. on Ind. Electron., vol. 70, no. 8, pp. 799 7913-7923, Aug. 2023.
 - 31.S. S. Lee, C. Shen Lim, Y. P. Siwakoti and K. -B. Lee, "Single-Stage Common-Ground Boost Inverter (S2CGBI) for Solar Photovoltaic Systems," 2019 IEEE Energy Conversion Congress and Exposition (ECCE), Baltimore, MD, USA, 2019, pp. 4229-4233.
 - 32.L. Rosado, J. Samanes, E. Gubia and J. Lopez, "Selective Harmonic Mitigation: Limitations of Classical Control Strategies and Benefits of Model Predictive Control," in IEEE Transactions on Industry Applications, vol. 59, no. 5, pp. 6082-6094, Sept.-Oct. 2023.
 - 33.M. Merai, M. W. Naouar, I. Slama-Belkhodja and E. Monmasson, "An Adaptive PI Controller Design for DC-Link Voltage Control of Single-Phase Grid-

- Connected Converters," in IEEE Transactions on Industrial Electronics, vol. 66, no. 8, pp. 6241-6249, Aug. 2019.
- 34.K. Zeb et al., "High-performance and Multi-functional Control of Transformerless Single-phase Smart Inverter for Grid-connected PV System," in Journal of Modern Power Systems and Clean Energy, vol. 9, no. 6, pp. 1386-1394, November 2021.
 - 35.M. Ghiasi et al., "Multipurpose FCS Model Predictive Control of VSC-Based Microgrids for Islanded and Grid-Connected Operation Modes," in IEEE Systems Journal, vol. 17, no. 2, pp. 2558-2569, June 2023.
 - 36.Ranjan Bana, M. Amin and M. Molinas, "ANN-Based Surrogate PI and MPC Controllers for Grid-Connected VSC System: Small-Signal Analysis and Comparative Evaluation," in IEEE Journal of Emerging and Selected Topics in Power Electronics, vol.12, no.1, pp 566-578, Feb. 2024.
 - 37.F. Haroon, M. Aamir and A. Waqar, "Second-Order Rotating Sliding Mode Control with Composite Reaching Law for Two Level Single Phase Voltage Source Inverters," in IEEE Access, vol. 10, pp. 60177-60188, 2022.
 - 38.B. Long, P. J. Lu, K. T. Chong, J. Rodriguez and J. M. Guerrero, "Robust Fuzzy-Fractional-Order Nonsingular Terminal Sliding-Mode Control of LCL-Type Grid-Connected Converters," in IEEE Transactions on Industrial Electronics, vol. 69, no. 6, pp. 5854-5866, June 2022.
 - 39.M. Fliess, J. Levine, P. Martin and P. Rouchon, "A Lie-Backlund approach to equivalence and flatness of nonlinear systems," in IEEE Transactions on Automatic Control, vol. 44, no. 5, pp. 922-937, May 1999.
 - 40.Y. Liu, X. Chen, Y. Wu, K. Yang, J. Zhu and B. Li, "Enabling the Smart and Flexible Management of Energy Prosumers via the Energy Router With Parallel Operation Mode," in IEEE Access, vol. 8, pp. 35038-35047, 2020.
 - 41.M. Najafzadeh, N. Strzelecka, O. Husev, I. Roasto, K. Nassereddine, D. Vinnikov, and R. Strzelecki, "Grid-Forming Operation of Energy-Router Based on Model Predictive Control with Improved Dynamic Performance." Energies, 15, no. 11 (2022): 4010.

- 42.M.H. Athari, M.M. Ardehali. "Operational performance of energy storage as function of electricity prices for on-grid hybrid renewable energy system by optimized fuzzy logic controller." *Renewable Energy*, 85 (2016): 890-902.
- 43.J. Liu et al., "A home energy router and energy management strategy for AC/DC hybrid sources and consumers," in *Proc. 13th IEEE Conference on Industrial Electronics and Applications*, 2018.
- 44.C. Tu, L. Guan, F. Xiao and Z. Lan, "Study on an novel multi-port energy router for AC-DC hybrid microgrid," in *proc. of 13th IEEE Conference on Industrial Electronics and Applications (ICIEA)*, Wuhan, China, 2018, pp. 2654-2659.
- 45.I. Fagarasan, I. Stamatescu, N. Arghira, D. Hossu, A. Hossu and S. S. Iliescu, "Control Techniques and Strategies for Microgrids: Towards an Intelligent Control," *2017 21st International Conference on Control Systems and Computer Science (CSCS)*, Bucharest, Romania, 2017, pp. 630-635, doi: 10.1109/CSCS.2017.96.
- 46.Y. Liu et al., "Dispatchable droop control strategy for DC microgrid," *Energy Reports*, vol. 9, suppl. 12, pp. 98–102, 2023.
- 47.U. B. Tayab, M. A. B. Roslan, L. J. Hwai, and M. Kashif, "A review of droop control techniques for microgrid," *Renewable and Sustainable Energy Reviews*, vol. 76, pp. 717–727, 2017.
- 48.S. G. Ndeh, D. K. Ngwashi, L. K. Letting, C. D. Iweh, and E. Tanyi, "Power sharing enhancement through a decentralized droop-based control strategy in an islanded microgrid," *e-Prime – Advances in Electrical Engineering, Electronics and Energy*, vol. 7, 100433, 2024.
- 49.W. Wang, X. Lei, B. Wei, K. He and P. Yang, "Research on adaptive droop control strategy of DC active power and voltage in DC microgrid," in *Proc. 2023 Int. Conf. Power Energy Syst. Appl. (ICoPESA)*, Nanjing, China, 2023, pp. 627–632.
- 50.S. Prakash, V. Nougain and S. Mishra, "Adaptive Droop-Based Control for Active Power Sharing in Autonomous Microgrid for Improved Transient Performance," in *IEEE Journal of Emerging and Selected Topics in Power Electronics*, vol. 9, no. 3, pp. 3010-3018, June 2021, doi: 10.1109/JESTPE.2020.2988712.

- 51.Q. -C. Zhong, "Robust Droop Controller for Accurate Proportional Load Sharing Among Inverters Operated in Parallel," in IEEE Transactions on Industrial Electronics, vol. 60, no. 4, pp. 1281-1290, April 2013, doi: 10.1109/TIE.2011.2146221.
- 52.A. Basati, A. Fakharian and J. M. Guerrerro, "An intelligent droop control for improve voltage regulation and equal power sharing in islanded DC microgrids," 2017 5th Iranian Joint Congress on Fuzzy and Intelligent Systems (CFIS), Qazvin, Iran, 2017, pp. 190-195, doi: 10.1109/CFIS.2017.8003681.
- 53.T. L. Vandoorn, J. D. M. De Kooning, B. Meersman, and L. Vandevelde, "Communication-based secondary control in microgrids with voltage-based droop control," in Proc. IEEE PES Transmission & Distribution Conf. Expo., Orlando, FL, USA, 2012, pp. 1–6.
- 54.L. Meng, T. Dragicevic, J. Roldán-Pérez, J. C. Vasquez and J. M. Guerrero, "Modeling and Sensitivity Study of Consensus Algorithm-Based Distributed Hierarchical Control for DC Microgrids," in IEEE Transactions on Smart Grid, vol. 7, no. 3, pp. 1504-1515, May 2016, doi: 10.1109/TSG.2015.2422714.
- 55.R. Li, S. Liu, M. Xia and X. Liu, "Analysis of Effects of Communication Conditions on Distributed Secondary Control for DC Microgrids," 2020 IEEE 9th International Power Electronics and Motion Control Conference (IPEMC2020-ECCE Asia), Nanjing, China, 2020, pp. 2933-2938, doi: 10.1109/IPEMC-ECCEAsia48364.2020.9368071.
- 56.A. Lahmer, J. -W. Chang, H. Jeong and S. Chae, "Distributed Hierarchical Control of Energy Storage Systems in a DC Microgrid under Consensus Based Adaptive Droop Control Method," 2023 11th International Conference on Power Electronics and ECCE Asia (ICPE 2023 - ECCE Asia), Jeju Island, Korea, Republic of, 2023, pp. 568-573, doi: 10.23919/ICPE2023-ECCEAsia54778.2023.10213736.
- 57.L. Meng, T. Dragicevic, J. M. Guerrero and J. C. Vasquez, "Dynamic consensus algorithm based distributed global efficiency optimization of a droop controlled DC microgrid," 2014 IEEE International Energy Conference (ENERGYCON),

Cavtat, Croatia, 2014, pp. 1276-1283, doi: 10.1109/ENERGYCON.2014.6850587.

- 58.O. Husev, D. Vinnikov, S. Kouro, F. Blaabjerg, and C. Roncero-Clemente, "Dual-purpose converters for DC or AC grid as energy transition solution: Perspectives and challenges," IEEE Ind. Electron. Mag., early access.
59. S. A. Q. Mohammed and J.-W. Jung, "A state-of-the-art review on soft-switching techniques for DC–DC, DC–AC, AC–DC, and AC–AC power converters," IEEE Trans. Ind. Informat., vol. 17, no. 10, pp. 6569–6582, Oct. 2021.
- 60.E. Jayashree and G. Uma, "Analysis, design and implementation of a quasi-resonant DC–DC converter," IET Power Electron., vol. 4, no. 7, pp. 785–792, 2011.
- 61.T. Zhu, F. Zhuo, F. Zhao, F. Wang, H. Yi and T. Zhao, "Optimization of Extended Phase-Shift Control for Full-Bridge CLLC Resonant Converter with Improved Light-Load Efficiency," in IEEE Trans. on Power Electron., vol. 35, no. 10, pp. 11129-11142, Oct. 2020.
- 62.N. Hou and Y. W. Li, "Overview and Comparison of Modulation and Control Strategies for a Nonresonant Single-Phase Dual-Active-Bridge DC–DC Converter," in IEEE Trans. on Power Electron., vol. 35, no. 3, pp. 3148-3172, March 2020.
- 63.U. Badstuebner, J. Biela, and J. W. Kolar, "Design of a 99%-efficient, 5-kW, phase-shift PWM DC–DC converter for telecom applications," in Proc. IEEE Appl. Power Electron. Conf. Expo. (APEC), Palm Springs, CA, USA, 2010, pp. 773–780.
- 64.F. M. Ibanez, "Bidirectional Series Resonant DC/AC Converter for Energy Storage Systems," in IEEE Trans. on Power Electron., vol. 34, no. 4, pp. 3429-3444, April 2019.
- 65.S. -H. Lee, W. -J. Cha and B. -H. Kwon, "High-Efficiency Soft-Switching AC–DC Converter With Single-Power-Conversion Method," in IEEE Transactions on Industrial Electronics, vol. 64, no. 6, pp. 4483-4490, June 2017.

- 66.D. Rothmund, D. Bortis, J. Huber, D. Biadene, and J. W. Kolar, “10-kV SiC-based bidirectional soft-switching single-phase AC/DC converter concept for medium-voltage solid-state transformers,” in *Proc. IEEE Int. Symp. Power Electron. Distrib. Gener. Syst. (PEDG)*, Florianopolis, Brazil, 2017, pp. 1–8.
- 67.M. Llomplat, J. E. Bosso, E. R. Carballo, and G. O. García, “Novel modified phase-shift modulation strategy for isolated AC–DC power converters,” *IET Power Electron.*, vol. 13, no. 5, pp. 1022–1032, 2020.
- 68.A. F. B. Santos, G. P. Duggan, C. D. Lute, and D. J. Zimmerle, “An efficiency comparison study for small appliances operating in DC and AC in minigrids,” in *Proc. IEEE Global Humanitarian Technology Conf. (GHTC)*, San Jose, CA, USA, 2018, pp. 1–2.
- 69.T. Mishima, S. Sakamoto and C. Ide, "ZVS Phase-Shift PWM-Controlled Single-Stage Boost Full-Bridge AC–AC Converter for High-Frequency Induction Heating Applications," in *IEEE Trans. on Ind. Electron.*, vol. 64, no. 3, pp. 2054–2061, March 2017.
- 70.F. Melzi, A. Same, M. Zayani, and L. Oukhellou, “A dedicated mixture model for clustering smart meter data: Identification and analysis of electricity consumption behaviors,” *Energies*, vol. 10, no. 10, p. 1446, Sep. 2017.
- 71.A. Stippich et al., “From AC to DC: Benefits in household appliances,” in *Proc. Int. ETG Congr.*, Bonn, Germany, 2017, pp. 1–6.
- 72.D. L. Gerber, V. Vossos, W. Feng, A. Khandekar, C. Marnay, and B. Nordman, “A simulation-based comparison of AC and DC power distribution networks in buildings,” in *Proc. IEEE Int. Conf. DC Microgrids (ICDCM)*, Nuremberg, Germany, 2017, pp. 588–595.
- 73.AA. Goikoetxea, J. M. Canales, R. Sanchez, and P. Zumeta, “DC versus AC in residential buildings: Efficiency comparison,” in *Proc. IEEE EUROCON*, Zagreb, Croatia, 2013, pp. 1–5.
- 74.A. Santos, G. Duggan, S. Frank, D. Gerber, and D. Zimmerle, “Endpoint use efficiency comparison for AC and DC power distribution in commercial buildings,” *Energies*, vol. 14, no. 18, p. 5863, 2021.

- 75.IEC, LVDC: Electricity for the 21st Century, IEC Technology Report, Geneva, Switzerland, 2017. [Online]. Available: <https://www.iec.ch/basecamp/LVdc-electricity-21st-century>.
- 76.European Commission, "Renewable energy targets," [Online]. Available: https://energy.ec.europa.eu/topics/renewable-energy/renewable-energy-directive-targets-and-rules/renewable-energy-targets_en#the-2030-targets
- 77..P. Li, "Energy storage is the core of renewable technologies," in IEEE Nanotechnology Magazine, vol. 2, no. 4, pp. 13-18, Dec. 2008, doi: 10.1109/MNANO.2009.932032.
- 78.Hamidieh and M. Ghassemi, "Microgrids and Resilience: A Review," in IEEE Access, vol. 10, pp. 106059-106080, 2022, doi: 10.1109/ACCESS.2022.3211511.
- 79.M. Najafzadeh, R. Ahmadihangar, O. Husev, I. Roasto, T. Jalakas and A. Blinov, "Recent Contributions, Future Prospects and Limitations of Interlinking Converter Control in Hybrid AC/DC Microgrids," in IEEE Access, vol. 9, pp. 7960-7984, 2021, doi: 10.1109/ACCESS.2020.3049023.
- 80.T. Dragičević, X. Lu, J. C. Vasquez and J. M. Guerrero, "DC Microgrids—Part II: A Review of Power Architectures, Applications, and Standardization Issues," in IEEE Transactions on Power Electronics, vol. 31, no. 5, pp. 3528-3549, May 2016, doi: 10.1109/TPEL.2015.2464277.
- 81.D. Kumar, F. Zare and A. Ghosh, "DC Microgrid Technology: System Architectures, AC Grid Interfaces, Grounding Schemes, Power Quality, Communication Networks, Applications, and Standardizations Aspects," in IEEE Access, vol. 5, pp. 12230-12256, 2017, doi: 10.1109/ACCESS.2017.2705914.
- 82.S. K. Sahoo, A. K. Sinha, and N. K. Kishore, "Control techniques in AC, DC, and hybrid AC–DC microgrid: A review," IEEE J. Emerg. Sel. Topics Power Electron., vol. 6, no. 2, pp. 738–759, 2018.
- 83.M. Chen, S. Ma, H. Wan, J. Wu, and Y. Jiang, "Distributed control strategy for DC microgrids of photovoltaic energy storage systems in off-grid operation," Energies, vol. 11, no. 10, p. 2637, 2018.

- 84.B. Aluisio, S. Bruno, L. De Bellis, M. Dicorato, G. Forte, and M. Trovato, "DC-microgrid operation planning for an electric vehicle supply infrastructure," *Appl. Sci.*, vol. 9, no. 13, p. 2687, 2019.
- 85.E. L. Carvalho, A. Blinov, A. Chub, P. Emiliani, G. de Carne and D. Vinnikov, "Grid Integration of DC Buildings: Standards, Requirements and Power Converter Topologies," in *IEEE Open Journal of Power Electronics*, vol. 3, pp. 798-823, 2022, doi: 10.1109/OJPEL.2022.3217741.
- 86.N. Papanikolaou, A. Kyritsis, M. Loupis, C. Tzotzos and E. Zoga, "Design Considerations for Single-Phase Line Frequency Transformers Applied at Photovoltaic Systems," in *IEEE Power and Energy Technology Systems Journal*, vol. 2, no. 3, pp. 82-93, Sept. 2015, doi: 10.1109/JPETS.2015.2433391.
- 87.M. A. Hannan et al., "State of the Art of Solid-State Transformers: Advanced Topologies, Implementation Issues, Recent Progress and Improvements," in *IEEE Access*, vol. 8, pp. 19113-19132, 2020, doi: 10.1109/ACCESS.2020.2967345.
- 88.X. She, A. Q. Huang and R. Burgos, "Review of Solid-State Transformer Technologies and Their Application in Power Distribution Systems," in *IEEE Journal of Emerging and Selected Topics in Power Electronics*, vol. 1, no. 3, pp. 186-198, Sept. 2013, doi: 10.1109/JESTPE.2013.2277917.
- 89.M. -H. Ryu, H. -S. Kim, J. -W. Baek, H. -G. Kim and J. -H. Jung, "Effective Test Bed of 380-V DC Distribution System Using Isolated Power Converters," in *IEEE Transactions on Industrial Electronics*, vol. 62, no. 7, pp. 4525-4536, July 2015, doi: 10.1109/TIE.2015.2399273.
- 90.IEEE Standard for Interconnection and Interoperability of Distributed Energy Resources with Associated Electric Power Systems Interfaces--Amendment 1: To Provide More Flexibility for Adoption of Abnormal Operating Performance Category III," in *IEEE Std 1547a-2020 (Amendment to IEEE Std 1547-2018)* , vol., no., pp.1-16, 15 April 2020, doi: 10.1109/IEEESTD.2020.9069495.
- 91.S. Rivera, R. Lizana F., S. Kouro, T. Dragičević and B. Wu, "Bipolar DC Power Conversion: State-of-the-Art and Emerging Technologies," in *IEEE Journal of*

Emerging and Selected Topics in Power Electronics, vol. 9, no. 2, pp. 1192-1204, April 2021, doi: 10.1109/JESTPE.2020.2980994.

- 92.S. Dey, V. K. Bussa and R. K. Singh, "Transformerless Hybrid Converter With AC and DC Outputs and Reduced Leakage Current," in IEEE Journal of Emerging and Selected Topics in Power Electronics, vol. 7, no. 2, pp. 1329-1341, June 2019, doi: 10.1109/JESTPE.2018.2883243.
- 93.G. Buticchi, D. Barater, E. Lorenzani and G. Franceschini, "Digital Control of Actual Grid-Connected Converters for Ground Leakage Current Reduction in PV Transformerless Systems," in IEEE Transactions on Industrial Informatics, vol. 8, no. 3, pp. 563-572, Aug. 2012, doi: 10.1109/TII.2012.2192284.
- 94.T. R. Oliveira, W. W. A. G. Silva, S. I. Seleme and P. F. Donoso-Garcia, "PLL-Based Feed-Forward Control to Attenuate Low-Frequency Common-Mode Voltages in Transformerless LVDC Systems," in IEEE Transactions on Industry Applications, vol. 55, no. 3, pp. 3151-3159, May-June 2019, doi: 10.1109/TIA.2019.2891435.
- 95.J. Qiu, Y. He, C. Lei, Q. Jiao and J. Liu, "An Improved LMSVM Method for Leakage Current Suppression and Neutral-Point Voltage Control in Transformerless NPC Three-Level Inverters," in IEEE Journal of Emerging and Selected Topics in Power Electronics, vol. 10, no. 3, pp. 3100-3113, June 2022, doi: 10.1109/JESTPE.2021.3106339.
- 96.L. Zhou, F. Gao and T. Xu, "Implementation of Active NPC Circuits in Transformer-Less Single-Phase Inverter With Low Leakage Current," in IEEE Transactions on Industry Applications, vol. 53, no. 6, pp. 5658-5667, Nov.-Dec. 2017, doi: 10.1109/TIA.2017.2736965.
- 97.S. Iturriaga-Medina et al., "Leakage-Ground Currents Compensation in a Transformerless HB-NPC Topology Using a DC-Link-Tied LC Filter for Photovoltaic Applications," in IEEE Journal of Emerging and Selected Topics in Power Electronics, vol. 10, no. 4, pp. 4725-4737, Aug. 2022, doi: 10.1109/JESTPE.2021.3132239.

- 98.G. Escobar, P. R. Martinez-Rodriguez, S. Iturriaga-Medina, J. C. Mayo-Maldonado, J. Lopez-Sarabia and O. M. Micheloud-Vernackt, "Mitigation of Leakage-Ground Currents in Transformerless Grid-Tied Inverters via Virtual-Ground Connection," in IEEE Journal of Emerging and Selected Topics in Power Electronics, vol. 8, no. 3, pp. 3111-3123, Sept. 2020, doi: 10.1109/JESTPE.2019.2933399.
- 99.J. Mohammadi, F. Badrkhani Ajaei and G. Stevens, "Grounding the DC Microgrid," in IEEE Transactions on Industry Applications, vol. 55, no. 5, pp. 4490-4499, Sept.-Oct. 2019, doi: 10.1109/TIA.2019.2928278.
- 100.M. Pourmirasghariyan, S. F. Zarei, and M. Hamzeh, "DC-system grounding: Existing strategies, performance analysis, functional characteristics, technical challenges, and selection criteria—A review," Electr. Power Syst. Res., vol. 206, p. 107769, 2022.
- 101.J. Park, "Ground fault detection and location for ungrounded DC traction power systems," IEEE Trans. Veh. Technol., vol. 64, no. 12, pp. 5667–5676, Dec. 2015.
- 102.S. Beheshtaein, R. M. Cuzner, M. Forouzesh, M. Savaghebi and J. M. Guerrero, "DC Microgrid Protection: A Comprehensive Review," in IEEE Journal of Emerging and Selected Topics in Power Electronics, doi: 10.1109/JESTPE.2019.2904588.
- 103.Rahimpour, Saeed, Oleksandr Husev, and Dmitri Vinnikov. "Design and Analysis of a DC Solid-State Circuit Breaker for Residential Energy Router Application." Energies 15, no. 24 (2022): 9434.
- 104.J. -D. Park and J. Candelaria, "Fault Detection and Isolation in Low-Voltage DC-Bus Microgrid System," in IEEE Transactions on Power Delivery, vol. 28, no. 2, pp. 779-787, April 2013, doi: 10.1109/TPWRD.2013.2243478.
- 105.L. Xu et al., "A Review of DC Shipboard Microgrids—Part II: Control Architectures, Stability Analysis, and Protection Schemes," in IEEE Transactions on Power Electronics, vol. 37, no. 4, pp. 4105-4120, April 2022, doi: 10.1109/TPEL.2021.3128409.

106. A. A. Sheikh et al., "A Brief Review on DC Microgrid Protection," 2020 IEEE First International Conference on Smart Technologies for Power, Energy and Control (STPEC), Nagpur, India, 2020, pp. 1-6, doi: 10.1109/STPEC49749.2020.9297770.
107. L. Zhang, N. Tai, W. Huang, J. Liu and Y. Wang, "A review on protection of DC microgrids," in Journal of Modern Power Systems and Clean Energy, vol. 6, no. 6, pp. 1113-1127, November 2018, doi: 10.1007/s40565-018-0381-9.
108. R. Mohanty and A. K. Pradhan, "Protection of DC and hybrid AC-DC microgrids with ring configuration," 2017 7th International Conference on Power Systems (ICPS), Pune, India, 2017, pp. 607-612, doi: 10.1109/ICPES.2017.8387365.
109. M. Noritake, T. Iino, A. Fukui, K. Hirose and M. Yamasaki, "A study of the safety of the DC 400 V distribution system," INTELEC 2009 - 31st International Telecommunications Energy Conference, Incheon, Korea (South), 2009, pp. 1-6, doi: 10.1109/INTLEC.2009.5351768.
110. O. Husev, O. Matushkin, D. Vinnikov, C. Roncero-Clemente and S. Kouro, "Novel Concept of Solar Converter With Universal Applicability for DC and AC Microgrids," in IEEE Transactions on Industrial Electronics, vol. 69, no. 5, pp. 4329-4341, May 2022, doi: 10.1109/TIE.2021.3086436.
111. M. Vygoder, M. Milton, J. D. Gudex, R. M. Cuzner and A. Benigni, "A Hardware-in-the-Loop Platform for DC Protection," in IEEE Journal of Emerging and Selected Topics in Power Electronics, vol. 9, no. 3, pp. 2605-2619, June 2021, doi: 10.1109/JESTPE.2020.3017769.
112. Y. -C. Liu and C. -Y. Lin, "Insulation fault detection circuit for ungrounded DC power supply systems," SENSORS, 2012 IEEE, Taipei, Taiwan, 2012, pp. 1-4, doi: 10.1109/ICSENS.2012.6411550.
113. D. Salomonsson, L. Soder and A. Sannino, "Protection of Low-Voltage DC Microgrids," in IEEE Transactions on Power Delivery, vol. 24, no. 3, pp. 1045-1053, July 2009, doi: 10.1109/TPWRD.2009.2016622.
114. NL: DC Installations for low Voltage, Standard NPR 9090:2018, Royal Dutch Standardization Institute (NEN), The Netherlands, Sep. 2018.

115. A. Blinov, I. Roasto, A. Chub, P. Emiliani, and D. Vinnikov, "Electric power management and control in DC buildings—State-of-the-art and emerging technologies," in *Power Quality: Infrastructures and Control*, 2023, pp. 67–96.
116. W. Li, Y. Gu, H. Luo, W. Cui, X. He and C. Xia, "Topology Review and Derivation Methodology of Single-Phase Transformerless Photovoltaic Inverters for Leakage Current Suppression," in *IEEE Transactions on Industrial Electronics*, vol. 62, no. 7, pp. 4537-4551, July 2015, doi: 10.1109/TIE.2015.2399278.
117. Y. Gu, W. Li, Y. Zhao, B. Yang, C. Li and X. He, "Transformerless Inverter With Virtual DC Bus Concept for Cost-Effective Grid-Connected PV Power Systems," in *IEEE Transactions on Power Electronics*, vol. 28, no. 2, pp. 793-805, Feb. 2013, doi: 10.1109/TPEL.2012.2203612.
118. M. N. H. Khan, M. Forouzesh, Y. P. Siwakoti, L. Li, T. Kerekes and F. Blaabjerg, "Transformerless Inverter Topologies for Single-Phase Photovoltaic Systems: A Comparative Review," in *IEEE Journal of Emerging and Selected Topics in Power Electronics*, vol. 8, no. 1, pp. 805-835, March 2020, doi: 10.1109/JESTPE.2019.2908672.
119. A. Demetriou, D. Buxton and C. A. Charalambous, "Stray Current DC Corrosion Blind Spots Inherent to Large PV Systems Fault Detection Mechanisms: Elaboration of a Novel Concept," in *IEEE Transactions on Power Delivery*, vol. 33, no. 1, pp. 3-11, Feb. 2018, doi: 10.1109/TPWRD.2016.2538789.
120. A. Dimitriou and C. A. Charalambous, "DC Interference Modeling for Assessing the Impact of Sustained DC Ground Faults of Photovoltaic Systems on Third-Party Infrastructure," in *IEEE Transactions on Industrial Electronics*, vol. 66, no. 4, pp. 2935-2945, April 2019, doi: 10.1109/TIE.2018.2844841.
121. Y. Wu and P. Zhang, "A Novel Online Monitoring Scheme for Underground Power Cable Insulation Based on Common-Mode Leakage Current Measurement," in *IEEE Transactions on Industrial Electronics*, vol. 69, no. 12, pp. 13586-13596, Dec. 2022, doi: 10.1109/TIE.2022.3142434.

122. International Electrotechnical Commission, IEC 60950 – Information Technology Equipment – Safety – Part 1: General Requirements, 3rd ed., Geneva, Switzerland, 2005. [Online]. Available: <https://webstore.iec.ch/publication/4020>.
123. IEEE Standard for Interconnection and Interoperability of Distributed Energy Resources with Associated Electric Power Systems Interfaces, IEEE Std 1547-2018 (Revision of IEEE Std 1547-2003), Piscataway, NJ, USA, 2018, pp. 1–138.
124. Mohammadi, F. Badrkhani Ajaei and G. Stevens, "Grounding the AC Microgrid," in IEEE Transactions on Industry Applications, vol. 55, no. 1, pp. 98-105, Jan.-Feb. 2019, doi: 10.1109/TIA.2018.2864106.
125. J. Yang, X. Xiao, W. Su, X. Si, J. Zhang and X. Zhang, "Comparison of Grounding Modes of MMC-Based Flexible DC Distribution System," in IEEE Access, vol. 9, pp. 19696-19706, 2021, doi: 10.1109/ACCESS.2021.3049886.
126. International Electrotechnical Commission, IEC 60364-1 – Low-Voltage Electrical Installations – Part 1: Fundamental Principles, Assessment of General Characteristics, Definitions, Geneva, Switzerland, 2005.
127. P. Sattari and S. Panetta, "High-Resistance Grounding Design for Industrial Facilities: Providing Continuity of Service in Complex Distribution Systems," in IEEE Industry Applications Magazine, vol. 26, no. 2, pp. 18-27, March-April 2020, doi: 10.1109/MIAS.2019.2943653.
128. J. Lopez-Sarabia, G. E. Valderrama, P. R. Martinez-Rodriguez, S. Iturriaga-Medina, J. C. Mayo-Maldonado and D. d. Puerto-Flores, "DC-Link Capacitors' Voltage Balance in an HB-NPC Five-Level Grid-Tied Inverter via the Common-Mode Control Component," in IEEE Journal of Emerging and Selected Topics in Power Electronics, vol. 10, no. 3, pp. 3242-3255, June 2022, doi: 10.1109/JESTPE.2021.3128041.
129. M. Valdes, T. Papallo, and B. Premerlani, "Finding fault—Locating a ground fault in low-voltage, high-resistance grounded systems via the single-processor concept for circuit protection," IEEE Ind. Appl. Mag., vol. 13, no. 5, pp. 24–30, Sep.–Oct. 2007.

130. D. Paul, "DC traction power system grounding," *IEEE Trans. Ind. Appl.*, vol. 38, no. 3, pp. 818–824, May–Jun. 2002.
131. M. Mobarrez, D. Fregosi, S. Bhattacharya and M. A. Bahmani, "Grounding architectures for enabling ground fault ride-through capability in DC microgrids," 2017 IEEE Second International Conference on DC Microgrids (ICDCM), Nuremburg, Germany, 2017, pp. 81-87, doi: 10.1109/ICDCM.2017.8001026.
132. M. Naghizadeh, E. Farjah, T. Ghanbari, H. Pourgharibshahi and M. T. Andani, "Efficient Grounding Method for DC Microgrid with Multiple Grounding Points," 2018 Clemson University Power Systems Conference (PSC), Charleston, SC, USA, 2018, pp. 1-6, doi: 10.1109/PSC.2018.8664021.
133. J. Karppanen et al., "Effect of Voltage Level Selection on Earthing and Protection of LVDC Distribution Systems," 11th IET International Conference on AC and DC Power Transmission, Birmingham, 2015, pp. 1-8, doi: 10.1049/cp.2015.0057.
134. J. Yang, J. E. Fletcher, and J. O'Reilly, "Short-circuit and ground fault analyses and location in VSC-based DC network cables," *IEEE Trans. Ind. Electron.*, vol. 59, no. 10, pp. 3827–3837, Oct. 2012.
135. B. Jacobson and J. Walker, "Grounding considerations for DC and mixed DC and AC power systems," *Naval Eng. J.*, vol. 119, no. 2, pp. 49–62, 2007.
136. K. Hirose et al., "Grounding concept considerations and recommendations for 400VDC distribution system," 2011 IEEE 33rd International Telecommunications Energy Conference (INTELEC), Amsterdam, Netherlands, 2011, pp. 1-8, doi: 10.1109/INTLEC.2011.6099881.
137. L. Mackay, K. F. Yanez Martinez, E. Vandeventer, L. Ramirez-Elizondo and P. Bauer, "Capacitive grounding for DC distribution grids with two grounding points," 2017 IEEE Second International Conference on DC Microgrids (ICDCM), Nuremburg, Germany, 2017, pp. 76-80, doi: 10.1109/ICDCM.2017.8001025.
138. S. A. Saleh, S. Kanukollu and A. Al-Durra, "Performance Assessment of Frequency Selective Grounding for Grid-Connected Photovoltaic Systems," in

- IEEE Transactions on Power Delivery, vol. 38, no. 2, pp. 1138-1147, April 2023, doi: 10.1109/TPWRD.2022.3209876.
139. W. Zhang, T. Wei, Q. Chen, Y. Cui, W. Liu and J. Yang, "Study on Grounding Modes of AC/DC Hybrid Distribution System," 2019 IEEE International Conference on Energy Internet (ICEI), Nanjing, China, 2019, pp. 42-46, doi: 10.1109/ICEI.2019.00014.
140. Hai Yan Lu, Jian Guo Zhu and S. Y. R. Hui, "Experimental determination of stray capacitances in high frequency transformers," in IEEE Transactions on Power Electronics, vol. 18, no. 5, pp. 1105-1112, Sept. 2003, doi: 10.1109/TPEL.2003.816186.
141. K. Fu, W. Chen, and S. Lin, "A general transformer evaluation method for common-mode noise behavior," Energies, vol. 12, no. 10, p. 1984, 2019.
142. T. R. de Oliveira, A. S. Bolzon and P. F. Donoso-Garcia, "Grounding and safety considerations for residential DC microgrids," IECON 2014 - 40th Annual Conference of the IEEE Industrial Electronics Society, Dallas, TX, USA, 2014, pp. 5526-5532, doi: 10.1109/IECON.2014.7049345.
143. D. Zhang, D. Cao, J. Huber, J. Everts and J. W. Kolar, "Non-Isolated Three-Phase Current DC-Link Buck-Boost EV Charger with Virtual Output Midpoint Grounding and Ground Current Control," in IEEE Transactions on Transportation Electrification, doi: 10.1109/TTE.2023.3282978.
144. C. Roncero-Clemente et al., "Feasibility Study of Three-Phase Modular Converter for Dual-Purpose Application in DC and AC Microgrids," in IEEE Journal of Emerging and Selected Topics in Power Electronics, doi: 10.1109/JESTPE.2023.3247960.
145. Lee, Y. Yang and Y. P. Siwakoti, "A Novel Single-Stage FiveLevel Common-Ground-Boost-Type Active Neutral-Point-Clamped (5L-CGBT-ANPC) Inverter," in IEEE Transactions on Power Electronics, vol. 36, no. 6, pp. 6192-6196, June 2021.
146. N. Vosoughi, S. H. Hosseini and M. Sabahi, "A New Single-Phase Transformerless Grid-Connected Inverter With Boosting Ability and Common

- Ground Feature," in IEEE Transactions on Industrial Electronics, vol. 67, no. 11, pp. 9313-9325, Nov. 2020, doi: 10.1109/TIE.2019.2952781.
147. T. H. Shahsavar et al., "A New Flying Capacitor-Based Buck–Boost Converter for Dual-Purpose Applications," in IEEE Journal of Emerging and Selected Topics in Industrial Electronics, vol. 4, no. 2, pp. 447-459, April 2023, doi: 10.1109/JESTIE.2023.3238322.
 148. M. Azizi, S. Rahimpour, O. Husev and O. Veligorskyi, "Back-to-Back Energy Router Based on Common-Ground Inverters," 2023 IEEE 17th International Conference on Compatibility, Power Electronics and Power Engineering (CPE-POWERENG), Tallinn, Estonia, 2023, pp. 1-6, doi: 10.1109/CPE-POWERENG58103.2023.10227480.
 149. R. Barzegarkhoo, Y. P. Siwakoti, N. Vosoughi and F. Blaabjerg, "Six-Switch Step-Up Common-Grounded Five-Level Inverter With Switched-Capacitor Cell for Transformerless Grid-Tied PV Applications," in IEEE Transactions on Industrial Electronics, vol. 68, no. 2, pp. 1374-1387, Feb. 2021, doi: 10.1109/TIE.2020.2967674.
 150. O. Husev, N. V. Kurdkandi, M. G. Marangalu, D. Vinnikov and S. H. Hosseini, "A New Single-Phase Flying Inductor-Based Common Grounded Converter for Dual-Purpose Application," in IEEE Transactions on Industrial Electronics, vol. 70, no. 8, pp. 7913-7923, Aug. 2023, doi: 10.1109/TIE.2022.3215832.
 151. R. Barzegarkhoo, S. S. Lee, Y. P. Siwakoti, S. A. Khan and F. Blaabjerg, "Design, Control, and Analysis of a Novel Grid-Interfaced Switched-Boost Dual T-Type Five-Level Inverter With Common-Ground Concept," in IEEE Transactions on Industrial Electronics, vol. 68, no. 9, pp. 8193-8206, Sept. 2021, doi: 10.1109/TIE.2020.3018073.
 152. H. N. Hokmabad, T. H. Shahsavar, O. Matiushkin, T. Jalakas, O. Husev and J. Belikov, "Single Cell Energy Router Justification for Three Phase Near Zero Energy Buildings," 2025 IEEE Applied Power Electronics Conference and Exposition (APEC), Atlanta, GA, USA, 2025, pp. 1622-1628.

153. M. Mehrasa, E. Pouresmaeil, S. Taheri, I. Vechiu and J. P. S. Catalão, "Novel Control Strategy for Modular Multilevel Converters Based on Differential Flatness Theory," in IEEE Journal of Emerging and Selected Topics in Power Electronics, vol. 6, no. 2, pp. 888-897, June 2018.
154. H. A. Khalid, C. Cecati, N. A. Al-Emadi, A. Gastli and L. Ben-Brahim, "Differential Flatness-Based Performance Enhancement of a Vector Controlled VSC With an LCL-Filter for Weak Grids," in IEEE Access, vol. 9, pp. 33557-33568, 2021.
155. P. Mungporn et al., "Dynamics improvement of 3-phase inverter with output LC-filter by using differential flatness based control for grid connected applications," in Proceedings of the 2016 19th International Conference on Electrical Machines and Systems (ICEMS), Chiba, Japan, 2016, pp. 1-6.
156. A. Houari, H. Renaudineau, J. -P. Martin, S. Pierfederici and F. Meibody-Tabar, "Flatness-Based Control of Three-Phase Inverter With Output LC Filter," in IEEE Transactions on Industrial Electronics, vol. 59, no. 7, pp. 2890-2897, July 2012.
157. M.I. Isabel-Montero, E. Romero-Cadaval, and F. Barrero-González., "Comparison of control strategies for shunt active power filters in three-phase four-wire systems," IEEE Transactions on Power Electronics, Vol. 22, No. 1, January 2007.
158. M. Gonzales, V. Cardenas and F. Pazos, "DQ transformation development for single-phase systems to compensate harmonic distortion and reactive power," 9th IEEE International Power Electronics Congress, pp. 177-182, 2004.
159. C. Roncero-Clemente, E. Romero-Cadaval, O. Husev and D. Vinnikov, "P and Q control strategy for single phase Z/qZ source inverter based on d-q frame," 2014 IEEE 23rd International Symposium on Industrial Electronics (ISIE), Istanbul, Turkey, 2014, pp. 2048-2053.
160. E. Song, A. F. Lynch and V. Dinavahi, "Experimental Validation of Nonlinear Control for a Voltage Source Converter," in IEEE Transactions on Control Systems Technology, vol. 17, no. 5, pp. 1135-1144, Sept. 2009.

161. A. Gensior, H. Sira-Ramirez, J. Rudolph and H. Guldner, "On Some Nonlinear Current Controllers for Three-Phase Boost Rectifiers," in *IEEE Transactions on Industrial Electronics*, vol. 56, no. 2, pp. 360-370, Feb. 2009.
162. O. Husev, C. Roncero-Clemente, E. Makovenko, S. P. Pimentel, D. Vinnikov and J. Martins, "Optimization and Implementation of the Proportional-Resonant Controller for Grid-Connected Inverter With Significant Computation Delay," in *IEEE Transactions on Industrial Electronics*, vol. 67, no. 2, pp. 1201-1211, Feb. 2020.
163. Z. Pan, F. Dong, J. Zhao, L. Wang, H. Wang and Y. Feng, "Combined Resonant Controller and Two-Degree-of-Freedom PID Controller for PMSLM Current Harmonics Suppression," in *IEEE Transactions on Industrial Electronics*, vol. 65, no. 9, pp. 7558-7568, Sept. 2018.
164. R. Chattopadhyay, A. De and S. Bhattacharya, "Comparison of PR controller and damped PR controller for grid current control of LCL filter based grid-tied inverter under frequency variation and grid distortion," 2014 IEEE Energy Conversion Congress and Exposition (ECCE), Pittsburgh, PA, USA, 2014, pp. 3634-3641.
165. R. A. Mastromauro, M. Liserre, and A. Dell'Aquila, "Control issues in single-stage photovoltaic systems: MPPT, current and voltage control," *IEEE Trans. Ind. Inform.*, vol. 8, no. 2, pp. 241–254, May 2012.
166. L. Harnefors, A. G. Yepes, A. Vidal and J. Doval-Gandoy, "Passivity-Based Stabilization of Resonant Current Controllers With Consideration of Time Delay," in *IEEE Transactions on Power Electronics*, vol. 29, no. 12, pp. 6260-6263, Dec. 2014.
167. D. Minoli, K. Sohraby and B. Occhiogrosso, "IoT Considerations, Requirements, and Architectures for Smart Buildings—Energy Optimization and Next-Generation Building Management Systems," in *IEEE Internet of Things Journal*, vol. 4, no. 1, pp. 269-283, Feb. 2017, doi: 10.1109/JIOT.2017.2647881.
168. C. Balasubramanian and R. L. Raja Singh, "IoT Based Energy Management System in Smart Grid," 2023 *Innovations in Power and Advanced Computing*

Technologies (i-PACT), Kuala Lumpur, Malaysia, 2023, pp. 1-6, doi: 10.1109/i-PACT58649.2023.10434561.

169. S. Wang, X. Wang and W. Wu, "Cloud Computing and Local Chip-Based Dynamic Economic Dispatch for Microgrids," in *IEEE Transactions on Smart Grid*, vol. 11, no. 5, pp. 3774-3784, Sept. 2020, doi: 10.1109/TSG.2020.2983556.

APPENDIX A

List of publications of the applicant

1. M. Azizi, O. Husev, C. Roncero-Clemente, O. Veligorskyi and R. Strzelecki, "Fast and Robust Energy Router Control in Dynamic Conditions Using Flatness-Based Control Theory," 2025 IEEE 19th International Conference on Compatibility, Power Electronics and Power Engineering (CPE-POWERENG), Antalya, Turkiye, 2025, pp. 1-6, doi: <https://doi.org/10.1109/CPE-POWERENG63314.2025.11027260>. Flatness-based control theory is developed to enhance the dynamic performance of a multiport energy router. The presented method controls the grid-side inverter and regulates the dc link voltage. The simulation results confirm the proper performance of this method, and the comparisons made validate the high speed and accuracy of the system responses compared to conventional solutions. Keywords—Flatness-based control theory, multiport energy router, dynamic conditions, hybrid nanogrid. Conference Scopus.
2. M. Azizi, O. Husev, R. Mbayed, E. Monmasson, J. Martins and O. Veligorskyi, "Energy Router: A Sustainable Solution for Future Residential Buildings," in IEEE Power Electronics Magazine, vol. 12, no. 1, pp. 75-86, March 2025, doi: <https://doi.org/10.1109/MPEL.2024.3525349>. This article provides a detailed review of power electronics solutions for ZEBs and offers strategies to address related challenges. By exploring the promising future of the low-voltage dc (LVdc) industry in ZEBs, it presents and compares grid connection scenarios and evaluates their overall efficiencies across hybrid, dc, and ac technologies. Furthermore, it addresses the integration of dc and ac systems in energy resources (ER), proposing solutions for challenges related to protection, grounding, and leakage currents. Finally, it examines the latest EMS solutions, emphasizing the shift to full digitalization through a combination of cloud-based and edge-computing platforms. Keywords: {Photovoltaic systems; Renewable energy sources; Energy consumption; Low voltage; Reviews; Buildings; Standardization; Microgrids; Power electronics; Protection}, Scopus Q2 Journal.

3. M. Azizi, O. Husev, O. Veligorskyi, M. Turzvínski and R. Strzelecki, "Dc Leakage Current in Isolated Grid-Connected dc Nanogrid - Origins and Elimination Methods," 2024 IEEE 18th International Conference on Compatibility, Power Electronics and Power Engineering (CPE-POWERENG), Gdynia, Poland, 2024, pp. 1-6, doi: <https://doi.org/10.1109/CPE-POWERENG60842.2024.10604426>. This study deals with the leakage current in the galvanically isolated dc nanogrid. Then, it examines the dc leakage current and its relationship with the dc nanogrid grounding and finally provides solutions to remove the dc components in the leakage current. Keywords: Grid-connected dc nanogrid, Isolation, grounding type, dc leakage current, capacitive grounding. Conference Scopus.
4. Azizi, M., Husev, O., Veligorskyi, O., Rahimpour, S., & Roncero-Clemente, C. (2023). Grounding and Isolation Requirements in DC Microgrids: Overview and Critical Analysis. *Energies*, 16(23), 7747. <https://doi.org/10.3390/en16237747> DC microgrids, along with existing AC grids, are a future trend in energy distribution systems. At the same time, many related issues are still undefined and unsolved. In particular, uncertainty prevails in isolation requirements between AC grids and novel microgrids as well as in the grounding approaches. This paper presents a critical technical analysis and an overview of possible grounding approaches in DC systems and the feasibility of avoiding isolation between AC and DC grids. Keywords: DC microgrids; isolation requirements; grounding approach ,Scopus Q2 Journal.
5. M. Azizi, S. Rahimpour, O. Husev and O. Veligorskyi, "Back-to-Back Energy Router Based on Common-Ground Inverters," 2023 IEEE 17th International Conference on Compatibility, Power Electronics and Power Engineering (CPE-POWERENG), Tallinn, Estonia, 2023, pp. 1-6, <https://doi.org/10.1109/CPE-POWERENG58103.2023.10227480>. This paper proposes an energy router based on a back-to-back structure with common-ground inverters. Connecting the neutral wire of the ac system to the negative port of the dc link eliminates leakage currents and ensures safety. The operation mode of the common-ground inverter has been investigated, and the simulation results confirm the accuracy of the overall

structure and benefits compared to classical H-bridge inverter. Keywords: Energy router, non-isolated, common-ground inverters, back-to-back structure. Keywords: {Photovoltaic systems; Power engineering; Electric potential; Simulation; Wires; Voltage; Inverters; Energy router; non-isolated; common-ground inverters; back-to-back structure}, conference Scopus.

6. M. Azizi, O. Husev, D. Vinnikov and O. Veligorskyi, "Comparative Evaluation of Isolated dc-dc Converters for Low Power Applications," 2022 IEEE 20th International Power Electronics and Motion Control Conference (PEMC), Brasov, Romania, 2022, pp. 7-12, doi: <https://doi.org/10.1109/PEMC51159.2022.9962944>. This article examines and evaluates five popular types of isolated dc-dc converters for low-power applications. Using simulations, converters have been evaluated and compared from different perspectives. Keywords— Isolated dc-dc converters, Component design, Flyback, Forward, Push-pull, Full-bridge. Conference Scopus.
7. Azizi, M., Husev, O., & Vinnikov, D. (2022). Single-Stage Buck–Boost Inverters: A State-of-the-Art Survey. *Energies*, 15(5), 1622. <https://doi.org/10.3390/en15051622>. In this paper, the state of the art of single-stage buck–boost inverters is discussed. The advantages and disadvantages of each structure are examined from different perspectives, such as the number of components, losses, and performance. Finally, in a general comparison, the properties of all structures are discussed and summarized in a table. Keywords: single-stage inverter; buck–boost operation; survey, Scopus Q2 Journal.

Continued **Appendix A**

Approval of the results of the dissertation. The main provisions of the dissertation were reported and discussed at four international scientific and technical conferences, namely:

- 20th International Power Electronics and Motion Control Conference (PEMC) IEEE 2022 (Brasov, Romania) 25-28 September 2022.
- 17th International Conference on Compatibility, Power Electronics and Power Engineering (CPE-PowerENG) 2023 (Tallinn, Estonia), 14-16 June 2023.
- 18th International Conference on Compatibility, Power Electronics and Power Engineering (CPE-PowerENG) 2024 (Gdynia, Poland), 24-26 June 2024.
- 19th International Conference on Compatibility, Power Electronics and Power Engineering (CPE-PowerENG) 2024 (Antalya, Turkey), 20-22 May 2025.

APPENDIX B

| | | |
|--|--|---|
| МІНІСТЕРСТВО ОСВІТИ І НАУКИ УКРАЇНИ |  | MINISTRY OF EDUCATION AND SCIENCE OF UKRAINE |
| НАЦІОНАЛЬНИЙ УНІВЕРСИТЕТ «ЧЕРНІГІВСЬКА ПОЛІТЕХНІКА» | тел. +38(0462) 665-103; факс +38(0462) 665-105 E-mail: estu@stu.cn.ua www.stu.cn.ua Код ЄДРПОУ 05460798 | CHernihiv Polytechnic National University |
| вул. Шевченка, 95, Чернігів, 14030, Україна | | 95, Shevchenko str., Chernihiv, 14030, Ukraine |

12.11.2025 № 202/02-2252/PC
На № _____ від _____

CERTIFICATE ON IMPLEMENTATION

of the results of MOHAMMADREZA Azizi dissertation “Energy Router for Hybrid Microgrids for efficient and robust energy and power management” for the degree of Doctor of Philosophy in the specialty 141 Electric Power Engineering, Electrical Engineering, and Electromechanics

The results of scientific research presented in MOHAMMADREZA Azizi dissertation have been implemented in the educational process and project activities of Chernihiv Polytechnic National University:

1. At the Department of Electrical Engineering and Information Measuring Technologies, during classes in the disciplines “Smart Cities and Climate Adaptation and Mitigation Strategies” and “Smart Grid Technologies in Electric Power Engineering” in the process of training Master students majoring in 141 Electric Power Engineering, Electrical Engineering, and Electromechanics.

2. In the project “Research and Education Network for Smart and Green Energy Systems and Business Models” (SMARTGYsum) under the Horizon 2020 MSCA-ITN-2020 program “Innovative Training Networks”.

Vice-Rector for Scientific Work



Anatolii PRYSTUPA